Air Force Institute of Technology

AFIT Scholar

Theses and Dissertations | Student Graduate Works

12-13-2001

Air Vehicle Path Planning

Jeffrey M. Hebert

Follow this and additional works at: https://scholar.afit.edu/etd

 Part of the Navigation, Guidance, Control and Dynamics Commons

Recommended Citation

Hebert, Jeffrey M., "Air Vehicle Path Planning" (2001). *Theses and Dissertations*. 4349.
https://scholar.afit.edu/etd/4349

This Dissertation is brought to you for free and open access by the Student Graduate Works at AFIT Scholar. It has been accepted for inclusion in Theses and Dissertations by an authorized administrator of AFIT Scholar. For more information, please contact AFIT.ENWL.Repository@us.af.mil.

AIR VEHICLE PATH PLANNING

DISSERTATION

Jeffrey M. Hebert, Captain, USAF

AFIT/DS/ENG/01-04

DEPARTMENT OF THE AIR FORCE
AIR UNIVERSITY

AIR FORCE INSTITUTE OF TECHNOLOGY

Wright-Patterson Air Force Base, Ohio

APPROVED FOR PUBLIC RELEASE; DISTRIBUTION UNLIMITED

Report Documentation Page

Report Date	**Report Type**	**Dates Covered (from... to)**
13 Dec 2001	Final	Oct 1999 - Nov 2001

Title and Subtitle Air Vehicle Path Planning	**Contract Number**
	Grant Number
	Program Element Number
Author(s) Capt Jeffrey M. Hebert, USAF	**Project Number**
	Task Number
	Work Unit Number
Performing Organization Name(s) and Address(es) Air Force Institute of Technology Graduate School of Engineering and Management (AFIT/EN) 2950 P Street, Bldg 640 Wright-Patterson AFB, OH 45433-7765	**Performing Organization Report Number** AFIT/DS/ENG/01-04
Sponsoring/Monitoring Agency Name(s) and Address(es) Mr. Phillip R. Changler UAV Control Tech Lead AFRL/VACA 2210 8th Street Bldg 146, Room 305 Wright-Patterson AFB, OH 45433-7532	**Sponsor/Monitor's Acronym(s)**
	Sponsor/Monitor's Report Number(s)
Distribution/Availability Statement Approved for public release, distribution unlimited	
Supplementary Notes	

Abstract
This dissertation explores optimal path planning for air vehicles. An air vehicle exposed to illumination by a tracking radar is considered and the problem of determining an optimal planar trajectory connecting two prespecified points is addressed. An analytic solution yielding the trajectory minimizing the received radar energy reflected from the target is derived using the Calculus of Variations. Additionally, the related problem of an air vehicle tracked by a passive sensor is also solved. Using the insights gained from the single air vehicle radar exposure minimization problem, a hierarchical cooperative control law is formulated to determine the optimal trajectories that minimize the cumulative exposure of multiple air vehicles during a rendezvous maneuver. The problem of one air vehicle minimizing exposure to multiple radars is also addressed using a variational approach, as well as a sub-optimal minmax argument. Local and global optimality issues are explored. A novel decision criterion is developed determining the geometric conditions dictating when it is preferable to go between or around two radars. Lastly, an optimal minimum time control law is obtained for the search and target identification mission of an autonomous air vehicle. This work demonstrates that an awareness of the consequences of embracing sub-optimal and non-globally optimal solutions for optimization problems, such as air vehicle path planning, is essential.

Subject Terms
Planning, Optimization, Calculus of Variations, Unmanned, Uninhabited Air Vehicle, Aircraft

Report Classification	**Classification of this page**
unclassified	unclassified
Classification of Abstract	**Limitation of Abstract**
unclassified	UU

Number of Pages
195

The views expressed in this dissertation are those of the author and do not reflect the official policy or position of the United States Air Force, Department of Defense or the United States Government.

AFIT/DS/ENG/01-04

AIR VEHICLE PATH PLANNING

DISSERTATION

Presented to the Faculty

School of Engineering and Management

Air Force Institute of Technology

Air University

Air Education and Training Command

In Partial Fulfillment of the Requirements for the

Degree of Doctor of Philosophy

Jeffrey M. Hebert, B.S., M.S.E.E.

Captain, USAF

November 2001

APPROVED FOR PUBLIC RELEASE; DISTRIBUTION UNLIMITED

AFIT/DS/ENG/01-04

AIR VEHICLE PATH PLANNING

Jeffrey M. Hebert, B.S., M.S.E.E.

Captain, USAF

Approved:

Dr. Meir Pachter Thesis Advisor	Date
Lt Col David Jacques Committee Member	Date
Lt Col Raymond Hill Committee Member	Date
Dr. Yung Kee Yeo Dean's Representative	Date

Accepted:

Robert A. Calico, Jr.
Dean, Graduate School of Engineering and Management

Acknowledgements

I would like to express most sincere thanks to my advisor, Prof. Meir Pachter, for sharing with me his perspectives on mathematics, engineering, problem solving and life in general. He was exceptionally generous in making time to meet with me, and I benefited greatly from our conversations. I would also like to thank Lt Col Dave Jacques for not only his excellent comments and suggestions, but also for his academic and professional mentorship throughout the entire program. I owe several debts of gratitude to Lt Col Ray Hill, especially for his generosity and encouragement.

I would especially like to thank my fellow classmate, Maj Dave Lucia, for his friendship and sound advice. Our musical collaborations were tremendously rewarding and provided me a much needed creative outlet. Thanks also to Maj Jon Anderson, Maj Jim Rogers, Capt John Erickson, Capt Dave Laird, Capt Kevin LaRochelle, Capt Chuck Ormsby, Capt Mark Suriano, Capt Jesse Zydallis and all my classmates, for their support, encouragement and camaraderie.

I would like to thank my family for their love and support throughout this journey. I would especially like to thank my parents for instilling in me the drive and self-confidence it takes to complete an endeavor such as this. Lastly, my wife has been exceptionally understanding and supportive throughout my time at AFIT. I could never have done any of this without her.

Jeffrey M. Hebert

Table of Contents

List of Figures

List of Tables

Abstract

This dissertation explores optimal path planning for air vehicles. An air vehicle exposed to illumination by a tracking radar is considered and the problem of determining an optimal planar trajectory connecting two prespecified points is addressed. An analytic solution yielding the trajectory minimizing the received radar energy reflected from the target is derived using the Calculus of Variations. Additionally, the related problem of an air vehicle tracked by a passive sensor is also solved.

Using the insights gained from the single air vehicle radar exposure minimization problem, a hierarchical cooperative control law is formulated to determine the optimal trajectories that minimize the cumulative exposure of multiple air vehicles during a rendezvous maneuver. The problem of one air vehicle minimizing exposure to multiple radars is also addressed using a variational approach, as well as a sub-optimal minmax argument. Local and global optimality issues are explored. A novel decision criterion is developed determining the geometric conditions dictating when it is preferable to go between or around two radars. Lastly, an optimal minimum time control law is obtained for the target identification and classification mission of an autonomous air vehicle.

This work demonstrates that an awareness of the consequences of embracing sub-optimal and non-globally optimal solutions for optimization problems, such as air vehicle path planning, is essential.

AIR VEHICLE PATH PLANNING

I. Introduction

1.1 Overview

In response to the lessons learned from recent conflicts, the Air Force is expanding the uses and roles of the Uninhabited Air Vehicle (UAV). Traditionally used for reconnaissance, UAVs are now being considered for combat operations, including autonomous attack. The Uninhabited Combat Air Vehicle (UCAV) is envisioned to carry out the "dull, dirty and dangerous" missions of suppression of enemy air defenses and the prosecution of time critical targets; missions that often involve high risk to pilots and demand high endurance [25]. Similarly, air weapons designers are researching standoff miniature munitions that autonomously search, detect, identify, attack and destroy time critical and ground *mobile* targets of military significance [21].

The intention to develop a significant military force consisting of UAVs, UCAVs and autonomous munitions provides both opportunities and imperatives for research. *If these uninhabited air vehicles are to make effective contributions to air power, a progression from single vehicle autonomy to multiple vehicle cooperative behavior is required.* The purpose of this research is to contribute to the development of a theory of path planning for autonomous air vehicles.

1.2 Historical Overview

1.2.1 Single Vehicle Path Planning. The single vehicle path planning problem entails finding a path from point A to point B, such that one minimizes or avoids risk, while subject to constraints, e.g., limited fuel, minimum time, etc., see, e.g., Fig. 1.1.

The task of planning optimal and sub-optimal paths for single vehicle operations has been addressed by the disciplines of Control Engineering, Operations Research and Computer Science. In general, path planning is approached using four methods: trajectory optimization, route planning, analogy-based path planning and game theoretic methods.

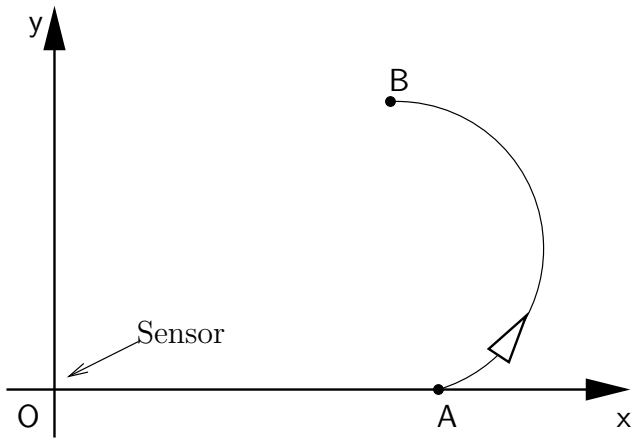

Figure 1.1 Simple Path Planning Problem

1.2.1.1 Trajectory Optimization. One approach used to solve air vehicle path planning problems is trajectory optimization. Trajectory optimization seeks time histories of state and/or control variables of a dynamic model which minimizes a particular cost function or performance index. Closed form solutions of these time histories are rarely obtained. Thus, numerical techniques are usually employed.

Trajectory optimization problems are generally posed as continuous time non-linear optimization problems that are addressed using non-linear parameter optimization, Calculus of Variations, optimal control theory or dynamic programming. Discrete time and/or linear approximations are commonly made. Many classic trajectory optimization problems have been solved using these tools and techniques, such as the brachristichrone problem, the isoperimetric problem, numerous minimum-time performance problems, Zermelo's navigation problem and others - see, e.g., [16, 8, 7].

Numerical codes have been developed for trajectory optimization purposes. Recently, Bryson [7] published an extensive set of methods and codes for trajectory optimization. Furthermore, commercial software packages, such as the MATLAB Optimization Toolbox [13], and software libraries such as Numerical Recipes [36] and IMSL [43], contain many tested and widely used routines. Of particular interest in this work are shooting methods for two-point boundary value problems. Roberts and Shipman [40] have authored a classic text on the subject. FORTRAN implementations of the shooting method are available from many sources [11, 43, 36].

1.2.1.2 Route Planning. Generally, in operational contexts, route planning is performed rather than trajectory optimization. A route consists of a two or more waypoints connected, usually, by straight lines. Often these problems employ a discretization or gridding scheme, where the space of feasible waypoints is predefined and in general, bounded.

A subset of route planning problems involve the situation where a set of waypoints is provided and one must determine the optimal visitation sequence that minimizes some cost function. All but the simplest route planning problems are solved numerically via dynamic programming, network/graph theory or combinatorial optimization. Efficient search methods and heuristics are employed to make the computational burden reasonable. Unless complete enumeration is feasible, optimal solutions cannot be guaranteed.

1.2.1.3 Analogy-based Path Planning. Analogy-based path planning involves transforming the path planning problem to an entirely different problem that has already been solved or to one that has a convenient method of solution. Transformations can be found from a variety of concepts such as physics, geometry and biology.

Techniques developed for robotic motion planning include a method of path planning using potential fields. This technique has been used by several researchers [27, 17, 5] at Air Force Research Laboratory (AFRL) investigating optimal path planning for autonomous air vehicles. The AFRL technique relies upon a defined grid and a system of connections between nodes on the grid, based upon physical laws such as the attraction and repulsion of magnetic fields. Bortoff [5] employed a potential field method by representing the path of a UAV through a radar threat zone as a chain of spring-mass systems. The radars generated virtual forces proportional to the $1/R^4$ distance law and "pushed" the spring mass system away. The chain is initialized in some arbitrary configuration and through simulation, reaches it's potential energy minimum, which is a weighted sum of the path length and the distance from the radar. Potential fields, however popular, have shortcomings. Koren and Borenstien [24] identified four significant problems with the potential field approach: trap situations due to local minima, no passage through closely spaced obstacles, oscillations in the presence of obstacles, and oscillations in narrow passageways.

Helgason, et al [20], developed a geometric algorithm that finds a path through threat regions modelled as circles. The routes were selected by moving between waypoints in a fashion tangential to the threat circles. The waypoints are identified by circumscribing various triangles around the threat circles in a branch-and-bound scheme. In a similar manner, Asseo [4] developed an algorithm to avoid threat zones represented as circles. Asseo generates routes consisting of linear segments tangent to the threat circles, however Asseo also admits circular segments as well, travelling along the threat circles for some segments. Compared to the grid search algorithms, these geometric approaches impose a minor computational burden, yet they make no claims of optimality.

1.2.2 Game Theoretic Path Planning. Contained mainly to applications involving economics and warfare, game theory emerged in the late 1940s from the fields of Applied Mathematics and Operations Research. Games of pursuit and evasion are commonly studied using the methods of game theory. In general, these games consist of the pursuer P attempting to *capture* the evader E by closing the distance PE to within some prescribed positive quantity. For example, the pursuer could be a torpedo, a fighter aircraft or a guided missile, and the evader could be a warship, a bomber aircraft or a tank.

The simplest games often involve one pursuer and one evader, and the dynamics of their motion is governed by differential equations with bounds on speed and rates of turn. Consider the game of the homicidal chauffeur, see, e.g., [22]. The pursuer (the chauffeur) and his quarry are restricted to movement in the plane. The pursuer moves at a fixed speed, w_1, with a bounded turning radius, R. The evader moves at a constant speed, $w_2 < w_1$, however, the evader can change direction at any moment. Capture occurs when the pursuer and evader are separated by a distance $PE \leq l$.

Two forms of the homicidal chauffeur game are typically studied. In the *game of kind*, we are concerned with determining the conditions under which the pursuer can capture the evader, viz., what values of the parameters $w_1/w_2, R$ and l guarantee that P can capture E? Alternatively, assume the game is designed such that P can always capture E. When we are concerned with optimizing the time of capture, we are playing a *game of degree*.

Here, the evader hopes to maximize the time before capture, while the pursuer is working to minimize this quantity.

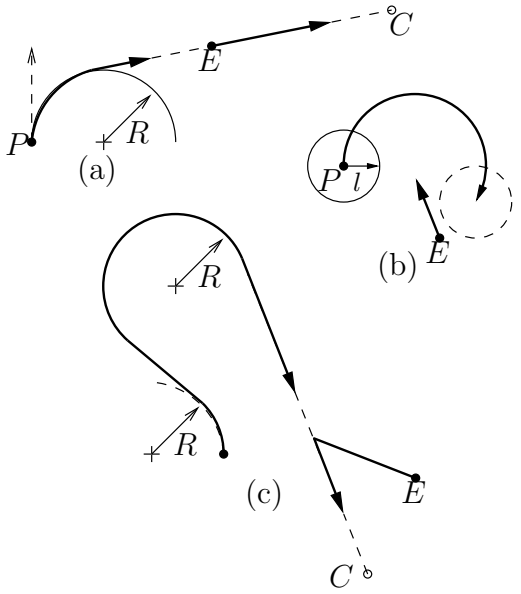

Figure 1.2 Isaac's Illustration Concerning the Game of the Homicidal Chauffeur

The game of the homicidal chauffeur has many interesting scenarios arising from different initial starting conditions. For example, consider Fig. 1.2, from Isaacs [22]. At (a) of Fig. 1.2 we have the pursuer travelling initially up, with the evader ahead and to the right. The optimal strategy is for P to turn hard to the right, following the curve of a minimum radius turn, until the pursuer's velocity vector is aligned with E. The game ends with capture of E at the point C. Now consider Fig. 1.2 at (b), where P is still proceeding initially up, however E is to the rear of P. If the pursuer makes the same hard turn to the right, E has an opportunity to get inside the pursuer's turning radius, thus allowing E to avoid capture. To capture E, the pursuer must first make an indirect move. In (c), a "swerve" maneuver is depicted, whereby P initially turns hard to the left, away from E, until a subsequent hard turn to the right will result in the advantageous situation of (a).

More complicated games can involve multiple pursuers and evaders, such as the football problem: several tacklers against a ball carrier, or the case of a few fighter aircraft against a fleet of bombers. For more information on game theoretic path planning, the reader is referred to the text by Isaacs [22]. Isaacs highlights many different types of two

player games of pursuit and evasion, and these results lend themselves naturally to the problem of path planning for air vehicles.

1.2.3 Multiple Vehicle Control. Path planning for multiple vehicles will use one or more of the path planning methods previously described for single vehicles. Multiple vehicle path planning can be organized into two distinct frameworks: hierarchical cooperative control and reactive control.

1.2.3.1 Hierarchical Cooperative Control. Hierarchical control systems are typified by a segmentation of functionality, where the layers of control coordinate with each other in a predicable and deliberate fashion. Decisions can be made by a centralized leader or by a team of decision makers in a decentralized manner.

Centralized hierarchical control can be achieved through encapsulation or recursion. Much work in this area of is focused on formation flight control, e.g., reducing pilot workload on Special Operations Forces missions [9] or minimizing fuel expenditure for cargo aircraft. Freund and Hoyer [15] describe a method for controlling multiple robots where the dynamic equations for individual robots are coupled and fed to a hierarchical coordinator which handles the problems of collision avoidance, obstacle avoidance and path planning - see, e.g., Fig. 1.3.

McLain [28] details an approach to coordinating the rendezvous of multiple UAVs using a decomposition strategy. This decentralized approach was driven by a state machine residing on each UAV whereupon an identical "team-optimal" estimated time of arrival (ETA) solution is determined by each UAV. Once an ETA is determined and coordinated, the individual UAVs solve local optimization problems to plan paths to meet the ETA goal, as well as maximize their own survivability.

Hierarchical control schemes often attempt to take advantage of high-level knowledge-based representations or maps of the environment. Typically these maps are generated *a priori* and can be updated with on-line sensor information. Paths are planned based upon the knowledge that is available to the air vehicles, and robustness to uncertainty or partial knowledge is an active area of research.

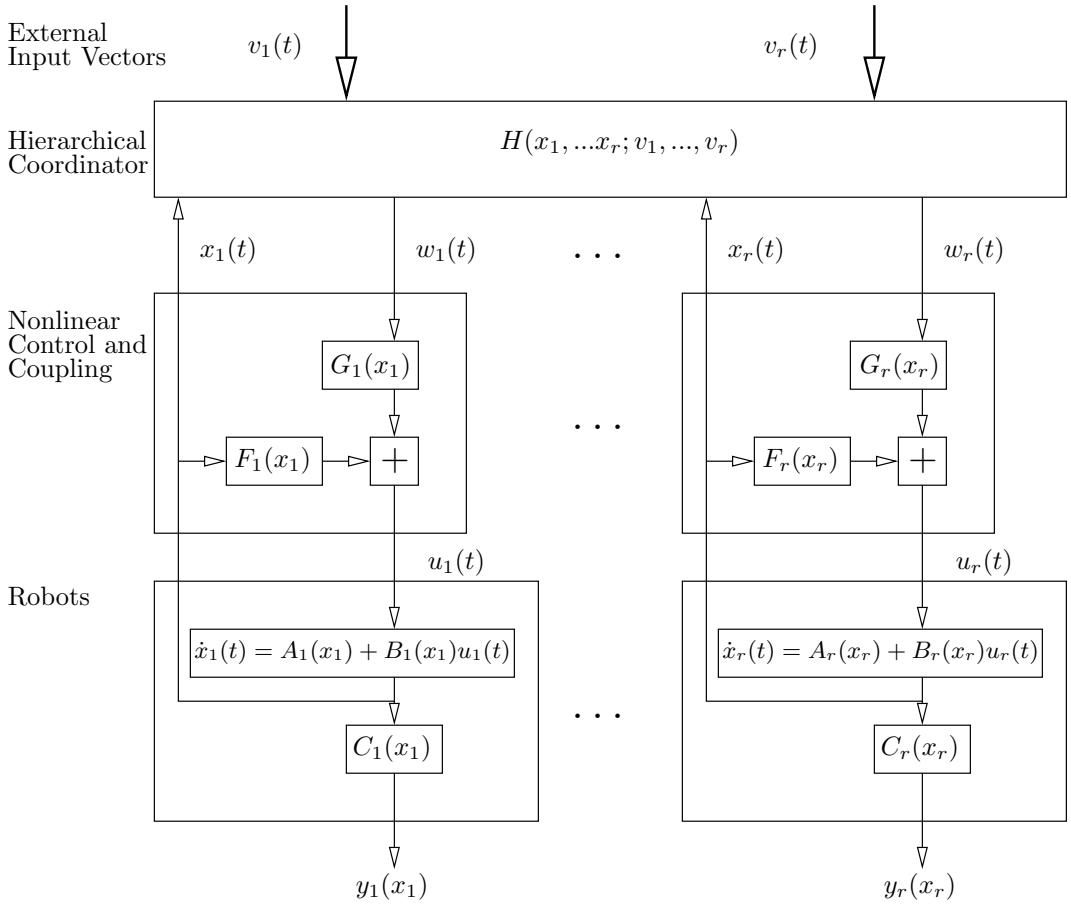

Figure 1.3 Freund and Hoyer's Hierarchical Control Structure

1.2.3.2 Robotic Navigation and Reactive Control. The problem of safely navigating robots through a cluttered environment is closely related to the problem of routing autonomous aircraft. Although methods involving hierarchical planning in robotic navigation have been successful, dissatisfaction with their performance led to the emergence of the reactive control approach. Influenced by the Behaviorist school of psychology, Brooks developed the subsumption architecture [6], in which a model or representation of the world is eschewed in favor of a system of simple behaviors (like wander, avoid obstacles, move to goal). In the subsumption architecture, the intended behavior of the robot emerges from the interaction of the simple behaviors with the environment. Reactive control research is concerned with how best to coordinate these simple behaviors to achieve desired emergent

behaviors. In principle, the subsumptive architecture promotes quick response to changes in the world and hence, adaptability to unplanned circumstances.

Arkin, Ram and others have made numerous contributions [39, 38, 37] to the area of reactive control for robotic navigation, addressing some of the shortcomings [24] of the purely reactive control model. Much of the work has focused on how the robots adapt their behavioral structure and control parameters using machine learning techniques. The work on reactive control of robots has been extended to include cooperative behaviors amongst the robots. Arkin and Balch give a short history of the development of multi-agent robotic systems [3]. Currently, the most popular application of multiple robot research is the RoboCup robotic soccer initiative [41].

Although the two approaches of hierarchical planning and reactive control seem orthogonal to each other in terms of their philosophy, Arkin eloquently describes the need to synthesize the two approaches in "Towards the Unification of Navigation Planning and Reactive Control"[2]. He states, "The reality is that the hierarchical school is involved with plan formulation while the reactive school copes with plan execution and the issues of dynamic replanning." Suggesting that the two approaches are addressing two different problems, Arkin suggests, "we look not towards the superiority of one navigational methodology over the other, but rather toward a synthetic, integrative approach that applies both of these paradigms to the issues of navigational planning..."

1.3 Problem Statement

Previous work in air vehicle path planning has focussed on ad-hoc or heuristic optimization methods. Thus, extending existing path planning methods to multiple vehicles, while seeking insight into the nature of optimal solutions, is difficult. The development of a comprehensive theory of cooperative control for air vehicles is a vast problem, beyond the scope of a single dissertation. A realistic, yet challenging, problem statement for this dissertation is as follows:

> The objective is to develop a mathematically rigorous approach to a problem in air vehicle path planning, seeking fundamental truths concerning autonomous air vehicles and their cooperative control.

It is hoped that these fundamental truths, will guide planners in the development of tools for more complex air vehicle path planning scenarios. To this end, the scenarios of minimizing exposure to a threat radar and target classification are selected as the basis for this research.

1.4 Key Results

The analysis conducted in this research has led to the following key results:

- A closed form solution to the single vehicle radar exposure minimization problem.
  - The solution is shown to satisfy necessary and sufficient conditions for a weak local minimum as well as the Weierstrass necessary conditions for a strong local minimum.
  - The solution is shown to exist if, and only if, the angle included between the departure and destination points is less than 60°.
  - A closed form expression for the optimal cost is obtained.
  - An expression for the optimal path length, not available in closed form, is derived using elliptic integrals. This formulation allows for efficient and accurate computation of the optimal path length.
  - A method for determining optimal path length constrained solutions to the single vehicle radar exposure minimization problem is presented and conditions for the existence of these solutions are identified.
- A similar analysis is conducted for the single vehicle passive sensor exposure minimization problem to include a closed form solution and closed form expressions for the optimal path length and cost. A comparison between the solutions to the passive sensor and radar exposure minimization problem is made.
- It is verified that the Voronoi edge is the locally optimal solution for exposure minimization against two radars. The issues of global versus local optimality are explored yielding analytic results identifying the conditions where going around (between) two

radars is preferable to going between (around) two radars. A suboptimal algorithm for n-radar exposure minimization is developed and examined.

- A hierarchical cooperative control algorithm is formulated to determine optimal trajectories minimizing radar exposure for two (or more) air vehicles performing isochronous rendezvous. The constructive nature of the algorithm renders the existence of these solutions readily verifiable.
- The automatic target recognition process is modelled and a novel optimization problem is formulated and solved. Minimum time trajectories for air vehicles with a minimum turning radius are employed to integrate these concepts and a solution to the autonomous air vehicle search problem is presented.

1.5 Organization

This dissertation is organized as follows: The essential elements of radar technology and optimization theory utilized in this research are presented in Chapter 2. In Chapter 3, the single vehicle radar exposure minimization problem is addressed, including derivations of the optimal trajectory, its cost and path length. Next, an analysis is conducted for the problem of minimizing exposure to a passive sensor in Chapter 4. Similarly, closed form solutions for the optimal trajectory, cost and path length are derived. Chapter 5 contains a description of the numerical methods developed and employed in this research, including a novel discrete formulation of the problem, as well as an exposition on the shooting method for solving two point boundary value problems. Chapter 6 describes an extension of the results of Chapter 2 to address several new problems. A hierarchical cooperative control algorithm is formulated for the problem of isochronous rendezvous of multiple air vehicles. Additionally, the problem of a single vehicle minimizing exposure to two radars is studied and novel analytic results are derived. A suboptimal technique for minimizing exposure to n-radars is presented. In Chapter 7, the process of automatic target recognition is modelled and an optimization problem is suggested. An optimal minimum time control law is developed for the problem of autonomous target classification. Chapter 8 provides a discussion of these results and recommendations for further research. Lastly, appendices, a succinct list of relevant references and a vita are provided.

1.6 Summary

The forthcoming application of UAVs and UCAVs to the battlefield motivated the need for path planning tools that consider autonomous vehicles and the cooperative control of multiple air vehicles. The multidisciplinary nature of path planning has been illustrated and the different disciplines and approaches to path planning were discussed. The problem statement motivated the need for mathematical rigor and the key results obtained through this research were summarized.

In the next chapter, some basic theory of radar technology is presented, setting the stage for the development of the cost functionals used in this research. Additionally, requisite elements of the Calculus of Variations and optimization theory will be covered.

II. Underlying Topics

2.1 Introduction

The dissertation research is concerned with the theoretical nature of path planning problems for air vehicles. This section provides the basic theory that underlies the problem. Since the research emphasizes analytic solutions, only the basic science behind radar technology is considered. More detailed treatments of radar systems can be found in the literature [42]. Most of the analytic work will involve optimization and the essential elements of the Calculus of Variations are presented. For complete treatments of the Calculus of Variations and Optimal Control, the reader is referred to [16, 26, 18, 8].

2.2 Radar

Radar, or "radio detection and ranging", is one of the primary sensors used by hostile forces against air vehicles. In the simplest terms, a radar transmits an electromagnetic signal and then "listens" for an echo signal reflected from the target. By sensing the time delay between the transmitted pulse and the reflected echo, the range to the target can be determined. The range to a target is given by

$$R = \frac{c\Delta t}{2}$$

where c is the velocity of propagation of the radar signal and Δt is the time elapsed from transmission to reception of the echo signal. In general, the target azimuth is detected by rotating the radar antenna and sensing the location of the antenna when an echo is received. The radial velocity of the target can be estimated by further processing the received signal to sense the Doppler frequency shift.

The typical radar configuration consists of a collocated transmitter and receiver. This is known as a *monostatic* radar configuration. When the receiver and transmitter are separated geographically, this is known as a *bistatic* radar configuration. Bistatic radar configurations, while important, will not be explicitly considered in this dissertation.

2.2.1 The Radar Equation. The basic relationship that determines the maximum range at which a radar can detect a given target is known as the radar range equation. Consider the radar transmitter to have an omnidirectional antenna. The power of the signal radiating from the antenna P_t would be uniformly distributed about a sphere with surface area $4\pi r^2$. The power density of the radar is given by dividing the signal power by the surface area. Since radars use a directional antenna, we can adjust the signal power by a gain factor G_t. Thus, the power density at the target is given by

$$\text{power density at the target} = \frac{P_t G_t}{4\pi R^2}$$

where R is the range from the radar to the target.

As the echo propagates away from the target and toward the radar receiving antenna, the power density of the echo decays with the same $4\pi R^2$ factor, assuming a monostatic radar configuration. Thus given an effective area A_e of the receiving antenna, and the radar cross section of the target σ, the echo power at the radar receiver is given by

$$P_r = \frac{P_t G_t \sigma A_e}{(4\pi R^2)^2} \tag{2.1}$$

The "radar equation", Eq. (2.1), can be written as a ratio of the received radar power to the transmitted power,

$$\frac{P_r}{P_t} = \frac{G_t \sigma A_e}{(4\pi)^2 R^4}$$

and is a crucial factor in the detection of targets by a radar system [42].

2.3 Optimization

This section covers the optimization theory that will be used in the dissertation research. Analytic solutions will be sought, and the two main optimization tools to be used are non-linear programming and the Calculus of Variations.

2.3.1 Calculus of Variations. The Calculus of Variations is essentially concerned with finding the extremals of a functional and classifying them as minima or maxima.

Following the development in [16], we define a functional as a correspondence that assigns a definite real number to each function (or curve) belonging to some class. Thus, a functional can be thought of as a function where the independent variable is itself a function.

We concern ourselves with functionals of the form

$$J[y] = \int_a^b F(x, y, y')\, dx, \quad y(a) = A, \quad y(b) = B \tag{2.2}$$

where $J[y]$ is defined on some normed linear space. We define the *increment* of a functional as

$$\Delta J[h] = J[y + h] - J[y]$$

where $h = h(x)$ is the increment of the independent variable $y = y(x)$. If y is fixed, then $\Delta J[h]$ is itself a functional. In general, $\Delta J[h]$ is non-linear. Suppose we express $\Delta J[h]$ as

$$\Delta J[h] = \varphi[h] + \varepsilon \|h\|$$

where $\varphi[h]$ is a linear functional and $\varepsilon \to 0$ as $\|h\| \to 0$. The functional $J[y]$ is differentiable and the linear functional $\varphi[h]$ is called the *variation* of $J[h]$ and is denoted by $\delta J[h]$.

Theorem 2.3.1. *A necessary condition for the differentiable functional $J[y]$ to have an extremum for $y = \hat{y}$ is that its variation vanish for $y = \hat{y}$, i.e., that*

$$\delta J[y] = 0$$

for $y = \hat{y}$ and all admissible h.

Proof. See Theorem 2, Section 3 in [16]. □

2.3.1.1 The Euler Equation. We now consider one of the most well known results of the Calculus of Variations, the Euler equation.

Theorem 2.3.2. *Let $J[y]$ be a functional of the form*

$$\int_a^b F(x, y, y')\, dx$$

defined on the set of functions $y(x)$ which have continuous first derivatives in $[a, b]$ and satisfy the boundary conditions $y(a) = A, y(b) = B$. Then a necessary condition for $J[y]$ to have an extremum for a given function $y(x)$ is that $y(x)$ satisfy Euler's equation

$$F_y - \frac{d}{dx} F_{y'} = 0 \tag{2.3}$$

Proof. See Section 4.1 in [16]. □

The solution of Euler's equation in general involves solving a second order differential equation. There are special cases where Euler's equation can be reduced to a first order differential equation or another simplified expression.

Case 1: Assume the functional is of the form

$$\int_a^b F(x, y')\, dx$$

That is, the integrand $F(x, y')$ does not depend on y. Thus $F_y = 0$ and Euler's equation reduces to

$$\frac{d}{dx} F_{y'} = 0$$

We can integrate to obtain a first order differential equation

$$F_{y'} = C$$

where C is a constant of integration.

Case 2: Assume the functional is of the form

$$\int_a^b F(y, y')\, dx$$

That is, the integrand $F(y, y')$ does not depend on x. In this case it can be shown that Euler's equation can be reduced to

$$\frac{d}{dx}(F - y' F_{y'}) = 0$$

Similarly, we can integrate to obtain a first order differential equation

$$F - y'F_{y'} = C$$

where C is a constant of integration.

Case 3: Assume the functional is of the form

$$\int_a^b F(x, y)\, dx$$

where the integrand $F(x, y)$ does not depend on y'. Thus $F_{y'} = 0$ and Euler's equation reduces to

$$F_y = 0$$

This equation is not a differential equation.

Case 4: Assume the functional is of the form

$$\int_a^b F(x, y)\sqrt{1 + y'^2}\, dx$$

In this case it can be shown that Euler's equation can be reduced to

$$F_y - F_x y' - F\frac{y''}{1 + y'^2} = 0.$$

This case often occurs when the functional involves integration with respect to an arc length s, where

$$ds = \sqrt{1 + y'^2}\, dx$$

Often, but not always, the "simplifications" offered by these special cases expedite the process of finding a solution to the Euler equation.

2.3.1.2 Constrained Optimization. Some problems posed in the Calculus of Variations involve constraints, or subsidiary conditions, that are imposed upon the admissible solutions. The *isoperimetric problem* is given as:

Find the curve $y = y(x)$ for which the functional

$$J[y] = \int_a^b F(x, y, y')\, dx$$

has an extremum, where the admissible curves satisfy the boundary conditions

$$y(a) = A, \quad y(b) = B,$$

and are such that another functional

$$K[y] = \int_a^b G(x, y, y')\, dx$$

takes a fixed value l.

Assuming the functionals F and G have continuous first and second derivatives, then by Theorem 1, Section 12.1 in [16], there exists a constant λ such that $y = y(x)$ is an extremal of the functional

$$\int_a^b \left[F(x, y, y') + \lambda G(x, y, y')\right]\, dx,$$

i.e., $y = y(x)$ satisfies the differential equation

$$F_y - \frac{d}{dx}F_{y'} + \lambda\left(G_y - \frac{d}{dx}G_{y'}\right) = 0 \tag{2.4}$$

The constant λ is analogous to the Lagrange multiplier used in parameter optimization problems. The solution of equation (2.4) will result in two unknown constants of integration and the unknown constant λ. These three unknowns are solved by enforcing the boundary conditions $y(a) = A$, $y(b) = B$ and the constraint $K[y] = l$. One can also specify an initial guess for the value for the parameter λ and iterate on the solution until the constraint $K[y] = l$ is satisfied. The latter technique is useful when numerical solutions to the two point boundary value problem are sought.

2.3.1.3 Weak and Strong Extremum. Not only are we concerned about the existence of an extremum for our functional $J[y]$, but we also wish to classify our extremum. Thus we obtain the following definitions:

Definition 2.3.1. *For $y = \hat{y}$, a* **weak extremum** *of the functional $J[y]$ exists if there is an $\varepsilon > 0$ such that $J[y] - J[\hat{y}]$ has the same sign for all y which satisfy $\|y - \hat{y}\|_1 < \varepsilon$ where*

$$\|y\|_1 = \max_{a \le x \le b} |y(x)| + \max_{a \le x \le b} |y'(x)|$$

denotes the norm in the space of all continuous functions that have continuous first derivatives on some closed interval $[a, b]$.

Definition 2.3.2. *For $y = \hat{y}$, a* **strong extremum** *of the functional $J[y]$ exists if there is an $\varepsilon > 0$ such that $J[y] - J[\hat{y}]$ has the same sign for all y which satisfy $\|y - \hat{y}\|_0 < \varepsilon$ where*

$$\|y\|_0 = \max_{a \le x \le b} |y(x)|$$

denotes the norm in the space of all continuous functions on some closed interval $[a, b]$.

Thus, every strong extremum is also simultaneously a weak extremum and any necessary condition generated for a weak extremum would also be a necessary condition for a strong extremum.

2.3.1.4 Necessary and Sufficient Conditions for a Weak Extremum. As shown in Theorem 2.3.1, the vanishing of the (first) variation $\delta J[h]$ of the functional $J[y]$ was a necessary condition for the existence of a (weak) extremal. Analogous to examining the second derivative in parameter optimization problems, to show sufficient conditions for a weak extremal we consider the second variation $\delta^2 J[h]$.

By applying Taylor's theorem to functionals of the form (2.2), with an increment $h(x)$ satisfying the boundary conditions

$$h(a) = 0, \quad h(b) = 0$$

one can obtain the second variation

$$\delta^2 J[h] = \frac{1}{2}\int_a^b \left(F_{yy}h^2 + 2F_{yy'}hh' + F_{y'y'}h'^2\right)\, dx. \tag{2.5}$$

Applying the condition that the increment must vanish on the boundary and integrating by parts yields a convenient form of the second variation

$$\delta^2 J[h] = \int_a^b \left(Ph'^2 + Qh^2\right)\, dx, \tag{2.6}$$

where

$$P = P(x) = \frac{1}{2}F_{y'y'}, \quad Q = Q(x) = \frac{1}{2}\left(F_{yy} - \frac{d}{dx}F_{yy'}\right)$$

Theorem 2.3.3 (Legendre). *A necessary condition for the functional of the form*

$$J[y] = \int_a^b F(x, y, y')\, dx, \quad y(a) = A, \quad y(b) = B$$

to have a minimum for the curve $y = y(x)$ is that the inequality

$$F_{y'y'} \geq 0$$

(Legendre's condition) be satisfied at every point of the curve.

Proof. See [16] Sec 25. □

Similarly, Legendre's condition for a maximum is $F_{y'y'} \leq 0$.

In order to demonstrate sufficient conditions for a weak extremum, we must introduce the the concept of conjugate points and a means to determine conjugate points in a closed interval. First we define the Jacobi equation of the functional (2.2).

Definition 2.3.3. *The Euler equation*

$$-\frac{d}{dx}\left(Ph'\right) + Qh = 0 \tag{2.7}$$

of the quadratic functional (2.6) is called the Jacobi equation of the original functional (2.2)

Next we define the conjugate point and introduce an important theorem relating the functional from which the Jacobi equation is derived.

Definition 2.3.4. *The point $\tilde{a}$ ($\neq a$) is said to be conjugate to the point a if the Jacobi equation (2.7) has a solution which vanishes for $x = a$ and $x = \tilde{a}$ but is not identically zero.*

Theorem 2.3.4. *The quadratic functional*

$$\int_a^b \left(Ph'^2 + Qh^2 \right) \, dx, \tag{2.8}$$

where

$$P(x) > 0 \qquad (a \leq x \leq b)$$

is positive definite for all $h(x)$ such that $h(a) = h(b) = 0$ if and only if the interval $[a, b]$ contains no points conjugate to a.

Proof. See [16] Sec. 26 Theorem 3. □

Showing that the interval $[a, b]$ contains no points conjugate to a can be accomplished by solving the Jacobi equation (2.7), thus satisfying the definition (2.3.4), or by proving equation (2.8) is positive definite and invoking Theorem 2.3.4. Proving equation (2.8) is positive definite can be accomplished by showing $Q \geq 0$ over the interval $[a, b]$. While this is sufficient to show the functional (2.8) is positive definite, it is not necessary.

Finally, we are able to state sufficient conditions for finding a weak extremum.

Theorem 2.3.5. *Suppose for some admissible curve $y = y(x)$, the functional (2.2) satisfies the following conditions:*

1. *The curve $y = y(x)$ is an extremal, i.e., satisfies Euler's equation*

$$F_y - \frac{d}{dx} F_{y'} = 0;$$

2. *Along the curve $y = y(x)$,*

$$P(x) \equiv \frac{1}{2} F_{y'y'} > 0$$

(the strengthened Legendre condition).

3. *The interval $[a, b]$ contains no points conjugate to the point a.*

Then the functional (2.2) has a weak minimum for $y = y(x)$.

Proof. See [16] Sec 28. □

2.3.1.5 Necessary and Sufficient Conditions for a Strong Extremum. Every strong extremum is also a weak extremum, however the converse is not generally true. Therefore, all of the necessary conditions for a weak extremum are also necessary conditions for a strong extremum. In order to state necessary conditions for a strong extremum as derived in [16], we need to introduce the Weierstrass E-function (excess function).

Definition 2.3.5. *The Weierstrass E-function of the functional*

$$J[y] = \int_a^b F(x, y, y')\, dx, \quad y(a) = A, \quad y(b) = B$$

is given by

$$E(x, y, z, w) = F(x, y, w) - F(x, y, z) - (w - z)F_{y'}(x, y, z)$$

Necessary conditions for a strong extremum are given by evaluating the Weierstrass E-function for a candidate extremal. The conditions given below are for strong minima, however they are extended to strong maxima by reversing the inequality.

Theorem 2.3.6 (Weierstrass' necessary condition). *If the functional*

$$J[y] = \int_a^b F(x, y, y')\, dx, \quad y(a) = A, \quad y(b) = B \tag{2.9}$$

has a strong minimum for the extremal γ, then

$$E(x, y, y', w) \geq 0 \tag{2.10}$$

along γ for every finite w.

Proof. See [16], Section 34. □

2.3.2 Numerical Methods. There are many methods available for solving variational problems numerically. The two methods discussed here are the direct method, where the cost function is approximated with discrete increments and the shooting method which iteratively seeks numerical solutions of the two point boundary value problem resulting from the Euler equation.

2.3.2.1 Direct Methods. One technique for minimizing the cost functional directly is the method of finite differences. Here an approximation to the cost funcional

$$J = \int F(x, y, \dot{y})\, dx$$

is performed by using numerical methods of integration and differentiation. This implies that the trajectory consists of some finite number of segments, e.g., N. For example, the derivative terms in the integrand of the cost functional can be replaced with the central difference approximation

$$\dot{y_i} \approx \frac{y_{i+1} - y_{i-1}}{2\,(t_{i+1} - t_{i-1})}$$

where $\dot{y_i}$ represents the derivative of y at the segment i. Integration can be performed using the trapezoidal rule, Simpson's rule, quadrature methods or any other numerical technique. A non-linear programming routine such as Sequential Quadratic Programming, can be used to choose the N points that minimize the approximate cost function. As N grows large, the sequence of N points should converge to the optimal trajectory. Issues such as numeric truncation, roundoff error and/or computational burden can limit the range of N.

Another direct method is that of piecewise linear approximation. Consider approximating the optimal trajectory from points A to B with a series of N straight line segments - see, e.g., Fig. 2.1. Writing one of these N segments in the two-point form of a line in polar coordinates, we have

$$R(\theta) = \frac{r_1 r_2 \sin(\theta_2 - \theta_1)}{r_1 \sin(\theta - \theta_1) - r_2 \sin(\theta - \theta_2)} \tag{2.11}$$

which has the first derivative

$$\dot{R}(\theta) = \frac{r_1 r_2 \sin(\theta_1 - \theta_2)\left[r_1 \cos(\theta - \theta_1) - r_2 \cos(\theta - \theta_2)\right]}{\left[r_1 \sin(\theta - \theta_1) - r_2 \sin(\theta - \theta_2)\right]^2} \tag{2.12}$$

Now the cost to travel from the point (r_1, θ_1) to the point (r_2, θ_2) can be written as

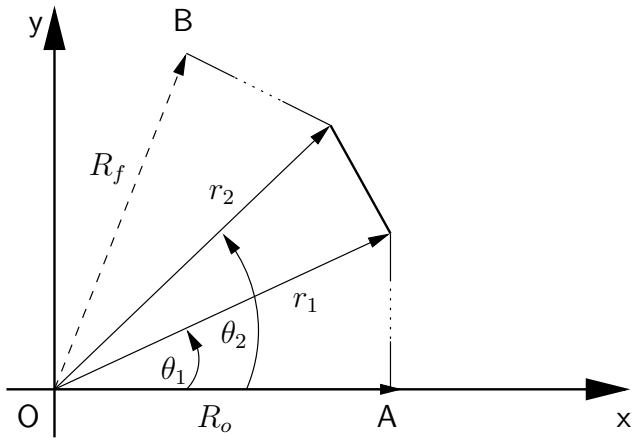

Figure 2.1 Line Segment Defined by Points (r_1, θ_1), (r_2, θ_2)

$$J_{1,2} = \int_{\theta_1}^{\theta_2} F(\theta, R, \dot{R})\, d\theta \tag{2.13}$$

Assume the substitution of Eqs. (2.11) and (2.12) into the cost function, Eq. (2.13) yields a closed form[1] for $J_{1,2}$. Eliminating dependence upon θ allows the cost of any given line segment to be explicitly determined for a given pair of points (r_1, θ_1), (r_2, θ_2). The total cost of the optimal path for some number N line segments is the summation of the costs for each segment, viz.,

$$\tilde{J}^* = \sum_{i=1}^{N} J_{i,i+1}$$

The original variational problem can now be approximated using discrete straight line segments and the resulting problem solved using non-linear programming techniques.

2.3.2.2 Shooting Methods. The shooting method is a numerical technique of solving two point boundary value problems. Here we are concerned about solving n

[1]This could be relaxed by substituting numerical integration for a closed form expression of $J_{1,2}$.

first order non-linear ordinary differential equations over a finite interval where r unknown boundary conditions exist at the initial point. All boundary conditions are given at the final point. In the shooting method, the missing initial conditions are guessed and the resulting system of ordinary differential equations is propagated forward in time. At the final time, the endpoints are compared to the known final boundary conditions and if the difference is not within some tolerance, a correction is made to the initial guess and the process of solving initial value problems is repeated.

Shooting methods can be applied to equality constrained variational problems where a Lagrange multiplier is used, e.g., the isoperimetric problem. In this case, in addition to solving for the missing initial condition, the value of the Lagrange multiplier must also be guessed and the shooting method must be iterated until the constraint condition is satisfied.

Shooting methods are sensitive to the initial guess of the derivative information. Thus this technique requires trial and error and can be difficult to automate compared to a finite difference method, for example. Some modifications to the shooting codes can improve their "robustness". Finite difference methods, for example, can be used as a starting point for the initial guess needed by a shooting method. Similarly, *continuation* is a technique where the shooting problem is formulated such that it depends on a parameter. The shooting problem is solved for one value of the parameter, presumably where the solution is readily obtained. The derivative information is used as a starting point for the next value of the parameter, and so on, thus the problem is "continued" over the range of the parameter. Shooting methods can also be employed "backwards" in time, where the initial boundary conditions are known and the final boundary values are guessed. Furthermore, multiple shooting methods that employ forward and backwards shooting, as well as unknown free parameters at both ends of the domain, have also been developed.

For a more detailed description of the shooting method, the reader can consult the text by Roberts and Shipman [40], the texts by Bryson [8, 7] or the many others that have been written on this topic. FORTRAN codes that implement the shooting method are available in [36, 11, 43].

2.4 Summary

In this chapter, the relevant elements of radar and optimization theory were presented. The main components of the Calculus of Variations were discussed and the numerical treatment of variational optimization problems was addressed.

In the next chapter, the radar exposure minimization problem is motivated from the radar equation, Eq. (2.1) and is formulated in the Calculus of Variations. A rigorous derivation and analysis of the solution of the radar exposure minimization problem for a single air vehicle will be presented.

III. Radar Exposure Minimization

3.1 Introduction

Many different performance objectives, or metrics, can be conceived when considering the problem of path planning for threat minimization. This work does not consider metrics such as probability of detection or probability of tracking. While such metrics may have appeal in operational contexts, they require knowledge of specific radar systems and their targets in order to be credible. The problem formulation that follows is deterministic, and is based upon the physics of radar signal propagation. Thus, the cost functional developed here applies *universally* to all monostatic radars.

In this chapter, the single vehicle radar exposure minimization problem is addressed. The problem is posed in the Calculus of Variations and an analytic solution is derived. Expressions for the optimal cost and optimal path length are provided. An optimal heading angle control law is developed as well as analytic solutions for the optimal maximum range attained from the radar.

3.2 Problem Formulation

Given a radar located at the origin O of the Euclidean plane, it is desired to find the optimal air vehicle trajectory that connects two pre-specified points A and B in the plane such that the received Radio Frequency (RF) energy reflected from the air vehicle is minimized; see, e.g., Fig. 3.1. According to the radar equation, Eq. (2.1), the ratio of the received RF power to the transmitted RF power reflected from the target is inversely proportional to R^4, where R is the slant range from the target to the monostatic radar. The cost to be minimized is then

$$\int_0^{\frac{l}{v}} \frac{1}{R^4(t)} dt$$

where v is the (constant) speed of the air vehicle and l is the path length.

Consider the trajectory in Fig. 3.1 to be given in polar form, as $R = R(\theta)$. Assume $R(\theta)$ is a single valued function, viz., we do not allow backtracking. We have, $v = \frac{ds}{dt}$, i.e.,

$dt = \frac{ds}{v}$, and ds, the element of arc length, is given in polar coordinates by

$$ds = \sqrt{\left(\frac{dR}{d\theta}\right)^2 + R^2}\, d\theta$$

Substituting into the cost equation we then obtain the functional

$$J[R(\theta)] = \int_0^{\theta_f} \frac{\sqrt{\dot{R}^2 + R^2}}{R^4}\, d\theta \tag{3.1}$$

The boundary conditions are

$$R(0) = R_o \tag{3.2}$$

$$R(\theta_f) = R_f, \quad 0 < \theta \leq \theta_f \tag{3.3}$$

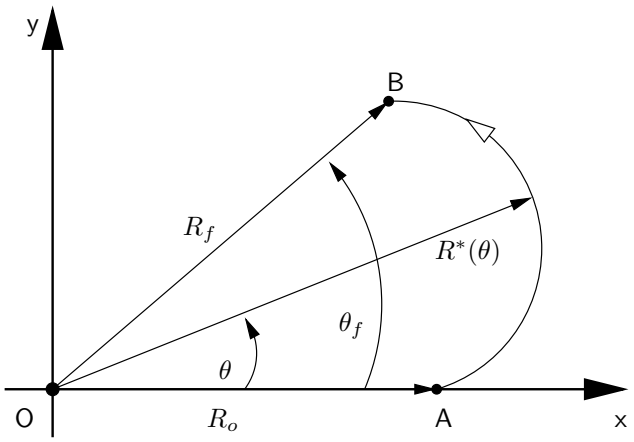

Figure 3.1 Illustration of the Radar Exposure Minimization Problem

3.3 Unconstrained Analytic Solution

Without loss of generality, assume $R_f \geq R_o$ and $0 < \theta_f \leq \pi$, see, e.g., Fig. 3.1. Polar coordinates are used. We have the following:

Theorem 3.3.1. *The optimal trajectory, connecting points A and B at a distance R_o and R_f from the radar located at the origin O, where θ_f is the angle $\angle AOB$, minimizing*

exposure to the radar according to Eqs. (3.1)-(3.3), is

$$R^*(\theta) = R_o \sqrt[3]{\frac{\sin(3\theta+\phi)}{\sin\phi}},\ 0 < \theta \leq \theta_f \tag{3.4}$$

where the angle

$$\phi = \text{Arctan}\left(\frac{\sin 3\theta_f}{\left(\frac{R_f}{R_o}\right)^3 - \cos 3\theta_f}\right) \tag{3.5}$$

Moreover, the length of the optimal path is given by the elliptic integral of the first kind

$$l^* = \frac{R_o}{\sqrt[3]{\sin\phi}} \int_0^{\theta_f} [\sin(3\theta+\phi)]^{-\frac{2}{3}}\ d\theta \tag{3.6}$$

and the cost function explicitly evaluates to

$$J^* = \frac{1}{3{R_o}^3} \frac{\sin 3\theta_f}{\sin(3\theta_f+\phi)} \tag{3.7}$$

This result holds provided $0 < \theta_f < \frac{\pi}{3}$*. However, if* $\frac{\pi}{3} \leq \theta_f \leq \pi$*, then an optimal path does not exist and a constraint on the path length must be included to render the optimization problem well posed.*

Proof. We have obtained a variational problem with an integrand which is not explicitly dependent upon the independent variable θ. In this case, the first integral form of the Euler equation [16] can be employed:

$$F - \dot{R}F_{\dot{R}} = C$$

where F is the integrand of the cost functional, Eq. (3.1), i.e.,

$$F = \frac{\sqrt{\dot{R}^2 + R^2}}{R^4}$$

This results in the first order differential equation

$$\frac{1}{R^2} = C\sqrt{\dot{R}^2 + R^2} \tag{3.8}$$

where C is a constant. Thus,

$$\dot{R} = \pm \frac{\sqrt{1/C^2 - R^6}}{R^2}$$

where $\frac{1}{C^2} > R^6 > 0$. Hence, we have obtained the non-linear ordinary differential equation

$$\frac{dR}{d\theta} = \pm \frac{\sqrt{1/C^2 - R^6}}{R^2}, \quad R(0) = R_o \equiv |OA| \tag{3.9}$$

The integration constant C will be determined by the terminal condition, $R(\theta_f) = R_f \equiv |OB|$.

Momentarily assume $R(\theta)$ is properly unimodal on $0 < \theta \leq \theta_f$, viz., $\exists\ \bar{\theta} \in (0, \theta_f]$ such that $R(\theta)$ is monotonically increasing (decreasing) on $(0, \bar{\theta}\,]$, and is monotonically decreasing (increasing) on $[\bar{\theta}, \theta_f]$. At $\theta = \bar{\theta}$, $R(\theta)$ is maximal and $\frac{dR}{d\theta}\big|_{\bar{\theta}} = 0$.

Let $R(\theta)$ be monotonically increasing on $0 < \theta \leq \bar{\theta}$ and let $R(\theta)$ be monotonically decreasing on $\bar{\theta} \leq \theta \leq \theta_f$. Consider $0 < \theta \leq \bar{\theta}$ where $R(\theta)$ is monotonically increasing, and

$$\frac{dR}{d\theta} = \frac{\sqrt{1/C^2 - R^6}}{R^2}$$

Thus,

$$d\theta = \frac{R^2}{\sqrt{1/C^2 - R^6}}\, dR$$

The solution of this ODE entails an integration. To this end, define the new variable

$$u = CR^3, \text{ i.e., } du = 3\,CR^2\, dR$$

Hence,

$$d\theta = \frac{1}{3} \frac{du}{\sqrt{1 - u^2}}$$

Integration yields $u = \sin(3\theta + \phi)$, where ϕ is the integration constant. Hence,

$$R^3(\theta) = \frac{1}{C} \sin(3\theta + \phi) \tag{3.10}$$

Therefore on $0 < \theta \leq \bar{\theta}$,

$$R(\theta) = \frac{1}{\sqrt[3]{C}} \sqrt[3]{\sin(3\theta + \phi)}, \quad 0 \leq \phi \tag{3.11}$$

Similarly, on $\bar{\theta} \leq \theta \leq \theta_f$,

$$R(\theta) = -\frac{1}{\sqrt[3]{C}} \sqrt[3]{\sin(3\theta - \psi)}, \ 0 \leq \psi \tag{3.12}$$

where $C > 0$.

We have three unknowns: ϕ, ψ, and $\bar{\theta}$, and three conditions: $R(0) = R_o$, $R(\theta_f) = R_f$ and $R(\bar{\theta}) = \max\limits_{0<\theta\leq\theta_f} R(\theta)$. The latter yields - see, e.g., Eqs. (3.11) and (3.12):

$$3\bar{\theta} + \phi = \frac{\pi}{2} \tag{3.13}$$

and

$$3\bar{\theta} - \psi = -\frac{\pi}{2}$$

Thus, combining Eqs. (3.13) and (3.3) yields

$$\phi + \psi = \pi$$

i.e.,

$$\psi = \pi - \phi \tag{3.14}$$

Hence, for $\bar{\theta} < \theta \leq \theta_f$, inserting Eq. (3.14) into (3.12) yields

$$\begin{aligned} R(\theta) &= -\frac{1}{\sqrt[3]{C}} \sqrt[3]{\sin(3\theta + \phi - \pi)} \\ &= \frac{1}{\sqrt[3]{C}} \sqrt[3]{\sin(3\theta + \phi)} \end{aligned}$$

Therefore, the formula

$$R(\theta) = \frac{1}{\sqrt[3]{C}} \sqrt[3]{\sin(3\theta + \phi)}$$

is *unique* and applies on the complete domain of $R(\theta)$, viz., it applies for $0 < \theta \leq \theta_f$.

Subsequently, we use the boundary conditions $R(0) = R_o$ and $R(\theta_f) = R_f$ to determine C and ϕ, respectively, viz.,

$$R_o = R(0) = \frac{1}{\sqrt[3]{C}} \sqrt[3]{\sin\phi}$$

Solving for C yields

$$C = \frac{\sin\phi}{{R_o}^3} \tag{3.15}$$

Thus, the extremizing trajectory is explicitly given by

$$R(\theta) = R_o \sqrt[3]{\frac{\sin(3\theta + \phi)}{\sin\phi}} \tag{3.16}$$

In addition,

$${R_f}^3 = R(\theta_f)^3 = {R_o}^3 \left(\frac{\sin(3\theta_f + \phi)}{\sin\phi} \right)$$

which yields

$$\phi = \text{Arctan} \left(\frac{\sin 3\theta_f}{\left(\frac{R_f}{R_o}\right)^3 - \cos 3\theta_f} \right)$$

The extremal $R(\theta)$, Eq. (3.16), satisfies the necessary and sufficient conditions for a weak local minimum, as well as the Weierstrass necessary conditions for a strong local minimum; see Appendix A.

Once the optimal path $R(\theta) = R^*(\theta)$ has been explicitly determined, it is possible to calculate the path length of the optimal trajectory. The path length is given by

$$l = \int_0^{\theta_f} \sqrt{\dot{R}^2(\theta) + R^2(\theta)}\, d\theta \tag{3.17}$$

Substituting (3.8) into (3.17) yields

$$l^* = \int_0^{\theta_f} \frac{1}{CR^2(\theta)}\, d\theta \tag{3.18}$$

Using Eqs. (3.4) and (3.15) yields

$$\begin{aligned} l^* &= \int_0^{\theta_f} \frac{{R_o}^3}{\sin\phi} \left(R_o \sqrt[3]{\frac{\sin(3\theta+\phi)}{\sin\phi}} \right)^{-2} \, d\theta \\ &= \frac{R_o}{\sqrt[3]{\sin\phi}} \int_0^{\theta_f} \left[\sin(3\theta+\phi)\right]^{-\frac{2}{3}} \, d\theta \end{aligned} \tag{3.19}$$

In Sec. 3.8, we explicitly show that the path length integral (3.19) evaluates into an elliptic integral of the first kind.

The cost function Eq. (3.1) can be simplified by substituting Eq. (3.8) to obtain

$$J = \frac{1}{C} \int_0^{\theta_f} \frac{1}{R^6} \, d\theta$$

Substituting for the previously determined integration constant (3.15), and optimal trajectory (3.4), yields

$$\begin{aligned} J^* &= \frac{\sin\phi}{{R_o}^3} \int_0^{\theta_f} \frac{1}{\sin^2(3\theta+\phi)} \, d\theta \\ &= \frac{\sin\phi}{3{R_o}^3} \int_\phi^{3\theta_f+\phi} \frac{1}{\sin^2(x)} \, d\theta \\ &= -\frac{\sin\phi}{3{R_o}^3} \cot x \Big|_\phi^{3\theta_f+\phi} \\ &= \frac{\sin\phi}{3{R_o}^3} \left[\cot\phi - \cot(3\theta_f+\phi)\right] \\ &= \frac{1}{3{R_o}^3} \frac{\sin 3\theta_f}{\sin(3\theta_f+\phi)} \end{aligned} \tag{3.20}$$

The optimal trajectory is parameterized by two non-dimensional parameters, viz., R_f/R_o and θ_f. The optimal trajectory represents the trade-off between minimizing the time of exposure (path length) and the RF power received by the radar over time, due to the air vehicle's proximity to the radar. The optimal trajectory no longer exists as the angle $\theta_f \to \frac{\pi}{3}$, a critical angle. In other words, the path length becomes infinite at this critical angular separation of the segments OA and OB. Furthermore, as the path length $l \to \infty$, the cost approaches a finite value - see, e.g., Fig. 3.2. Beyond the critical angle $\theta_f = \frac{\pi}{3}$, there does not exist a path that minimizes our cost function. That is, the

aforementioned trade-off breaks down and it is advantageous for the air vehicle to travel away from the radar. Thus, for $\theta_f \geq \frac{\pi}{3}$, a path length constraint must be included to render the optimization problem well posed.

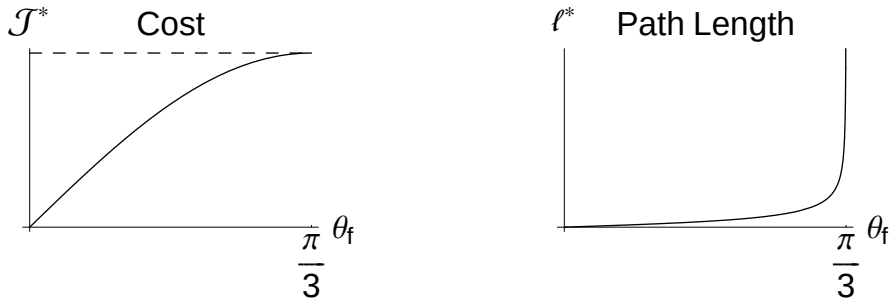

Figure 3.2 The Cost for the Radar Problem is Bounded as the Path Length Grows Without Bound

□

3.3.1 Relationship to Rose Functions. The optimal path given in Eq. (3.4) can be written in the form

$$R^*(\theta) = \frac{R_o}{\sqrt[3]{\sin\phi}} \sqrt[3]{\sin(3\theta + \phi)}$$

which is very similar to the equation of the three-leaved rose function or *Rhodonea* [14], given in polar coordinates as

$$r = a\cos 3\theta$$

The rose function amplitude parameter, a, is the maximum distance the rose function attains from the origin. The rose function is rotated about the origin by adding a parameter ϕ, such that

$$r = a\sin(3\theta + \phi)$$

Fig. 3.3 shows the three-leaved rose function plotted for $\phi = \{0, \frac{\pi}{4}\}$. For the radar problem, we are only concerned about the leaf in the first quadrant of the rose function plot, viz., when $0 \leq \theta \leq 60°$.

In our expression for $R^*(\theta)$, the rose function parameter a is represented by the term $\frac{R_o}{\sqrt[3]{\sin\phi}}$, and the sine term is taken to the third root. Since the distance from the origin

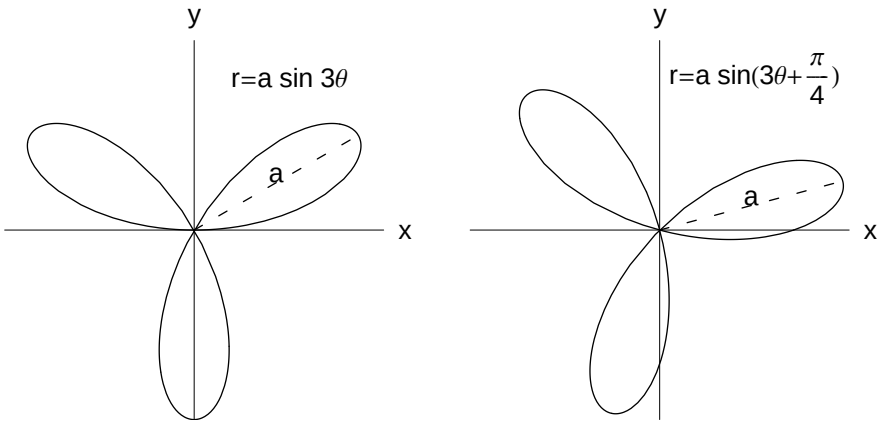

Figure 3.3 Three Leaved Rose Functions

in polar coordinates is real valued, and since complex values of $R(\theta)$ are not physically realizable in this problem, the sign of the original rose function is preserved. In other words, we are only concerned about the first "leaf" of the rose function as, evidently, $0 < \theta_f < 60°$. The shape of the rose function is distorted somewhat by the cubed root, as shown in Fig. 3.4.

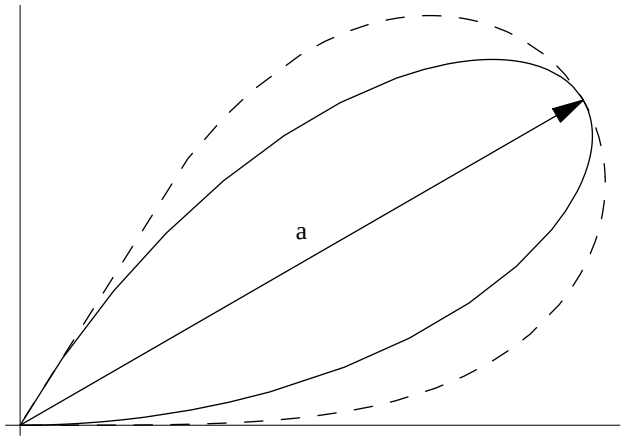

Figure 3.4 Comparison of $a \sin 3\theta$ (solid) and $a\sqrt[3]{\sin 3\theta}$ (dashed) for $0 \leq \theta \leq 60°$

3.3.2 Special Cases. Several interesting special cases concerning the optimal trajectory given by Eq. (3.4) are now considered.

In the case where $\theta_f = 0$ and $R_f > R_o$, the origin O and the points A and B are colinear, and the optimal trajectory is a straight line, as shown in Fig. 3.5.

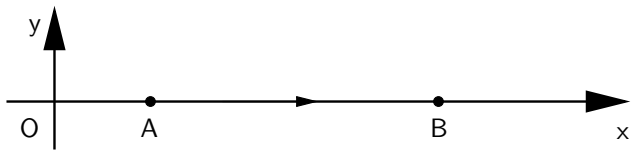

Figure 3.5 Optimal Trajectory for the Special Case where $\theta_f = 0$

Also, the following holds.

Corollary 3.3.1. *The optimal trajectory which connects points A and B at a distance $R_o = R_f$ from the radar located at the origin O, and minimizes exposure to the radar according to Eqs. (3.1)-(3.3), is*

$$R^*(\theta) = R_o \sqrt[3]{\frac{\cos(3\theta - \frac{3\theta_f}{2})}{\cos\frac{3\theta_f}{2}}}, \quad 0 < \theta \leq \theta_f \tag{3.21}$$

where θ_f is the angle $\angle AOB$. The length of the optimal trajectory is then given by

$$l^* = \frac{R_o}{\sqrt[3]{\cos\frac{3\theta_f}{2}}} \int_0^{\theta_f} \left[\cos\left(3\theta - \frac{3\theta_f}{2}\right)\right]^{-\frac{2}{3}} d\theta \tag{3.22}$$

which is an elliptic integral of the first kind. The cost function explicitly evaluates to

$$J^* = \frac{2}{3{R_o}^3} \sin\left(\frac{3\theta_f}{2}\right) \tag{3.23}$$

This result holds provided $0 < \theta_f < \frac{\pi}{3}$.

Proof. When $R_f = R_o$ we can write Eq. (3.5) as

$$\begin{aligned}
\phi &= \text{Arctan}\left(\frac{\sin 3\theta_f}{1 - \cos 3\theta_f}\right) \\
&= \text{Arctan}\left(\frac{\cos\frac{3\theta_f}{2}}{\sin\frac{3\theta_f}{2}}\right) \\
&= \text{Arctan}\left(\tan\left[\frac{\pi}{2} - \frac{3\theta_f}{2}\right]\right) \\
&= \frac{\pi}{2} - \frac{3\theta_f}{2}
\end{aligned} \tag{3.24}$$

The optimal trajectory $R^*(\theta)$ is then obtained by substituting (3.24) into (3.4), whereupon we obtain

$$\begin{aligned} R^*(\theta) &= R_o \sqrt[3]{\frac{\sin(3\theta + \frac{\pi}{2} - \frac{3\theta_f}{2})}{\sin(\frac{\pi}{2} - \frac{3\theta_f}{2})}} \\ &= R_o \sqrt[3]{\frac{\cos(3\theta - \frac{3\theta_f}{2})}{\cos\frac{3\theta_f}{2}}} \end{aligned}$$

Similarly, by substituting Eqs. (3.15) and (3.24) into the equation for the path length (3.18) yields

$$\begin{aligned} l^* &= \frac{{R_o}^3}{\sin\left(\frac{\pi}{2} - \frac{3\theta_f}{2}\right)} \int_0^{\theta_f} \frac{1}{R^2}\, d\theta \\ &= \frac{{R_o}^3}{\cos\frac{3\theta_f}{2}} \int_0^{\theta_f} \frac{1}{R^2}\, d\theta \end{aligned}$$

Substituting the expression for the optimal trajectory, $R^*(\theta)$, developed for this special case, we obtain

$$\begin{aligned} l^* &= \frac{{R_o}^3}{\cos\frac{3\theta_f}{2}} \int_0^{\theta_f} \frac{1}{{R_o}^2} \left[\sqrt[3]{\frac{\cos\frac{3\theta_f}{2}}{\cos(3\theta - \frac{3\theta_f}{2})}}\right]^2 d\theta \\ &= \frac{R_o}{\sqrt[3]{\cos\frac{3\theta_f}{2}}} \int_0^{\theta_f} \left[\cos\left(3\theta - \frac{3\theta_f}{2}\right)\right]^{-\frac{2}{3}} d\theta \end{aligned}$$

Finally, the cost for the optimal trajectory, J^*, is calculated by subsituting Eq. (3.24) into Eq. (3.20), which yields

$$\begin{aligned} J^* &= \frac{1}{3{R_o}^3} \frac{\sin 3\theta_f}{\sin(3\theta_f + \frac{\pi}{2} - \frac{3\theta_f}{2})} \\ &= \frac{1}{3{R_o}^3} \frac{\sin 3\theta_f}{\cos\frac{3\theta_f}{2}} \\ &= \frac{2}{3{R_o}^3} \sin\left(\frac{3\theta_f}{2}\right) \end{aligned} \tag{3.25}$$

□

In the symmetric special case where $R_f = R_o$, it is interesting to note that the relationship between ϕ and θ_f is *linear*. This relationship, given by Eq. (3.24), is depicted in Fig. 3.6. Furthermore, the angle ϕ is evaluated for some interesting θ_f in Table 3.1. We note that the angle $\theta_f \to \frac{\pi}{3}$ as $\phi \to 0$.

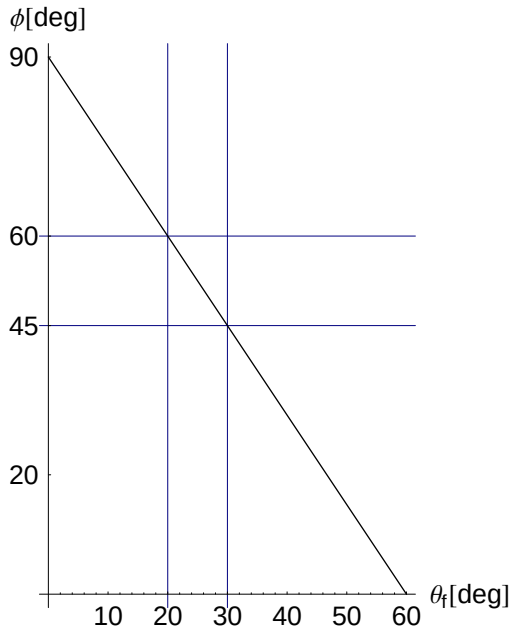

Figure 3.6 The Constant ϕ as a Function of θ_f for the Special Case $R_f = R_o$

Table 3.1 Interesting Values of ϕ for the Special Case $R_f = R_o = 1$

θ_f	ϕ	$\sin\phi$
$0^{\circ +}$	90°	1
10°	$\text{Arctan}\left(\frac{1}{2-\sqrt{3}}\right)$	$\frac{1}{2\sqrt{2-\sqrt{3}}}$
15°	$\text{Arctan}\left(\frac{1}{\sqrt{2}-1}\right)$	$\frac{1}{2\sqrt{1-\frac{1}{\sqrt{2}}}}$
20°	60°	$\frac{\sqrt{3}}{2}$
30°	45°	$\frac{1}{\sqrt{2}}$
45°	$\text{Arctan}\left(\frac{1}{\sqrt{2}+1}\right)$	$\frac{1}{2\sqrt{1+\frac{1}{\sqrt{2}}}}$
60°	0°	0

The optimal trajectory (3.4) is shown in Fig. 3.7 for the case where $R_f/R_o = 1$ and $\theta_f = 45^\circ$. By inspection of Fig. 3.7 we see that the extremal trajectory is indeed symmetric when $R_o = R_f$, as expected.

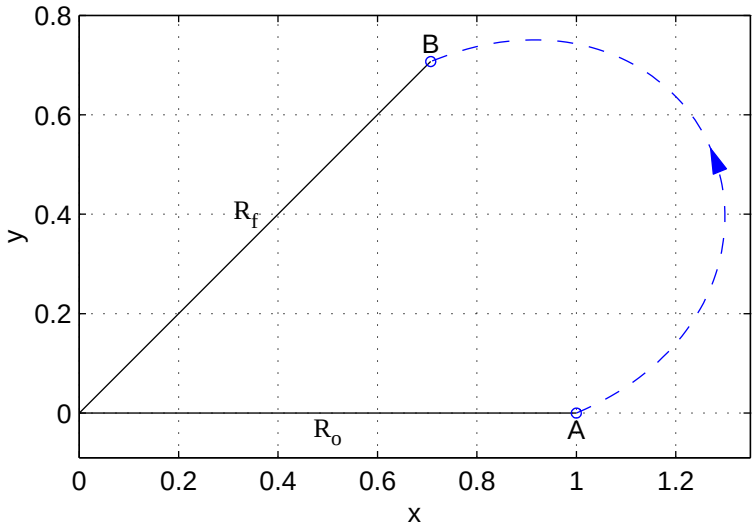

Figure 3.7 An Example of the Optimal Trajectory $R^*(\theta)$ for the Symmetric Case $R_f/R_o = 1$, $\theta_f = 45°$

3.4 Optimal Heading Angle

In this section we are concerned with calculating the optimal heading angle, $\varphi^*(\theta)$, of an aircraft flying the radar energy minimization trajectory specified by Eq. (3.4). The heading angle, for example, could be useful as a command generator in an autopilot mechanization.

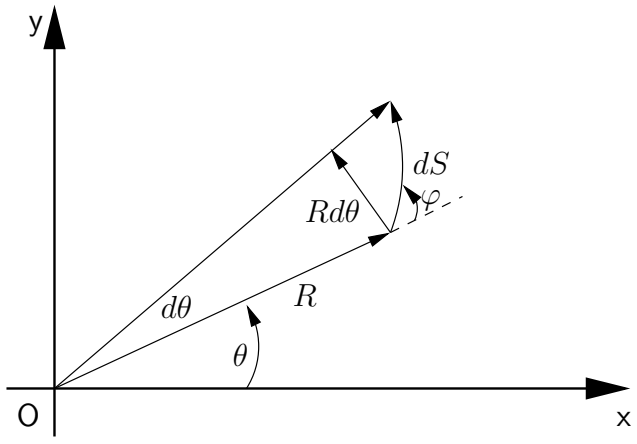

Figure 3.8 Angles of a Small Increment of θ

Consider Fig. 3.8, where we travel along a small increment, $d\theta$, of the trajectory. We can write

$$\begin{aligned} \sin\varphi &= \frac{R\, d\theta}{dS} \\ &= \frac{R}{\sqrt{\dot{R}^2 + R^2}} \end{aligned} \tag{3.26}$$

We now substitute Eq. (3.8) into Eq. (3.26) to obtain

$$\sin\varphi = C\, R^3 \tag{3.27}$$

where the constant C is given by Eq. (3.15). Substituting Eq. (3.10) into Eq. (3.27) yields

$$\sin\varphi = \sin(3\theta + \phi)$$

Thus, we have obtained a useful expression for the optimal heading angle,

$$\varphi^*(\theta) = 3\theta + \phi \tag{3.28}$$

Remark 3.4.1. *The constant ϕ, which depends only upon the problem parameters $\frac{R_f}{R_o}$ and θ_f and is specified in Eq.* (3.5)*, is the angle of departure, φ_d.*

Proof. The angle of departure is given under the condition $\theta = 0$. Thus, Eq. (3.28) becomes

$$\varphi_d = \varphi^*(0) = \phi \tag{3.29}$$

□

Likewise the angle of arrival, φ_a, is given under the condition $\theta = \theta_f$, thus

$$\varphi_a = \varphi^*(\theta_f) = 3\theta_f + \phi \tag{3.30}$$

It is interesting to revisit the plot of ϕ vs. θ_f, given in Fig. 3.6, for the symmetric special case where $R_f = R_o$. As the final angle θ_f approaches zero, the distance between

R_o and R_f becomes small and the optimal trajectory approaches a straight line. Thus, the angle of departure, or ϕ as depicted in Fig. 3.6, approaches 90°. Similarly, as θ_f approaches 60°, the path length of the extremal approaches infinity and thus the departure angle is shallow and approaches zero.

3.5 Solution Triangle

In this section we derive an alternate form of the extremal path formula and present a graphical interpretation of the relationship between the angles ϕ, θ_f and ψ. Assume a properly unimodal trajectory, viz., $3\theta_f+\phi \geq \frac{\pi}{2}$, and recall the optimal trajectory, Eq. (3.4), written here as

$$R^*(\theta) = R_o \sqrt[3]{\frac{\sin(3\theta+\phi)}{\sin\phi}} \tag{3.31}$$

over the interval $0 < \theta \leq \bar{\theta}$, where $R^*(\theta)$ is monotonically increasing, and which we know extends in reality to the domain $\bar{\theta} \leq \theta \leq \theta_f$.

Consider the interval $\bar{\theta} \leq \theta \leq \theta_f$, and take the point of view that the aircraft flies from point B toward point A until the maximal range from the radar is reached. The latter is larger than R_f and thus Eq. (3.31) applies

$$R^*(\theta) = R_f \sqrt[3]{\frac{\sin(3(\theta_f-\theta)+\psi)}{\sin\psi}}, \text{ for } \bar{\theta} \leq \theta \leq \theta_f \tag{3.32}$$

for some $\psi > 0$.

Obviously, for $\theta = \bar{\theta}$, Eq. (3.31) yields

$$\begin{aligned} R^*(\bar{\theta}) &= R_o \sqrt[3]{\frac{\sin(3\bar{\theta}+\phi)}{\sin\phi}} \\ &= R_o \frac{1}{\sqrt[3]{\sin\phi}} \end{aligned}$$

Similarly, Eq. (3.32) yields

$$R^*(\bar{\theta}) = R_f \sqrt[3]{\frac{\sin(3(\theta_f - \bar{\theta}) + \psi)}{\sin\psi}}$$
$$= R_f \frac{1}{\sqrt[3]{\sin\psi}}$$

Therefore

$$\frac{{R_o}^3}{\sin\phi} = \frac{{R_f}^3}{\sin\psi} \tag{3.33}$$

Moreover,

$$3\bar{\theta} + \phi = \frac{\pi}{2} \tag{3.34}$$

and

$$3(\theta_f - \bar{\theta}) + \psi = \frac{\pi}{2} \tag{3.35}$$

Combining Eqs. (3.34) and (3.35) yields

$$\phi + \psi + 3\theta_f = \pi \tag{3.36}$$

Hence, Eqs. (3.33) and (3.36) imply, in accordance with the "law of sines", that the angles ϕ and ψ are the angles of the triangle shown in Fig. 3.9.

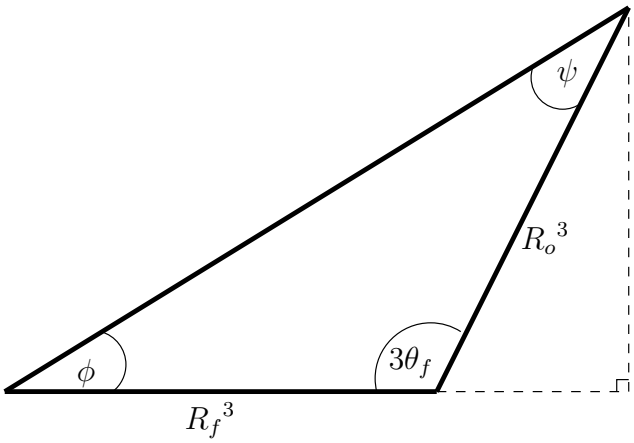

Figure 3.9 Solution Triangle

The "solution triangle" is determined by its sides ${R_o}^3$ and ${R_f}^3$ and the included angle $3\theta_f$. Consider the solution triangle in Fig. 3.9. We see that indeed,

$$\tan\phi = \frac{\sin 3\theta_f}{\left(\frac{R_f}{R_o}\right)^3 - \cos 3\theta_f} \tag{3.37}$$

$$\sin\phi = \frac{{R_o}^3 \sin 3\theta_f}{\sqrt{{R_o}^6 + {R_f}^6 - 2{R_o}^3{R_f}^3 \cos 3\theta_f}} \tag{3.38}$$

$$\cos\phi = \frac{{R_f}^3 - {R_o}^3 \cos 3\theta_f}{\sqrt{{R_o}^6 + {R_f}^6 - 2{R_o}^3{R_f}^3 \cos 3\theta_f}} \tag{3.39}$$

Similarly,

$$\tan\psi = \frac{\sin 3\theta_f}{\left(\frac{R_o}{R_f}\right)^3 - \cos 3\theta_f}$$

Clearly, in the symmetric case, viz., $R_o = R_f$, the solution triangle is isosceles and the angles ϕ and ψ are equal.

Remark 3.5.1. *The angle ψ is related to the angle of arrival, φ_a. Specifically,*

$$\varphi_a = \pi - \psi$$

Proof. The angle of arrival is given in Eq. (3.30) as $\varphi_a = 3\theta_f + \phi$. Substituting φ_a into Eq. (3.36) yields the result. □

Using Eq. (3.36), we can express Eq. (3.32) as

$$\begin{aligned} R^*(\theta) &= R_f \sqrt[3]{\frac{\sin(3(\theta_f - \theta) + \psi)}{\sin\psi}} \\ &= R_f \sqrt[3]{\frac{\sin(\pi - \phi - 3\theta)}{\sin(\pi - 3\theta_f - \phi)}} \\ &= R_f \sqrt[3]{\frac{\sin(3\theta + \phi)}{\sin(3\theta_f + \phi)}} \end{aligned} \tag{3.40}$$

Comparing the expression for the optimal trajectory obtained in Eq. (3.40) with the form in Eq. (3.4), we notice that the constant terms in Eq. (3.4) involve a parameterization in

the initial range, R_o, and the angle of departure, $\varphi_d = \phi$. Similarly, the constant terms in Eq. (3.40) involve a parameterization in the final range, R_f, and the angle of arrival, φ_a.

Remark 3.5.2. *Eq.* (3.40) *holds for the complete range of* θ*, viz.,* $0 < \theta \leq \theta_f$*, for all admissible* R_o *and* R_f*, and for the case where* $3\theta_f + \phi < \frac{\pi}{2}$*. Hence, we obtain an alternate expression Eq.* (3.40) *for the optimal trajectory.*

Proof. Recall the optimal trajectory, Eq. (3.4), is of the form

$$R^*(\theta) = \frac{1}{\sqrt[3]{C}} \sqrt[3]{\sin(3\,\theta + \phi)}$$

holds for the complete range of θ. Since $R(\theta_f) = R_f$, we have

$$R^*(\theta_f) = R_f = \frac{1}{\sqrt[3]{C}} \sqrt[3]{\sin(3\,\theta_f + \phi)}$$

Solving for C yields

$$C = \frac{\sin(3\,\theta_f + \phi)}{{R_f}^3}$$

Thus,

$$R^*(\theta) = R_f \sqrt[3]{\frac{\sin(3\theta + \phi)}{\sin(3\theta_f + \phi)}} \tag{3.41}$$

□

Remark 3.5.3. *An alternate expression for the optimal cost,* J^**, given in Eq. (3.20), is*

$$J^* = \frac{1}{3{R_o}^3{R_f}^3} \sqrt{{R_o}^6 + {R_f}^6 - 2{R_o}^3{R_f}^3 \cos 3\theta_f} \tag{3.42}$$

Proof. Recall the trigonometric identity

$$\sin(3\theta_f + \phi) = \sin 3\theta_f \cos\phi + \cos 3\theta_f \sin\phi$$

Substituting Eqs. (3.38) and (3.39) yields

$$\sin(3\theta_f + \phi) = \frac{{R_f}^3 \sin 3\theta_f}{\sqrt{{R_o}^6 + {R_f}^6 - 2{R_o}^3{R_f}^3 \cos 3\theta_f}} \tag{3.43}$$

Thus, substituting Eq. (3.43) into the optimal cost, Eq. (3.20) results in

$$J^* = \frac{1}{3{R_o}^3{R_f}^3}\sqrt{{R_o}^6 + {R_f}^6 - 2{R_o}^3{R_f}^3 \cos 3\theta_f}$$

□

We can also express the optimal cost from Eq. (3.42) as

$$3{R_o}^3{R_f}^3 J^* = \sqrt{{R_o}^6 + {R_f}^6 - 2{R_o}^3{R_f}^3 \cos 3\theta_f}$$

where we see that the right hand side is now the distance between the two lines having lengths ${R_o}^3$ and ${R_f}^3$ separated by the angle $3\theta_f$. Thus, one can visualize the relationship between the geometry of a radar problem and its cost - see, e.g., Fig 3.10.

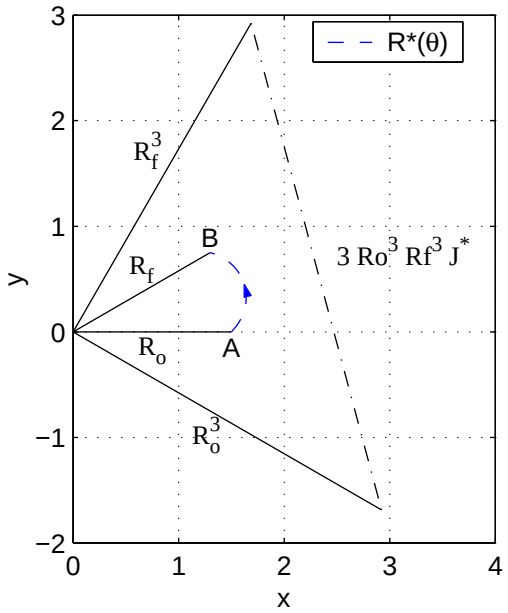

Figure 3.10 Graphical Representation of the Optimal Cost $3{R_o}^3{R_f}^3$ for the Case $R_o = R_f = 1.5$ and $\theta_f = 30°$

Recall that when $\theta_f = 0$, the optimal trajectory is the line segment AB. The cost of this line segment can be obtained from Eq. (3.42) by letting $\theta_f = 0$, see, e.g., Fig. 3.11. We see that the optimal (minimal) cost for a straight line trajectory is given by

$$J^* = \frac{1}{3}\left(\frac{1}{{R_o}^3} - \frac{1}{{R_f}^3}\right) \tag{3.44}$$

When $\theta_f \to 60°$, the path length approaches infinity and the cost is given by

$$J^* \to \frac{1}{3}\left(\frac{1}{{R_o}^3} + \frac{1}{{R_f}^3}\right) \tag{3.45}$$

Letting $\theta_f = \pi/3$, we find the cost for a trajectory of infinite length. This trajectory is the "go-around" trajectory, in which the air vehicle attempts to minimize it's exposure to the radar by beginning at the point A and running straight to infinity, then returning from infinity in a straight line to the point B, see, e.g., Fig. 3.12. We have the following:

Remark 3.6.1. *The cost of the"go around" trajectory has the same value as the cost function for* $\pi \geq \theta_f \geq \frac{\pi}{3}$*, i.e., Eq.* (3.45)*.*

Proof. From Eq. (3.44), evidently, the cost of progressing along a straight line from the point A to ∞ is

$$J_A^\infty = J_\infty^A = \frac{1}{3\,{R_o}^3}$$

and similarly from ∞ to the point B

$$J_B^\infty = J_\infty^B = \frac{1}{3\,{R_f}^3}$$

See, e.g., Fig. 3.11 and Fig. 3.12. □

Remark 3.6.2. *The optimal trajectory,* $R^*(\theta)$*, in Eq.* (3.4) *always has a lower cost than the "go around" trajectory, for* $0 < \theta_f < 60°$*.*

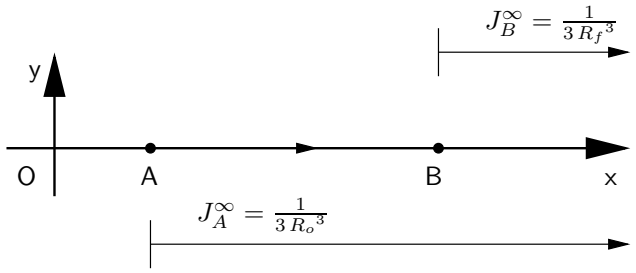

Figure 3.11 Cost for a Straight Line Trajectory, $\theta_f = 0$

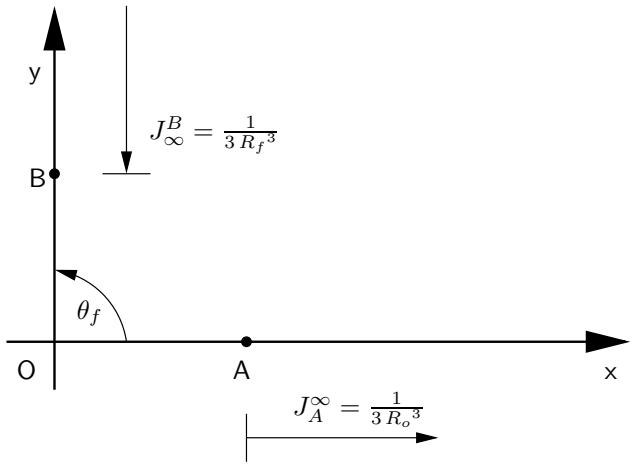

Figure 3.12 Cost for a Trajectory $\theta_f \geq 60°$

Proof. In Appendix A, the extremal trajectory is shown to be a local minimum. The "go-around" trajectory, has a cost given in Eq. (3.45). For all $\theta_f \in (0, \pi/3)$,

$$\frac{1}{3}\left(\frac{1}{{R_o}^3} + \frac{1}{{R_f}^3}\right) > \frac{1}{3{R_o}^3{R_f}^3}\sqrt{{R_o}^6 + {R_f}^6 - 2{R_o}^3{R_f}^3\cos 3\theta_f}$$

Thus, the cost of the extremal trajectory is less than the "go-around" trajectory. □

Proposition 3.6.1. *The optimal trajectory, $R^*(\theta)$, in Eq. (3.4), is globally optimal.*

Proof. The optimal trajectory $R^*(\theta)$ is a unique solution of the Euler equation. There are no constraints imposed on the solution. There are no other trajectories satisfying the boundary conditions having a lower cost. The locally optimal solution is globally optimal. □

3.7 Maximum Range

The maximum range, $R^*_{\max}(\theta)$, attained by an air vehicle on an optimal radar avoidance trajectory is sought. We have the following:

Remark 3.7.1. *Without loss of generality, let $R_f \geq R_o$. For the optimal trajectory described in Theorem 3.3.1, the maximal range from the radar is explicitly given by*

$$R^*_{\max} = \begin{cases} R^*(\bar{\theta}) = \sqrt[3]{\frac{\sqrt{{R_f}^6 + {R_o}^6 - 2{R_f}^3{R_o}^3\cos 3\theta_f}}{\sin 3\theta_f}}\ , & \textit{for} \quad 3\theta_f + \phi > \frac{\pi}{2} \\ R_f\ , & \textit{for} \quad 3\theta_f + \phi \leq \frac{\pi}{2} \end{cases} \tag{3.46}$$

Proof. Consider the case where $3\theta_f + \phi > \frac{\pi}{2}$. The optimal trajectory is then properly unimodal. Hence,

$$\left.\frac{dR}{d\theta}\right|_{\bar{\theta}} = 0 \tag{3.47}$$

and our extremal evaluated at the point $\theta = \bar{\theta}$ is given by

$$R^*(\bar{\theta}) = \frac{R_o}{\sqrt[3]{\sin\phi}}$$

From the solution triangle, Fig. 3.9, we see

$$\sin\phi = \frac{{R_o}^3 \sin 3\theta_f}{\sqrt{{R_f}^6 + {R_o}^6 - 2{R_f}^3{R_o}^3\cos 3\theta_f}}$$

Thus

$$\begin{aligned} R^*_{\max}(\theta) = R^*(\bar{\theta}) &= R_o \sqrt[3]{\frac{\sqrt{{R_f}^6 + {R_o}^6 - 2{R_f}^3{R_o}^3\cos 3\theta_f}}{{R_o}^3 \sin 3\theta_f}} \\ &= \sqrt[3]{\frac{\sqrt{{R_f}^6 + {R_o}^6 - 2{R_f}^3{R_o}^3\cos 3\theta_f}}{\sin 3\theta_f}} \end{aligned}$$

Now consider the case where $3\theta_f + \phi \leq \frac{\pi}{2}$. In this case the trajectory $R^*(\theta)$ is entirely monotonic (increasing) and the condition $\left.\frac{dR}{d\theta}\right|_{\bar{\theta}} = 0$ does not occur. In this case, the maximal range is achieved at $R(\theta_f) = R_f$. □

Normalizing the expression for $R^*(\bar{\theta})$ we obtain

$$\frac{R^*(\bar{\theta})}{R_o} = \sqrt[3]{\frac{\sqrt{\left(\frac{{R_f}^6}{{R_o}^6}\right) + 1 - 2\left(\frac{{R_f}^3}{{R_o}^3}\right)\cos 3\theta_f}}{\sin 3\theta_f}} \tag{3.48}$$

Remark 3.7.2. *For the symmetric special case, the inequality $3\theta_f + \phi > \frac{\pi}{2}$ holds for all $R_o = R_f > 0$ and for all $\theta_f \in (0, \frac{\pi}{3})$. Hence, for the special case where $R_f = R_o$, the optimal trajectory described in Theorem 3.3.1 is always properly unimodal.*

Proof. Recall Eq. (3.24) which was developed for the symmetric special case $R_o = R_f$,

$$\phi = \frac{\pi}{2} - \frac{3\theta_f}{2}$$

Thus, we can write

$$\begin{aligned} 3\theta_f + \phi &= 3\theta_f + \frac{\pi}{2} - \frac{3\theta_f}{2} \\ &= \frac{3\theta_f}{2} + \frac{\pi}{2} \\ &> \frac{\pi}{2}, \quad \text{for any admissible } \theta_f \end{aligned}$$

□

Therefore, for the symmetric case $R_o = R_f$, we can write Eq. (3.48) as

$$\frac{R^*_{\max}}{R_o} = \frac{R^*(\bar{\theta})}{R_o} = \sqrt[3]{\frac{\sqrt{2}\sqrt{(1-\cos 3\theta_f)}}{\sin 3\theta_f}}, \quad 0 < \theta_f \leq \frac{\pi}{3} \tag{3.49}$$

Table 3.2 shows Eq. (3.49) evaluated at several interesting values of θ_f when $R_o = R_f$. A plot of the maximal distance from the radar, $R^*_{\max}$, is shown as a function of θ_f for the cases $\frac{R_f}{R_o} = 1, 2, 3, 4$.

3.8 Path Length Calculation

Accurate calculations for the path length of the optimal trajectory are desired. In this section, we show that the optimal path length, l^*, can be expressed as function of

Table 3.2 $R^*_{\max}/R_o$ for Interesting Values of θ_f when $R_o = R_f = 1$

θ_f	$R^*_{\max}/R_o$
$0^{\circ +}$	1
10°	$\sqrt[3]{2}\left(2-\sqrt{3}\right)^{\frac{1}{6}}$
15°	$\left(4-2\sqrt{2}\right)^{\frac{1}{6}}$
20°	$\sqrt[3]{\frac{2}{\sqrt{3}}}$
30°	$2^{\frac{1}{6}}$
45°	$\left(2\left(2+\sqrt{2}\right)\right)^{\frac{1}{6}}$
60°	∞

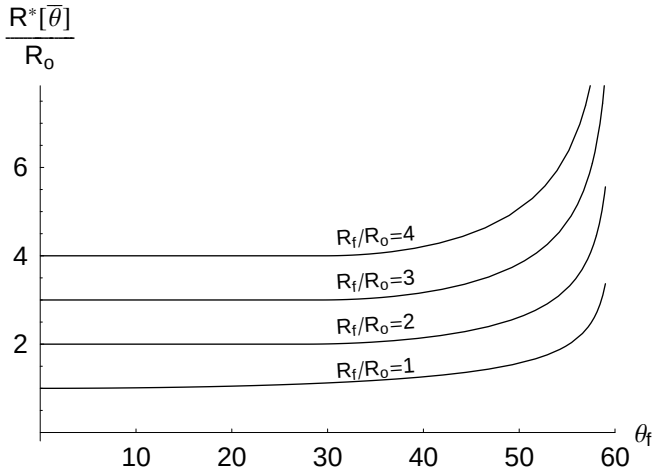

Figure 3.13 $R^*_{\max}/R_o$ as a Function of θ_f for the Cases $\frac{R_f}{R_o} = 1, 2, 3, 4$.

elliptic integrals. While not closed form, this formulation leads to efficient and accurate calculation of path length without resorting to numerical integration.

Consider the parametric equations for an elliptic arc, given by

$$x = a\cos\theta$$

$$y = b\sin\theta$$

where a is the semiminor axis and b is the semimajor axis. The length of an elliptic arc is given by

$$\begin{aligned} l &= \int_0^\gamma \sqrt{\dot{x}^2 + \dot{y}^2}\, d\theta \\ &= \int_0^\gamma \sqrt{a^2 \cos^2\theta + b^2 \sin^2\theta}\, d\theta \\ &= b \int_0^\gamma \sqrt{1 - k^2 \sin^2\theta}\, d\theta \end{aligned} \tag{3.50}$$

where $0 \leq \theta \leq \gamma$ and k is the eccentricity of the ellipse given by

$$k = \sqrt{1 - \frac{a^2}{b^2}}$$

The integral given in Eq. (3.50) cannot be evaluated in closed form and the class of problems given by integrals of the form in Eq. (3.50) are called *elliptic integrals* [1].

Specifically, an elliptic integral of the first kind is defined as

$$F(\gamma, k) = \int_0^\gamma \frac{d\theta}{\sqrt{1 - k^2 \sin^2\theta}}, \quad 0 < k < 1, \tag{3.51}$$

and when $\gamma = \pi/2$, Eq. (3.51) is considered a complete elliptic integral of the first kind, denoted

$$K(k) = \int_0^{\pi/2} \frac{d\theta}{\sqrt{1 - k^2 \sin^2\theta}}, \quad 0 < k < 1. \tag{3.52}$$

Values of the elliptic integral functions are tabulated in mathematics references [10, 29]. Elliptic integrals can also be evaluated as function calls in popular software packages such as *Mathematica* [45] or the FORTRAN IMSL libraries [43].

We claim that the path length integral given in Eq. (3.6) as

$$l^* = \frac{R_o}{\sqrt[3]{\sin\phi}} \int_0^{\theta_f} [\sin(3\theta + \phi)]^{-\frac{2}{3}}\, d\theta.$$

is an elliptic integral. This is shown by performing a change of variables. The first transformation $\theta = \frac{1}{3}x - \phi$ yields

$$l^* = \frac{1}{3}\frac{R_o}{\sqrt[3]{\sin\phi}}\int_{\phi}^{3\theta_f+\phi}\frac{1}{\sin^{\frac{2}{3}}x}\,dx \tag{3.53}$$

For the second transformation, let $u^3 = \sin x$. Thus

$$dx = \frac{3u^2}{\cos x}du \tag{3.54}$$

and

$$u = \sqrt[3]{\sin x} \tag{3.55}$$

Substituting Eqs. (3.54) and (3.55) into Eq. (3.53) yields

$$l^* = \frac{R_o}{\sqrt[3]{\sin\phi}}\int_{\sqrt[3]{\sin\phi}}^{\sqrt[3]{\sin(3\theta_f+\phi)}}\sec x\;du \tag{3.56}$$

We use the trigonometric identities

$$a = \sin x \Rightarrow \sec x = \frac{1}{\sqrt{1-a^2}}, \quad 0 \le x < \frac{\pi}{2} \tag{3.57}$$

$$a = \sin x \Rightarrow \sec x = \frac{-1}{\sqrt{1-a^2}}, \quad \frac{\pi}{2} < x \le \pi \tag{3.58}$$

to obtain

$$\frac{l^*}{R_o} = \frac{1}{\sqrt[3]{\sin\phi}}\int_{\sqrt[3]{\sin\phi}}^{\sqrt[3]{\sin(3\theta_f+\phi)}}\frac{(-1)^N du}{\sqrt{1-u^6}} \tag{3.59}$$

where

$$N = \begin{cases} 0\,, & 0 \le 3\theta_f + \phi \le \frac{\pi}{2} \\ 1\,, & \frac{\pi}{2} < 3\theta_f + \phi \le \pi \end{cases}$$

3.8.1 Monotonically Increasing Trajectories. When $0 < 3\theta_f + \phi \le \pi/2$, we have the case of a monotonically increasing trajectory, viz., $R^*_{\max} = R_f$. An example is shown in Fig. 3.14, where we plot the extremal $R^*(\theta)$ for $R_f/R_o = 10$, and $\theta_f = 20^\circ$.

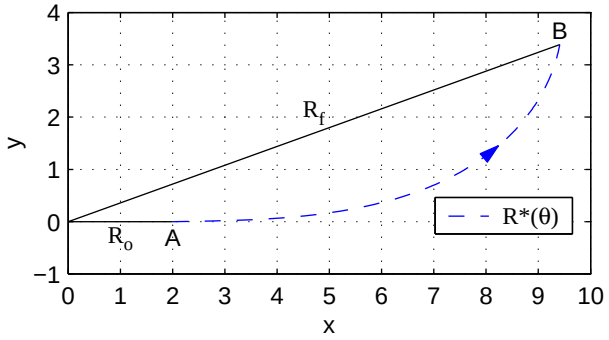

Figure 3.14 Monotonically Increasing Extremal for the Case $R_f/R_o = 10$ and $\theta_f = 20°$

The path length integral, Eq. (3.59), for a monotonically increasing trajectory can be written as

$$\frac{l^*}{R_o} = \frac{1}{\sqrt[3]{\sin\phi}} \left(\int_0^{\sqrt[3]{\sin(3\theta_f+\phi)}} \frac{du}{\sqrt{1-u^6}} - \int_0^{\sqrt[3]{\sin\phi}} \frac{du}{\sqrt{1-u^6}} \right) \tag{3.60}$$

From [10], the following useful relation can be found in a table of elliptic integrals of the first kind,

$$\int_0^Y \frac{d\tau}{\sqrt{1-\tau^6}} = \frac{1}{2\sqrt[4]{3}} F(\psi, k)$$

where

$$k^2 = \frac{2-\sqrt{3}}{4}$$

$$\psi = \text{Arccos}\left(\frac{1-(1+\sqrt{3})Y^2}{1+(\sqrt{3}-1)Y^2} \right)$$

Thus, we recognize Eq. (3.60) as the difference of two elliptic integrals of the first kind which has a solution of the form

$$\frac{l^*}{R_o} = \frac{1}{2\sqrt[4]{3}} \frac{1}{\sqrt[3]{\sin\phi}} \left[F(\psi_1, k) - F(\psi_2, k) \right]$$

where the parameters

$$k^2 = \frac{2-\sqrt{3}}{4} \tag{3.61}$$

$$\psi_1 = \text{Arccos}\left(\frac{1-(1+\sqrt{3})\left[\sin(3\theta_f+\phi)\right]^{2/3}}{1+(\sqrt{3}-1)\left[\sin(3\theta_f+\phi)\right]^{2/3}}\right) \tag{3.62}$$

$$\psi_2 = \text{Arccos}\left(\frac{1-(1+\sqrt{3})\left[\sin\phi\right]^{2/3}}{1+(\sqrt{3}-1)\left[\sin\phi\right]^{2/3}}\right) \tag{3.63}$$

For our example shown in Fig. 3.14, where $R_o = 1$, $R_f = 10$, and $\theta_f = 20°$, we compute $\frac{l^*}{R_o}$ using

$$\sin\phi = \frac{1}{2}\sqrt{\frac{3}{999001}} = 0.000866458$$

$$\psi_1 = \text{Arccos}\left(\frac{1-50\sqrt[3]{\frac{6}{999001}}\left(1+\sqrt{3}\right)}{1+50\sqrt[3]{\frac{6}{999001}}\left(\sqrt{3}-1\right)}\right) = 2.66935 \text{ rad}$$

$$\psi_2 = \text{Arccos}\left(\frac{2^{\frac{2}{3}}-\sqrt[3]{\frac{3}{999001}}\left(1+\sqrt{3}\right)}{2^{\frac{2}{3}}+\sqrt[3]{\frac{3}{999001}}\left(\sqrt{3}-1\right)}\right) = 0.25076 \text{ rad}$$

$$F(\psi_1, k) = 2.7229$$

$$F(\psi_2, k) = 0.250934$$

Thus, $\frac{l^*}{R_o} = 9.85108$.

3.8.2 Properly Unimodal Trajectories. Now consider evaluating the path length extremal when $\pi/2 < 3\theta_f + \phi \leq \pi$, i.e., the case of a properly unimodal extremal. In Sec. 3.7, we showed that $3\theta_f + \phi$ is always greater than $\pi/2$ for the symmetric case. An example of a properly unimodal trajectory is given in Fig. 3.7, which depicts the symmetric case where $R_f/R_o = 1$, and $\theta_f = 45°$.

The path length integral expressed in Eq. (3.59), can be rewritten as

$$\begin{aligned}
\frac{l^*}{R_o} &= \frac{1}{\sqrt[3]{\sin\phi}}\left(\int_{\sqrt[3]{\sin\frac{\pi}{2}}}^{\sqrt[3]{\sin(3\theta_f+\phi)}} \frac{-du}{\sqrt{1-u^6}} + \int_{\sqrt[3]{\sin\phi}}^{\sqrt[3]{\sin\frac{\pi}{2}}} \frac{du}{\sqrt{1-u^6}}\right) \\
&= \frac{1}{\sqrt[3]{\sin\phi}}\left(-\int_0^{\sqrt[3]{\sin(3\theta_f+\phi)}} \frac{du}{\sqrt{1-u^6}} + \int_0^{\sqrt[3]{\sin\frac{\pi}{2}}} \frac{du}{\sqrt{1-u^6}}\right. \\
&\left. + \int_0^{\sqrt[3]{\sin\frac{\pi}{2}}} \frac{du}{\sqrt{1-u^6}} - \int_0^{\sqrt[3]{\sin\phi}} \frac{du}{\sqrt{1-u^6}}\right) \\
&= \frac{1}{\sqrt[3]{\sin\phi}}\left(2\int_0^1 \frac{du}{\sqrt{1-u^6}} - \int_0^{\sqrt[3]{\sin(3\theta_f+\phi)}} \frac{du}{\sqrt{1-u^6}} - \int_0^{\sqrt[3]{\sin\phi}} \frac{du}{\sqrt{1-u^6}}\right) \qquad (3.64)
\end{aligned}$$

From [10] we recognize Eq. (3.64) as the difference of three elliptic integrals of the first kind and has a solution of the form

$$\frac{l^*}{R_o} = \frac{1}{2\sqrt[4]{3}}\frac{1}{\sqrt[3]{\sin\phi}}\left[2F(\psi_3,k) - F(\psi_1,k) - F(\psi_2,k)\right] \qquad (3.65)$$

where k, ψ_1 and ψ_2 are given in Eqs. (3.61)-(3.63) and

$$\begin{aligned}
\psi_3 &= \text{Arccos}\left(\frac{1-(1+\sqrt{3})\left[\sin(\pi/2)\right]^{2/3}}{1+(\sqrt{3}-1)\left[\sin(\pi/2)\right]^{2/3}}\right) \\
&= \pi \qquad (3.66)
\end{aligned}$$

Using some fundamental relations of elliptic integrals [10], namely

$$\begin{aligned}
F(m\pi \pm \gamma, k) &= 2mK(k) \pm F(\gamma,k) \\
F(0,k) &= 0
\end{aligned}$$

we recognize

$$\begin{aligned}
F(\psi_3,k) &= F(\pi,k) \\
&= 2K(k)
\end{aligned}$$

Thus, we can write Eq. (3.65) as

$$\frac{l^*}{R_o} = \frac{1}{2\sqrt[4]{3}} \frac{1}{\sqrt[3]{\sin\phi}} \left[4K(k) - F(\psi_1, k) - F(\psi_2, k)\right] \tag{3.67}$$

Remark 3.8.1. *For all symmetric cases when $R_f = R_o$,*

$$\sin\phi = \sin\left(3\theta_f + \phi\right) \tag{3.68}$$

Furthermore, the angle of departure is related to the angle of arrival by

$$\varphi_d = \pi - \varphi_a$$

Proof. Using Eq. (3.24),

$$\begin{aligned}
\sin\phi &= \sin\left(\frac{\pi}{2} - \frac{3\theta_f}{2}\right) \\
&= \sin\left(\frac{3\theta_f}{2} + \frac{\pi}{2}\right) \\
&= \sin\left(3\theta_f + \phi\right)
\end{aligned}$$

Similarly,

$$\begin{aligned}
\pi - \varphi_a &= \pi - (3\theta_f + \phi) \\
&= \pi - (3\theta_f + \frac{\pi}{2} - \frac{3\theta_f}{2}) \\
&= \frac{\pi}{2} - \frac{3\theta_f}{2} \\
&= \phi \\
&= \varphi_d
\end{aligned}$$

□

For our example shown in Fig. 3.7, where $R_f/R_o = 1$, and $\theta_f = 45^\circ$, we show how to compute the path length, $\frac{l^*}{R_o}$. Using Eq. (3.68) we see that $\psi_1 = \psi_2$ and

$$\begin{aligned}
\sin\phi &= \frac{1}{\sqrt{4+2\sqrt{2}}} = 0.382683 \\
\psi_1 = \psi_2 &= \text{Arccos}\left(\frac{1-\left(1+\sqrt{3}\right)\left(4+2\sqrt{2}\right)^{-1/2}}{1+\left(\sqrt{3}-1\right)\left(4+2\sqrt{2}\right)^{-1/2}}\right) = 1.89393 \text{ rad} \\
\psi_3 &= \pi \\
K(k) &= 1.59814 \\
F(\psi_1,k) = F(\psi_2,k) &= 1.93226
\end{aligned}$$

Thus, $\frac{l^*}{R_o} = 1.3229$.

3.8.3 General Result. We have the following:

Remark 3.8.2. *The optimal path length, l^*, for the trajectory minimizing the exposure to a monostatic radar given in Theorem 3.3.1, formulated using the Legendre form of the elliptic integrals is*

$$l^* = \begin{cases} \frac{R_o}{2\sqrt[4]{3}} \frac{1}{\sqrt[3]{\sin\phi}} \left[4K(k) - F(\psi_1,k) - F(\psi_2,k)\right], & 3\theta_f + \phi > \frac{\pi}{2} \\ \frac{R_o}{2\sqrt[4]{3}} \frac{1}{\sqrt[3]{\sin\phi}} \left[F(\psi_1,k) - F(\psi_2,k)\right], & 3\theta_f + \phi \leq \frac{\pi}{2} \end{cases}$$

where

$$\begin{aligned}
k &= \sqrt{\frac{2-\sqrt{3}}{4}} \\
\psi_1 &= \text{Arccos}\left(\frac{1-(1+\sqrt{3})\left[\sin(3\theta_f+\phi)\right]^{2/3}}{1+(\sqrt{3}-1)\left[\sin(3\theta_f+\phi)\right]^{2/3}}\right) \\
\psi_2 &= \text{Arccos}\left(\frac{1-(1+\sqrt{3})\left[\sin\phi\right]^{2/3}}{1+(\sqrt{3}-1)\left[\sin\phi\right]^{2/3}}\right)
\end{aligned}$$

□

Fig. 3.15 demonstrates how the length of the extremal aircraft trajectory l^* varies with increasing θ_f; the path lengths of optimal trajectories are plotted for $R_f/R_o = 1, 2, 3, 4$

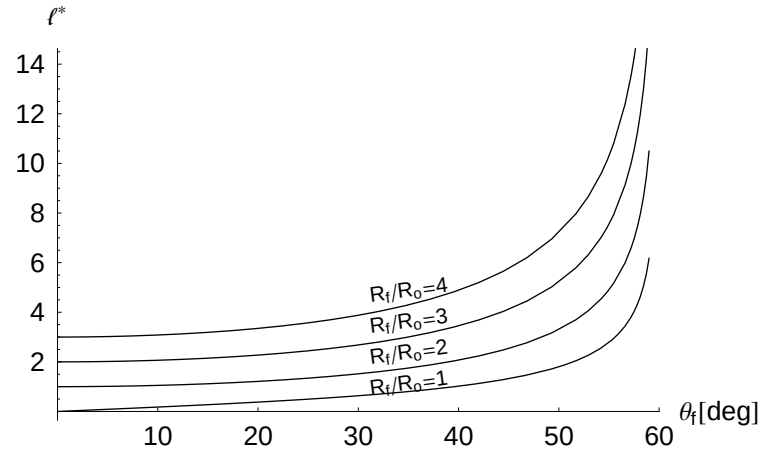

Figure 3.15 $l^*\left(\theta_f, \frac{R_f}{R_o}\right)$ for the Cases where $R_f/R_o = 1, 2, 3, 4$

and $\theta_f \in [0, 59^\circ]$. In Fig. 3.15, $l^*\left(\theta_f, \frac{R_f}{R_o}\right)$ is plotted and the asymptotic behavior of the path length, viz., $l^* \to \infty$ as $\theta_f \to 60^\circ$ is evident.

3.9 Summary

In this chapter, the radar exposure minimization problem was posed in the Calculus of Variations and a closed form, globally optimal, solution was presented. The solution was shown to exist if the final angle included between the endpoints of the trajectory, $\theta_f < 60^\circ$. The solution was shown to be related to the class of 3-leaved rose functions. An optimal heading angle control law was determined from the closed form solution. Alternative forms of the solution were presented via construction of a geometric tool, i.e., a solution triangle. An analytic expression for the optimal cost was obtained and is shown to approach a finite value as $\theta_f \to \infty$. Finally, the optimal path length was derived in terms of elliptic integral functions and the asymptotic behavior of the path length, viz., $l^* \to \infty$ as $\theta_f \to 60^\circ$, was demonstrated.

In the next chapter, a similar analysis will be performed for the case of minimizing exposure to a passive sensor. Closed form expressions are sought. In particular, the relationship between the solutions of the passive sensor and radar exposure minimization problems is revealed. Lastly, the path length constrained problem is posed for the passive sensor problem and the solution is shown to be a function of an elliptic integral.

IV. Minimizing Exposure to a Passive Sensor

4.1 Introduction

The problem minimizing the energy received by a passive sensor or emitter, e.g., an IR sensor or RF jammer, is formulated. In the following sections, a closed form solution to the passive sensor problem will be sought, as well as solutions for the optimal path length and optimal cost. A comparison will be made between the structure of the solution of the passive sensor problem and the solution of the radar exposure minimization problem presented in Chapter III. Finally, the path length constrained problem is addressed.

4.2 Unconstrained Analytic Solution

For a passive sensor, the received energy is inversely proportional to R^2. Hence, we obtain the variational problem

$$J[R(\theta)] = \int_0^{\theta_f} \frac{\sqrt{\dot{R}^2 + R^2}}{R^2}\, d\theta \tag{4.1}$$

with the familiar boundary conditions

$$R(0) = R_o \tag{4.2}$$

$$R(\theta_f) = R_f, \quad 0 < \theta \leq \theta_f \tag{4.3}$$

Without loss of generality, assume $R_f \geq R_o$ and $0 < \theta_f \leq \pi$. Polar coordinates are used. We have the following:

Theorem 4.2.1. *The optimal trajectory which connects points A and B at a distance R_o and R_f from the passive RF sensor located at the origin O, where θ_f is the angle $\angle AOB$, and minimizes the exposure to the RF sensor according to Eqs. (4.1)-(4.3), is*

$$R(\theta) = R_o \cos\theta + \frac{R_f - R_o \cos\theta_f}{\sin\theta_f} \sin\theta, \quad 0 < \theta_f < \pi \tag{4.4}$$

This trajectory is the arc AB of the circle which circumscribes $\triangle OAB$.

Proof. A candidate extremal which minimizes the cost functional (4.1), can be found by solving the differential equation that results from the Euler equation

$$F_R - \frac{d}{d\theta} F_{\dot{R}} = 0 \tag{4.5}$$

where F is the integrand of the cost functional, Eq. (4.1), i.e.,

$$F = \frac{\sqrt{\dot{R}^2 + R^2}}{R^2}$$

and we have the derivatives

$$F_R = \frac{-R(\theta)^2 - 2\,\dot{R}(\theta)^2}{R(\theta)^3 \sqrt{R(\theta)^2 + \dot{R}(\theta)^2}} \tag{4.6}$$

$$F_{\dot{R}} = \frac{\dot{R}(\theta)}{R(\theta)^2 \sqrt{R(\theta)^2 + \dot{R}(\theta)^2}}$$

$$\frac{d}{d\theta} F_{\dot{R}} = \frac{-3\,R(\theta)^2\,\dot{R}(\theta)^2 - 2\,\dot{R}(\theta)^4 + R(\theta)^3\,\ddot{R}(\theta)}{R(\theta)^3 \left(R(\theta)^2 + \dot{R}(\theta)^2\right)^{\frac{3}{2}}} \tag{4.7}$$

Substituting Eqs. (4.6) and (4.7) into the Euler equation (4.5) yields

$$\frac{-R(\theta) - \ddot{R}(\theta)}{\left(R(\theta)^2 + \dot{R}(\theta)^2\right)^{\frac{3}{2}}} = 0$$

which simplifies to

$$\ddot{R}(\theta) + R(\theta) = 0$$

Thus, we have obtained a second order, homogeneous, linear differential equation, which has the solution

$$R(\theta) = C_1 \cos\theta + C_2 \sin\theta \tag{4.8}$$

Applying the boundary conditions (4.2) and (4.2) we obtain

$$C_1 = R_o \tag{4.9}$$

$$C_2 = \frac{R_f - R_o \cos\theta_f}{\sin\theta_f} \tag{4.10}$$

Thus our candidate extremal is

$$R(\theta) = R_o \cos\theta + \frac{R_f - R_o \cos\theta_f}{\sin\theta_f} \sin\theta$$

Recall the equation of a circle passing through the origin in polar coordinates, given by

$$r = a\cos\theta + b\sin\theta \tag{4.11}$$

where a is the x-axis intercept and b is the y-axis intercept. We recognize Eq. (4.4) as a circle in the form of Eq. (4.11). The circle can be inscribed by a triangle, consisting of three points, given in Cartesian coordinates as:

$(x_1, y_1) = (0, 0)\,,$	the origin
$(x_2, y_2) = (R_o, 0)\,,$	the x-axis intercept and the point A
$(x_3, y_3) = (R_f \cos\theta_f, R_f \sin\theta_f)\,,$	the point B

□

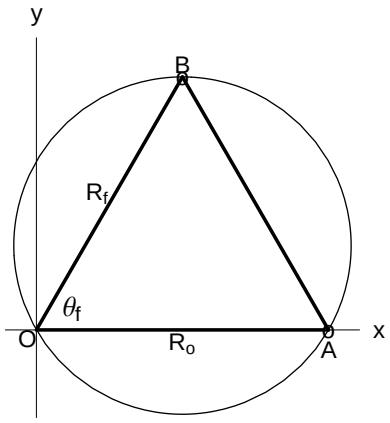

Figure 4.1 Triangle Inscribing the Circle Suggested by the Optimal Trajectory

The circle inscribing the triangle $\triangle OAB$ is depicted in Fig. 4.1. The center and radius of this circle can be identified by assigning coefficients to the quadratic curve [44]

$$ax^2 + cy^2 + dx + ey + f = 0$$

where

$$\begin{aligned}
c = a &= \begin{vmatrix} x_1 & y_1 & 1 \\ x_2 & y_2 & 1 \\ x_3 & y_3 & 1 \end{vmatrix} \\
&= R_o R_f \sin\theta_f \\
d &= -\begin{vmatrix} {x_1}^2 + {y_1}^2 & y_1 & 1 \\ {x_2}^2 + {y_2}^2 & y_2 & 1 \\ {x_3}^2 + {y_3}^2 & y_3 & 1 \end{vmatrix} \\
&= -R_f {R_o}^2 \sin\theta_f \\
e &= -\begin{vmatrix} {x_1}^2 + {y_1}^2 & x_1 & 1 \\ {x_2}^2 + {y_2}^2 & x_2 & 1 \\ {x_3}^2 + {y_3}^2 & x_3 & 1 \end{vmatrix} \\
&= R_o R_f \left(R_o \cos\theta_f - R_f\right) \\
f &= -\begin{vmatrix} {x_1}^2 + {y_1}^2 & x_1 & y_1 \\ {x_2}^2 + {y_2}^2 & x_2 & y_2 \\ {x_3}^2 + {y_3}^2 & x_3 & y_3 \end{vmatrix} \\
&= 0
\end{aligned}$$

Remark 4.2.1. *For the optimal trajectory described in Theorem 4.2.1, the circle circumscribing the triangle $\triangle OAB$ is centered at*

$$\left(\frac{R_o}{2}, \frac{R_f - R_o \cos\theta_f}{2\sin\theta_f}\right)$$

and has radius

$$r_0 = \frac{\sqrt{{R_f}^2 + {R_o}^2 - 2R_oR_f\cos\theta_f}}{2\sin\theta_f}$$

Proof. The center of the circle can be identified in Cartesian coordinates as

$$x_0 = -\frac{d}{2a} = \frac{R_o}{2}$$
$$y_0 = -\frac{e}{2a} = \frac{R_f - R_o\cos\theta_f}{2\sin\theta_f}$$

or equivalently in polar coordinates

$$r_0 = \frac{\sqrt{{R_f}^2 + {R_o}^2 - 2R_oR_f\cos\theta_f}}{2\sin\theta_f}$$
$$\theta_0 = \text{Arctan}\left(\frac{R_f - R_o\cos\theta_f}{R_o\sin\theta_f}\right)$$

Thus, the radius of the circle is given by r_0. □

The candidate extremal is defined for $0 < \theta \leq 180°$. A sample trajectory is plotted in Fig. 4.2 for the case where $R_f/R_o = 1$ and $\theta_f = 60°$. Recall that for the radar exposure minimization problem, the path length of the optimal trajectory for $\theta_f = 60°$ was infinite and for $\theta_f \geq 60°$ an optimal solution does not exist.

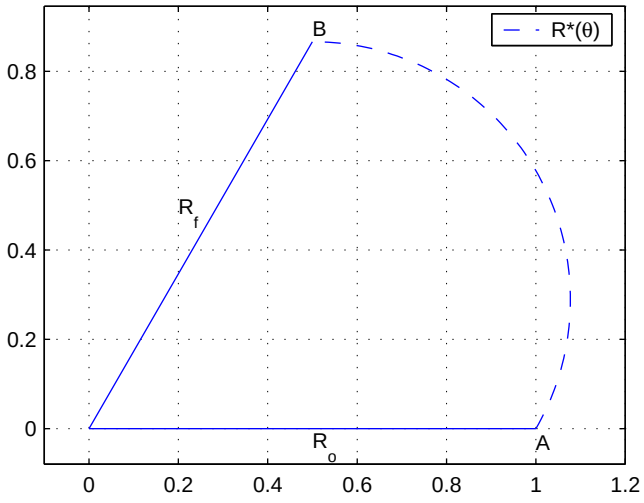

Figure 4.2 Passive Emitter Case: Extremal $R^*(\theta)$ for $R_f/R_o = 1$, $\theta_f = 60°$

Corollary 4.2.1. *The optimal trajectory which connects points A and B at a distance $R_o = R_f$ from the passive RF sensor located at the origin O, and minimizes the exposure to the RF sensor according to Eqs. (4.1)-(4.3), is*

$$R^*(\theta) = \frac{R_o}{\cos\frac{\theta_f}{2}} \cos\left(\theta - \frac{\theta_f}{2}\right) \tag{4.12}$$

Proof. When $R_o = R_f$ we can write Eq. (4.4) as

$$\begin{aligned} R^*(\theta) &= R_o \cos\theta + R_o \frac{1-\cos\theta_f}{\sin\theta_f} \sin\theta \\ &= R_o \left(\cos\theta + \tan\frac{\theta_f}{2} \sin\theta\right) \\ &= \frac{R_o}{\cos\frac{\theta_f}{2}} \left(\cos\theta\cos\frac{\theta_f}{2} + \sin\theta\sin\frac{\theta_f}{2}\right) \\ &= \frac{R_o}{\cos\frac{\theta_f}{2}} \cos\left(\theta - \frac{\theta_f}{2}\right) \end{aligned}$$

□

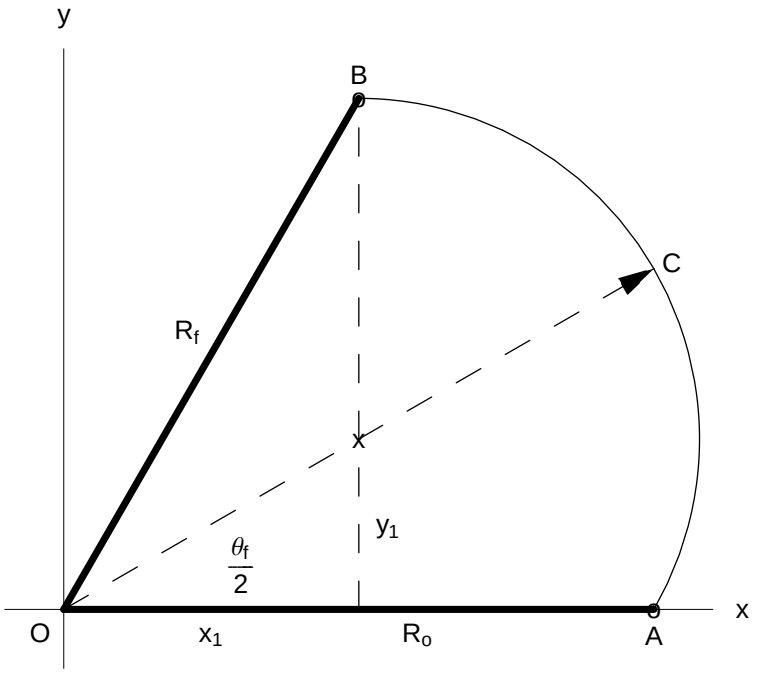

Figure 4.3 Geometric Construction for $R_o = R_f$

The center of the circle can be obtained by a geometric construction. Consider Fig. 4.3, where the angle θ_f is bisected. We know that the point C, halfway along the arc AB will be the maximum distance from the origin. Since the circle passes through the origin, the distance OC must be equal to the diameter, or twice the radius of the circle. Furthermore if OC is the diameter, then the center of the circle exists on OC. From Theorem 4.2.1, we know the center of the circle lies on the line

$$y = \frac{R_o}{2} \tag{4.13}$$

Thus the intersection of the bisector OC and the line in Eq. (4.13) is the center and is given by

$$(x_1, y_1) = \left(\frac{R_o}{2}, \frac{R_o}{2} \tan \frac{\theta_f}{2} \right)$$

Remark 4.2.2. *For the optimal trajectory described in Theorem 4.2.1, the optimal path length, viz., the length of the arc AB, is*

$$l = \theta_f \frac{\sqrt{{R_o}^2 + {R_f}^2 - 2R_o R_f \cos\theta_f}}{\sin\theta_f} \tag{4.14}$$

Proof. The path length is given by

$$l = \int_0^{\theta_f} \sqrt{\dot{R}^2(\theta) + R^2(\theta)}\, d\theta$$

where

$$\dot{R}(\theta) = -C_1 \sin\theta + C_2 \cos\theta$$

$$\dot{R}^2(\theta) = {C_1}^2 \sin^2\theta - 2C_1 C_2 \sin\theta\cos\theta + {C_2}^2 \cos^2\theta \tag{4.15}$$

$$R^2(\theta) = {C_1}^2 \cos^2\theta + 2C_1 C_2 \sin\theta\cos\theta + {C_2}^2 \sin^2\theta \tag{4.16}$$

Adding (4.15) and (4.16) and substituting into (3.17) yields

$$\begin{aligned} l &= \int_0^{\theta_f} \sqrt{{C_1}^2 + {C_2}^2}\, d\theta \\ &= \sqrt{{C_1}^2 + {C_2}^2} \int_0^{\theta_f} d\theta \\ &= \theta_f \sqrt{{C_1}^2 + {C_2}^2} \end{aligned} \tag{4.17}$$

Substituting (4.9) and (4.10) into (4.17)

$$\begin{aligned} l &= \theta_f \sqrt{{R_o}^2 + \left(\frac{R_f - R_o \cos\theta_f}{\sin\theta_f}\right)^2} \\ &= \theta_f \frac{\sqrt{{R_o}^2 + {R_f}^2 - 2R_oR_f\cos\theta_f}}{\sin\theta_f} \end{aligned}$$

we obtain the path length of the extremal. We notice that the path length is now expressed solely as a function of the boundary conditions R_f/R_o, and θ_f. □

Remark 4.2.3. *For the optimal trajectory described in Corollary 4.2.1, the path length, viz., the length of the arc AB, when $R_o = R_f$, is*

$$l = 2\, R_o\, \theta_f\, \frac{\sin\frac{\theta_f}{2}}{\sin\theta_f}$$

Proof. Let $R_o = R_f$. We can write Eq. (4.14) as

$$\begin{aligned} l &= \theta_f \frac{\sqrt{2\,{R_o}^2 - 2\,{R_o}^2\cos\theta_f}}{\sin\theta_f} \\ &= \sqrt{2}\, R_o\, \theta_f \frac{\sqrt{1-\cos\theta_f}}{\sin\theta_f} \\ &= 2\, R_o\, \theta_f\, \frac{\sin\frac{\theta_f}{2}}{\sin\theta_f} \end{aligned}$$

□

Remark 4.2.4. *For the optimal trajectory described in Theorem 4.2.1, the cost function explicitly evaluates to*

$$J = \frac{\sqrt{{R_o}^2 + {R_f}^2 - 2R_oR_f\cos\theta_f}}{R_oR_f} \tag{4.18}$$

Proof. It is also of interest to obtain a closed form expression for the cost function, given by

$$J = \int_0^{\theta_f} \frac{\sqrt{\dot{R}^2 + R^2}}{R^2}\, d\theta$$

Substituting Eqs. (4.15) and (4.16) we obtain

$$\begin{aligned} J &= \int_0^{\theta_f} \frac{\sqrt{{C_1}^2 + {C_2}^2}}{(C_1\cos\theta + C_2\sin\theta)^2}\, d\theta \\ &= \sqrt{{C_1}^2 + {C_2}^2} \int_0^{\theta_f} \frac{1}{(C_1\cos\theta + C_2\sin\theta)^2}\, d\theta \\ &= \sqrt{{C_1}^2 + {C_2}^2}\, \frac{\sin\theta}{{C_1}^2\cos\theta + C_1C_2\sin\theta}\Bigg|_0^{\theta_f} \\ &= \sqrt{{C_1}^2 + {C_2}^2}\frac{\sin\theta_f}{{C_1}^2\cos\theta_f + C_1C_2\sin\theta_f} \end{aligned} \tag{4.19}$$

Substituting (4.9) and (4.10) into (4.19)

$$\begin{aligned} J &= \sqrt{{R_o}^2 + \left(\frac{R_f - R_o\cos\theta_f}{\sin\theta_f}\right)^2}\, \frac{\sin\theta_f}{{R_o}^2\cos\theta_f + R_o\frac{R_f - R_o\cos\theta_f}{\sin\theta_f}\sin\theta_f} \\ &= \frac{\sqrt{{R_o}^2 + {R_f}^2 - 2R_oR_f\cos\theta_f}}{R_oR_f} \end{aligned}$$

□

We have obtained an expression for the cost which is only a function of the boundary conditions R_f/R_o and θ_f. This expression can be useful in comparing the cost of the optimal trajectory to sub-optimal trajectories

Remark 4.2.5. *For the optimal trajectory described in Corollary 4.2.1, i.e., when $R_o = R_f$, the cost function explicitly evaluates to*

$$J = 2\frac{\tan\frac{\theta_f}{2}}{R_o} \tag{4.20}$$

Proof. Let $R_o = R_f$. We can write Eq. (4.18) as

$$\begin{aligned} J &= \frac{\sqrt{2{R_o}^2 - 2{R_o}^2 \cos\theta_f}}{{R_o}^2} \\ &= 2\sqrt{\frac{1-\cos\theta_f}{2}}\frac{1}{R_o} \\ &= 2\frac{\tan\frac{\theta_f}{2}}{R_o} \end{aligned}$$

□

Using the expressions obtained for the path length l in Eq. (4.14) and explicit cost J in Eq. (4.20), we see that as the final angle $\theta_f \to \pi/3$, the path length $l \to \infty$. The optimal cost remains finite and approaches $\frac{2}{R_o}$; see, e.g., Fig. 4.4.

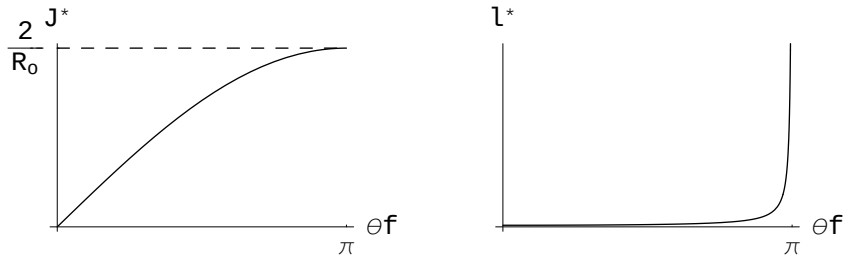

Figure 4.4 Asymptotic Behavior of the Optimal Cost and Path Length for $R_o = R_f$

4.3 Passive Sensor Maximum Range

Remark 4.3.1. *For the optimal trajectory described in Theorem 4.2.1, given by*

$$R^*(\theta) = R_o\cos\theta + \frac{R_f - R_o\cos\theta_f}{\sin\theta_f}\sin\theta$$

and without loss of generality $R_f \geq R_o$, the maximal range from the passive RF sensor is explicitly given by

$$R^*_{\max} = R^*(\bar{\theta}) = \frac{\sqrt{{R_o}^2 + {R_f}^2 - 2R_oR_f\cos\theta_f}}{\sin\theta_f} \tag{4.21}$$

Proof. Assuming the extremal is properly unimodal, the maximum range from the RF sensor achieved by the aircraft is obtained when $\frac{dR}{d\theta}|_{\bar{\theta}} = 0$. Thus,

$$\dot{R}(\bar{\theta}) = 0 = -R_o \sin\bar{\theta} + \left(\frac{R_f - R_o\cos\theta_f}{\sin\theta_f}\right)\cos\bar{\theta}$$

From which we can obtain

$$\tan\bar{\theta} = \frac{R_f - R_o\cos\theta_f}{R_o\sin\theta_f}$$

Using trigonometric identities we obtain

$$\sin\bar{\theta} = \frac{Rf - R_o\cos\theta_f}{\sqrt{{R_o}^2 + {R_f}^2 - 2R_oR_f\cos\theta_f}} \tag{4.22}$$

$$\cos\bar{\theta} = \frac{R_o\sin\theta_f}{\sqrt{{R_o}^2 + {R_f}^2 - 2R_oR_f\cos\theta_f}} \tag{4.23}$$

Substituting (4.22) and (4.23) into $R(\theta)$ yields

$$\max_{0<\theta\leq\theta_f} R(\theta) = R(\bar{\theta}) = \frac{\sqrt{{R_o}^2 + {R_f}^2 - 2R_oR_f\cos\theta_f}}{\sin\theta_f}$$

We also recognize that we can now write the path length, l, as a function of the maximum range to the sensor

$$l = R(\bar{\theta})\,\theta_f$$

Clearly, if the extremal is monotonically increasing, the maximum range is R_f, as $R_f \geq R_o$ is given. □

4.4 Alternate Derivation for Passive Sensor

The variational problem we have obtained in Eqs. (4.1)-(4.3) can also be solved using the first integral of the Euler equation [16], since the integrand of (4.1) does not depend upon the variable θ. The first integral of the Euler equation is given by

$$F - R'\,F_{R'} = C \tag{4.24}$$

where C is a constant. Evaluating Eq. (4.24) yields

$$\frac{1}{\sqrt{R(\theta)^2 + R'(\theta)^2}} = C$$

Thus, $\dot{R}(\theta) = \pm\sqrt{\frac{1}{C^2} - R^2(\theta)}$, where $\frac{1}{C^2} > R^2 > 0$. We have obtained a non-linear ODE,

$$\frac{dR}{d\theta} = \pm\sqrt{\frac{1}{C^2} - R^2}, \quad R(0) = R_o \tag{4.25}$$

where the integration constant C will be determined by the terminal condition $R(\theta_f) = R_f$.

We assume $R(\theta)$ is unimodal on $0 < \theta \leq \theta_f$. Hence, $\exists\ 0 < \bar{\theta} \leq \theta_f$ such that $R(\theta)$ is monotonically increasing (decreasing) on $[0, \bar{\theta}]$, and is monotonically decreasing (increasing) on $[\bar{\theta}, \theta_f]$. At $\theta = \bar{\theta}$, $R(\theta)$ is maximal and $\frac{dR}{d\theta}|_{\bar{\theta}} = 0$.

Consider $0 < \theta \leq \bar{\theta}$ where $R(\theta)$ is monotonically increasing, and

$$\frac{dR}{d\theta} = +\frac{\sqrt{1/C^2 - R^2}}{1}.$$

Thus,

$$d\theta = \frac{1}{\sqrt{1/C^2 - R^2}}\, dR \tag{4.26}$$

The solution of this ODE entails an integration. Eq. (4.26) is of the form

$$\int \frac{1}{\sqrt{a^2 - x^2}}\, dx = \text{Arcsin}\, \frac{x}{|a|}$$

Let $a = 1/C$. Thus the integration of (4.26) yields

$$\theta + \phi = \text{Arcsin}\, \frac{R}{|a|}$$

where ϕ is an integration constant. Hence,

$$R(\theta) = |a| \sin(\theta + \phi)$$

Similarly on $\bar{\theta} \leq \theta \leq \theta_f$,

$$R(\theta) = -|a| \sin(\theta - \psi)$$

We have three unknowns: ϕ, ψ, and $\bar{\theta}$, and three conditions: $R(0) = R_o$, $R(\theta_f) = R_f$ and $R(\bar{\theta}) = \max_{0<\theta\leq\theta_f} R(\theta)$. The latter yields

$$\bar{\theta} + \phi = \frac{\pi}{2}$$

and

$$\bar{\theta} - \psi = -\frac{\pi}{2}$$

thus

$$\begin{aligned} & \phi + \psi = \pi \\ \Longrightarrow \quad & \psi = \pi - \phi \end{aligned}$$

Hence, for $\bar{\theta} \leq \theta \leq \theta_f$,

$$\begin{aligned} R(\theta) &= -|a| \sin(\theta + \phi - \pi) \\ &= |a| \sin(\theta + \phi) \end{aligned}$$

Therefore, the formula

$$R(\theta) = |a| \sin(\theta + \phi)$$

applies for $0 < \theta \leq \theta_f$. To determine the integration constants, we substitute the boundary condition (4.2) to obtain

$$R(0) = R_o = |a| \sin \phi$$

Thus,

$$|a| = \frac{R_o}{\sin \phi} \tag{4.27}$$

Applying Eqs. (4.3) and (4.27) we obtain

$$\begin{aligned} R(\theta_f) = R_f &= \frac{R_o}{\sin\phi}\sin(\theta_f + \phi) \\ &= \frac{R_o}{\sin\phi}(\sin\theta_f\cos\phi + \cos\theta_f\sin\phi) \\ &= \frac{R_o\sin\theta_f}{\tan\phi} + R_o\cos\theta_f \end{aligned}$$

Solving for $\tan\phi$

$$\tan\phi = \frac{R_o\sin\theta_f}{R_f - R_o\cos\theta_f} \tag{4.28}$$

Which implies,

$$\sin\phi = \frac{R_o\sin\theta_f}{\sqrt{{R_o}^2 + {R_f}^2 - 2R_oR_f\cos\theta_f}} \tag{4.29}$$

$$\cos\phi = \frac{R_f - R_o\cos\theta_f}{\sqrt{{R_o}^2 + {R_f}^2 - 2R_oR_f\cos\theta_f}} \tag{4.30}$$

Thus, we can give an alternate expression for the extremal given in Eq. (4.4) as

$$R(\theta) = \frac{\sqrt{{R_o}^2 + {R_f}^2 - 2R_oR_f\cos\theta_f}}{\sin\theta_f}\sin(\theta + \phi) \tag{4.31}$$

where

$$\phi = \text{Arctan}\left(\frac{R_o\sin\theta_f}{R_f - R_o\cos\theta_f}\right) \tag{4.32}$$

We can show that the trajectory from Eq. (4.31) is explicitly the same as Eq. (4.4). Using a trigonometric identity, Eq. (4.31) becomes

$$R(\theta) = \frac{\sqrt{{R_o}^2 + {R_f}^2 - 2R_oR_f\cos\theta_f}}{\sin\theta_f}(\sin\theta\cos\phi + \cos\theta\sin\phi)$$

Substituting (4.29) and (4.30) we obtain

$$R(\theta) = \frac{R_f - R_o\cos\theta_f}{\sin\theta_f}\sin\theta + R_o\cos\theta \tag{4.33}$$

4.5 Comparison of Radar and Passive Sensor Cases

The optimal trajectories for minimizing the energy reflected to a monostatic radar and passive RF sensor share a very similar structure. Consider the equation for the optimal trajectory for the monostatic case, given by

$$\begin{aligned} R^*(\theta) &= R_o \sqrt[3]{\frac{\sin(3\theta+\phi)}{\sin\phi}} \\ &= R_o \sqrt[3]{\frac{\sin 3\theta\cos\phi + \cos 3\theta \sin\phi}{\sin\phi}} \\ &= R_o \sqrt[3]{\frac{\sin 3\theta}{\tan\phi} + \cos 3\theta} \end{aligned} \tag{4.34}$$

where

$$\phi = \text{Arctan}\left(\frac{\sin 3\theta_f}{\left(\frac{R_f}{R_o}\right)^3 - \cos 3\theta_f}\right)$$

Substituting

$$\tan\phi = \frac{{R_o}^3 \sin 3\theta_f}{{R_f}^3 - {R_o}^3 \cos 3\theta_f}$$

into Eq. (4.34) we obtain

$$R^*(\theta) = \sqrt[3]{\frac{{R_f}^3 - {R_o}^3\cos 3\theta_f}{\sin 3\theta_f}\sin 3\theta + {R_o}^3 \cos 3\theta} \tag{4.35}$$

Comparing the structure of Eq. (4.35) and (4.33), we see that both are essentially the sum of a sine and cosine term. The constants that multiply the sine and cosine terms are very similar in structure as well. Table 4.1 compares the equations for trajectories, path length and maximal range for the monostatic radar and passive sensor cases.

4.6 Constrained Analytic Solution

For the passive sensor exposure minimization problem, an optimal unconstrained solution exists for $0 \leq \theta_f \leq \pi$. Although this is a great advantage over the radar exposure minimization problem, it is still useful to to consider a path length constraint for the case of a passive sensor. The path length constrained formulation naturally applies when

Table 4.1 Comparison of Radar and Passive Emitter Equations

	Radar ($1/R^4$)	Passive Emitter ($1/R^2$)
$R^*(\theta)$	$\sqrt[3]{\frac{{R_f}^3-{R_o}^3\cos 3\theta_f}{\sin 3\theta_f}\sin 3\theta+{R_o}^3\cos 3\theta}$	$\frac{R_f-R_o\cos\theta_f}{\sin\theta_f}\sin\theta+R_o\cos\theta$
l^*	$\frac{R_o}{\sqrt[3]{\sin\phi}}\int_0^{\theta_f}\sin(3\theta+\phi)^{-\frac{2}{3}}\,d\theta$	$\frac{\sqrt{{R_o}^2+{R_f}^2-2R_oR_f\cos\theta_f}}{\sin\theta_f}\,\theta_f$
$R^*_{\max}$[1]	$\sqrt[3]{\frac{\sqrt{{R_f}^6+{R_o}^6-2{R_f}^3{R_o}^3\cos 3\theta_f}}{\sin 3\theta_f}}$	$\frac{\sqrt{{R_o}^2+{R_f}^2-2R_oR_f\cos\theta_f}}{\sin\theta_f}$

dealing with limited fuel resources or when attempting to coordinate the actions of multiple vehicles.

Consider the problem of minimizing exposure to a passive sensor located at the origin O, starting from some initial location $(R_o, 0)$, terminating at the point (R_f, θ_f), where the length of the trajectory, l, is given. This path length constraint, l, can be greater than or less than the optimal unconstrained path length, l^*, determined previously. Clearly, the path length constraint is bounded below by the minimum possible path length, viz. $l \geq \|AB\|$; see, e.g., Fig. 4.5.

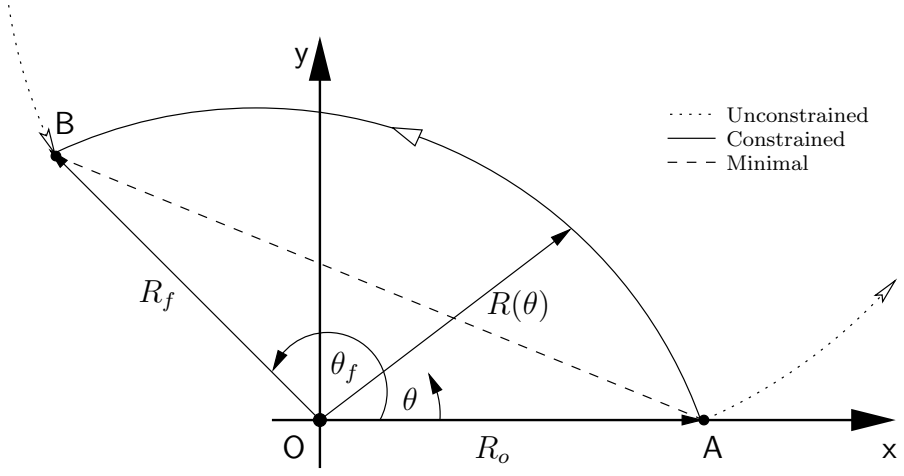

Figure 4.5 Notional Comparision of a Unconstrained Optimal Path, Constrained Optimal Path and a Minimum Length Path for the Passive Sensor Exposure Minimization Problem

[1]For properly unimodal case, i.e., when $3\theta_f + \phi > \pi/2$

Assuming a constant velocity for the vehicles, we wish to minimize the cost functional

$$J[R(\theta)] = \int_0^{\theta_f} \frac{\sqrt{\dot{R}^2 + R^2}}{R^2}\, d\theta$$

such that the admissible paths satisfy the conditions

$$\begin{aligned} R(0) &= R_o \\ R(\theta_f) &= R_f, \quad 0 < \theta \leq \theta_f \\ L[R(\theta)] &= \int_0^{\theta_f} \sqrt{\dot{R}^2 + R^2}\, d\theta = l \end{aligned}$$

where $L[R(\theta)]$ is a functional representing the path length constraint. The variational problem with subsidiary conditions is an isoperimetric problem - see, e.g., Section 2.3.1.2. We can express the augmented cost functional as

$$J = \int_0^{\theta_f} \left(\frac{\sqrt{\dot{R}^2 + R^2}}{R^2} + \lambda \sqrt{\dot{R}^2 + R^2} \right)\, d\theta \tag{4.36}$$

where λ is a parameter, sometimes called a Lagrange multiplier [16].

Since our functional J does not explicitly depend on θ, we can use the Euler equation of the form

$$F - \dot{R} F_{\dot{R}} = C$$

where C is a constant of integration and

$$\begin{aligned} F &= \left(\frac{\sqrt{\dot{R}^2 + R^2}}{R^2} + \lambda \sqrt{\dot{R}^2 + R^2} \right) \\ F_{\dot{R}} &= \frac{\lambda \dot{R}}{\sqrt{\dot{R}^2 + R^2}} + \frac{\dot{R}}{R^2 \sqrt{\dot{R}^2 + R^2}} \end{aligned}$$

Thus, the Euler equation becomes

$$\frac{1 + \lambda R^2}{\sqrt{\dot{R}^2 + R^2}} = C$$

Solving for $\dot{R}^2$ we obtain

$$\dot{R}^2 = \frac{1}{C^2}\left(1+\lambda R^2\right)^2 - R^2$$

Thus,

$$\begin{aligned}
\dot{R} &= \pm\sqrt{\frac{1}{C^2}\left(1+\lambda R^2\right)^2 - R^2} \\
&= \pm\sqrt{\frac{1}{C^2}\left(1+2\lambda R^2+\lambda^2 R^4\right) - R^2} \\
&= \pm\sqrt{\frac{\lambda^2}{C^2}R^4 + \left(\frac{2\lambda}{C^2}-1\right)R^2 + \frac{1}{C^2}} \\
&= \pm\frac{\lambda}{C}\sqrt{R^4 + \frac{2\lambda - C^2}{\lambda^2}R^2 + \frac{1}{\lambda^2}} \\
&= \pm\frac{\lambda}{C}\sqrt{\left(R^2-a^2\right)\left(R^2-b^2\right)} \\
&= \frac{dR}{d\theta}
\end{aligned}$$

where

$$\begin{aligned}
a^2 &= \frac{C^2 + C\sqrt{C^2-4\lambda} - 2\lambda}{2\lambda^2} \\
b^2 &= \frac{C^2 - C\sqrt{C^2-4\lambda} - 2\lambda}{2\lambda^2}
\end{aligned}$$

For the moment, consider only $\frac{dR}{d\theta} > 0$. We have

$$d\theta = \frac{dR}{\frac{\lambda}{C}\sqrt{\left(R^2-a^2\right)\left(R^2-b^2\right)}}$$

Integrating both sides

$$\begin{aligned}
\int d\theta &= \int \frac{dR}{\frac{\lambda}{C}\sqrt{\left(R^2-a^2\right)\left(R^2-b^2\right)}} \\
\frac{\lambda}{C}\int d\theta &= \int \frac{dR}{\sqrt{\left(R^2-a^2\right)\left(R^2-b^2\right)}} \\
\frac{\lambda}{C}\left(\theta+\phi\right) &= \int \frac{dR}{\sqrt{\left(R^2-a^2\right)\left(R^2-b^2\right)}}
\end{aligned}$$

Now let $t = \frac{R}{a} \implies dR = a\ dt$, thus

$$\begin{aligned}\frac{\lambda}{C}(\theta+\phi) &= \int \frac{a\ dt}{\sqrt{(a^2t^2-a^2)(a^2t^2-b^2)}} \\ &= \int \frac{a\ dt}{\sqrt{(-a^2)(1-t^2)(-b^2)\left(1-\frac{a^2}{b^2}t^2\right)}} \\ &= \frac{1}{b}\int \frac{dt}{\sqrt{(1-t^2)(1-k^2t^2)}}\end{aligned}$$

where $k^2 = \frac{a^2}{b^2}$, which is an elliptic integral of the first kind, denoted $F(\varphi, k)$, where

$$\varphi = \text{Arcsin}\left(\frac{R}{a}\right)$$

Thus,

$$\frac{\lambda}{C}(\theta+\phi) = F\left(\text{Arcsin}\left(\frac{R}{a}\right), \frac{a}{b}\right)$$

Taking the inverse of the elliptic integral and solving for R yields

$$R(\theta) = a\,\text{sn}\left[\frac{b\lambda(\theta+\phi)}{c}, \frac{a}{b}\right] \tag{4.37}$$

where $\text{sn}(\varphi, k)$ is the Jacobi elliptic function which is the inverse of the elliptic integral $F(\varphi, k)$. In this formulation, the desired path length l is not explicitly present. Instead, the parameter λ is chosen in an iterative fashion such that the constraint $L[R(\theta)] = l$ is satisfied.

The author is aware that the solution of the constrained passive sensor problem was obtained independently by Zabarankin, et. al., [46], and publication of their result is forthcoming.

4.7 Summary

In this chapter, the passive sensor exposure minimization problem has been addressed and a closed form solution has been obtained. The optimal solution was shown to be a circle and its radius and center were determined. Additionally, analytic solutions for the optimal path length and optimal cost were provided. A comparison between the solutions of the

passive sensor and radar exposure minimization problems reveal an interesting relationship in the structure of the two solutions. Finally, the path length constrained problem is addressed and the solution is shown to be a function of an elliptic integral.

Unlike the passive sensor problem, a tractable analytic expression for the constrained path length problem appears out of reach. In the next chapter, numerical methods are applied to the solution of both the unconstrained and constrained radar exposure minimization problem. Two methods of solution are demonstrated and specific limitations of the methods are discussed.

V. Numerical Methods of Solution

5.1 Introduction

In Chapter III we showed how the Calculus of Variations is used to find the optimal trajectory that minimizes exposure to a radar. A two-point boundary value problem is arrived at, which has a closed form solution given by Eq. (3.4).

Although numerical techniques are readily available for solving boundary value problems, e.g., [40, 7, 11], the insights gained from analyzing the closed form solution are invaluable. For example, consider the analyst who immediately employs a numerical technique, such as a shooting method, and wishes to evaluate trajectories for $\theta_f \geq 60°$. Countless hours could be saved if the analyst had the insight that the two-point boundary value problem does *not* have a solution for θ_f beyond $60°$. Even more pathetic is the analyst whose numerical experiments lead him to the incorrect conclusion that no solution then exists, for any value of θ_f. Conversely, direct numerical optimization methods that employ gridding or coarse discretization of the problem space can result in the incorrect conclusion that there *always* exists an optimal solution, for any value of θ_f, including $\theta_f \geq 60°$. While numerical results will be obtained for $\theta_f \geq 60°$, the ensuing discretized optimal trajectory, barring numerical precision issues, will invariably ride the boundary of the search space; the latter is arbitrarily imposed by the analyst. Hence, the analytical result that an optimal trajectory does not exist manages to manifest itself in the numerical work.

In this chapter, we present the results of using numerical methods to obtain the solution to the problem of minimizing the radar exposure cost functional, and compare them to the analytical results obtained in the previous sections. This comparison will aid in the validation of the numerical methods. The numerical methods will then be applied to the synthesis of optimal trajectories for $\theta_f \geq 60°$ where a path length constraint is imposed.

5.2 Finite Difference Approximation

This direct method employs a piecewise linear approximation as described in Sec. 2.3.2. Consider approximating the optimal trajectory from points A to B with a series of N

straight line segments. Neglecting the departure and destination points, the path can also be defined as a series of $N-1$ waypoints, equally spaced over the domain $(0, \theta_f)$ - see, e.g., Fig. 2.1. One of these N segments can be expressed as in the two-point form of a line in polar coordinates as in Eq. (2.11) which has the first derivative given by Eq. (2.12).

For example, consider the cost to travel the straight line segment from the point (r_1, θ_1) to the point (r_2, θ_2)

$$J_{1,2} = \int_{\theta_1}^{\theta_2} \frac{\sqrt{R^2 + \dot{R}^2}}{R^4}\, d\theta \tag{5.1}$$

Substituting Eqs. (2.11) and (2.12) into the cost function, Eq. (5.1) yields

$$J_{1,2} = \frac{\sqrt{{r_1}^2 + {r_2}^2 - 2r_1 r_2 \cos\Delta\theta}}{4\left(r_1 r_2 \sin\Delta\theta\right)^3} \left[4r_1 r_2 \Delta\theta \left(\cos\Delta\theta - \sin\Delta\theta\right) - \left({r_1}^2 + {r_2}^2\right)\left(2\Delta\theta - \sin 2\Delta\theta\right)\right]$$

where

$$\Delta\theta = \theta_1 - \theta_2$$

Thus we have eliminated any dependence upon θ and the cost of any given line segment is explicitly determined for a given pair of points (r_1, θ_1), (r_2, θ_2). The total cost of the optimal path, for N line segments, is the summation of the costs for each segment, viz.,

$$\tilde{J}^* = \sum_{i=1}^{N} J_{i,i+1}$$

In lieu of a more sophisticated gridpoint allocation algorithm, the approximation strategy employed is to increase the number of segments, N, until a user specified termination criterion is met, e.g., increase N, until

$$\left| \sum_{i=1}^{N} J_{i,i+1} - \sum_{k=1}^{N-1} J_{k,k+1} \right| < \epsilon \tag{5.2}$$

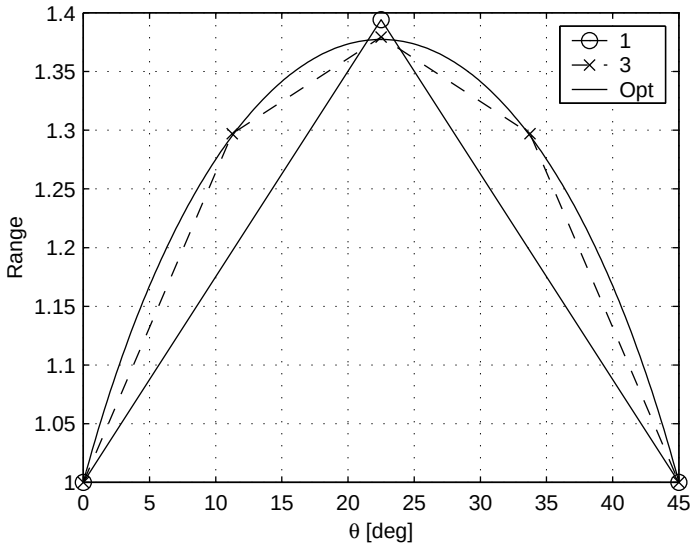

Figure 5.1 Comparison of Unconstrained Numerical and Analytic Optimization Results for 1 and 3 Waypoints, $R_f/R_o = 1$, $\theta_f = 45°$.

where ϵ is the user defined tolerance on the accuracy of $\tilde{J}^*$. A similar strategy can be used to approximate the path length, where

$$\tilde{l}^* = \sum_{i=1}^{N-1} \sqrt{{r_1}^2 + {r_2}^2 - 2r_1 r_2 \cos(\theta_i - \theta_{i+1})}$$

The piecewise linear approximation accurately portrays the discrete approximation to the cost function. This permits the variational problem to be approximated using non-linear programming techniques[1]. The optimization results that follow are performed in MATLAB using a Sequential Quadratic Programming (SQP) routine developed at AFIT [23], as well as the `fmincon.m` function from the MATLAB Optimization Toolbox [13]. Several optimization scenarios are considered.

5.2.1 Unconstrained Path Length. Consider the optimization problem as stated in Eqs. (3.1)-(3.3). Since $\theta_f \leq 60°$, no constraint on the path length need be imposed. The purpose of this optimization is to compare the analytic and numerical optimization results, viz., calibrate the numerical results. Fig. 5.1 shows the results of numerical optimization

[1]This approach also facilitates the development of a solution using the finite element method.

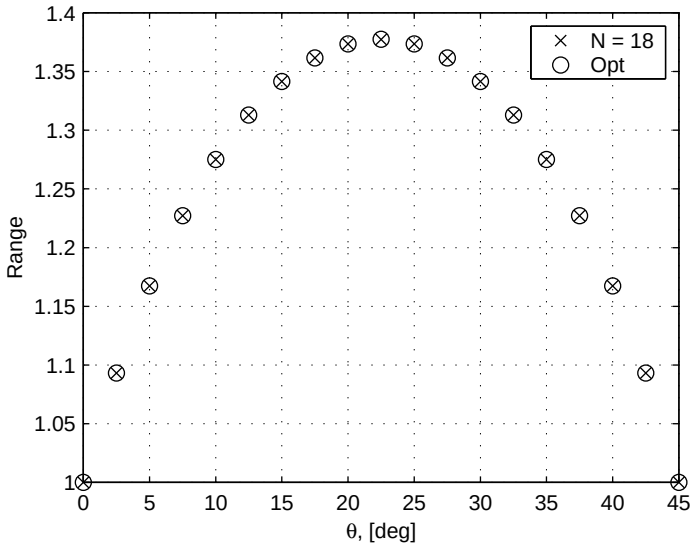

Figure 5.2 Comparison of Unconstrained Numerical and Analytic Optimization Results for 17 Waypoints, $R_f/R_o = 1$, $\theta_f = 45°$.

using the piecewise linear approximation developed above. A radar exposure minimization problem is solved for the cases of 1 and 3 waypoints and the analytic solution is also presented for comparison purposes. Interestingly, the numerically optimized paths fall mainly inside the optimal curve.

Employing this strategy and Eq. (5.2) with $\epsilon = 0.0001$, a trajectory of 17 waypoints was determined and is plotted in Fig 5.2. The same approximation strategy is used to determine the path length of the function. Table 5.1 compares the costs and path lengths of the $1, 3$ and 17 waypoint solutions with the optimal result for the case of $R_f/R_o = 1$, $\theta_f = 45°$. We can see that this piecewise linear approximation converges from above to the optimal solution as the number of waypoints is increased.

Difficulties can present themselves with the unconstrained problem when numerical optimization is employed. Clearly, obtaining good initial guesses for the value of the discrete waypoints will factor into the convergence and performance of the numerical optimization method. As $\theta_f \to \pi/3$, numerical methods have difficulty keeping up with the explosive nature of the solution - see, e.g., Novy [30].

Table 5.1 Comparison of Cost and Path Length for Unconstrained Radar Problem $R_f/R_o = 1$, $\theta_f = 45°$

Waypoints	Cost	Length
1	0.681329	1.212458
3	0.631784	1.292690
17	0.616710	1.321193
Optimal	0.615920	1.322899

5.2.2 Constrained Path Length. As we have shown, for $\theta_f \geq 60°$, a path length constraint must be included to make the optimization problem well posed. Clearly the minimum path length from points A to B is the length of the line segment AB. The problem can be stated as

$$\begin{aligned} \text{minimize} \quad & J[R(\theta)] = \int_0^{\frac{\pi}{4}} \frac{\sqrt{\dot{R}^2 + R^2}}{R^4}\, d\theta \\ \text{subject to:} \quad & R(0) = R_o = 1, \\ & R(\theta_f) = R_f = 1, \\ & l \leq R_o \theta_f = \frac{\pi}{4} \\ & 0 < \theta \leq \frac{\pi}{4} \end{aligned}$$

The inequality constraint $l \leq R_o\,\theta_f$, was chosen such that the path would be constrained about a circle of radius R_o. Moreover, for $\theta_f < 60°$, if the constrained path length $l > l^*$ from Eq. (3.6), then the constraint is not active.

Fig. 5.3 shows the results of the constrained numerical optimization for $R_o = R_f$, $\theta_f = 45°$. The discretization was performed with 8 waypoints evenly spaced over the domain of θ. As expected, the constrained solution is a segment of a circle with radius $R_o = 1$. The unconstrained analytic solution is also shown for comparison purposes.

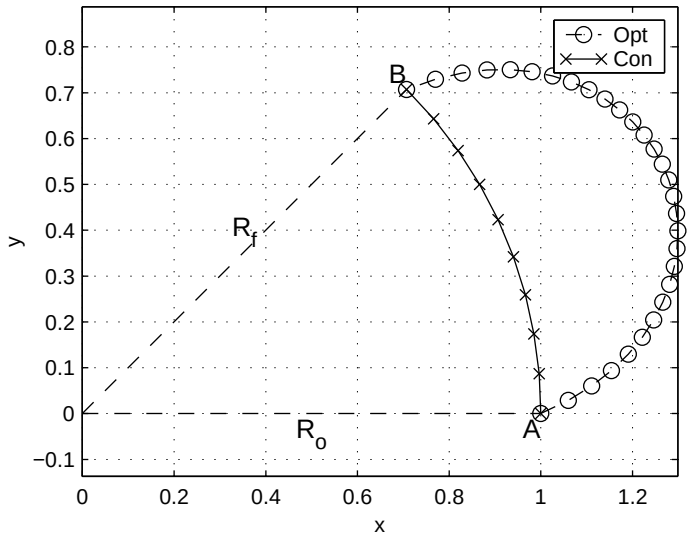

Figure 5.3 Comparison of Constrained Numerical Optimization and Unconstrained Analytic Optimization for $R_f/R_o = 1$, $\theta_f = 45°$

Lastly, we consider a case where $\theta_f > 60°$

$$\begin{aligned}
\text{minimize} \quad & J[R(\theta)] = \int_0^{\frac{13\pi}{18}} \frac{\sqrt{\dot{R}^2 + R^2}}{R^4}\, d\theta \\
\text{subject to:} \quad & R(0) = R_o = 1, \\
& R(\theta_f) = R_f = 1, \\
& 0 \leq \theta \leq \frac{13\pi}{18} \\
\text{and either:} \quad & \max R(\theta) \leq 4 \\
& \text{or} \\
& l < l_{\max R(\theta) \leq 4}
\end{aligned}$$

First, we use our numerical optimization method to solve the maximum range constrained problem. That is, we impose only $\max R(\theta) \leq 4$. Using an iterative scheme, the number of line segments is increased until the user defined tolerance on the cost, $\epsilon \leq 0.0001$. The length of the maximum range constrained trajectory, $l_{\max R(\theta) \leq 4} = 12.667841$, and the cost is 0.687642. Next, the path length constrained problem is solved using a similar iteration scheme, imposing the constrained path length $l_{\max R(\theta) \leq 4}$ previously calculated. The cost

for the latter trajectory is calculated as 0.684614. Fig. 5.4 depicts the results for the two different types of constraints.

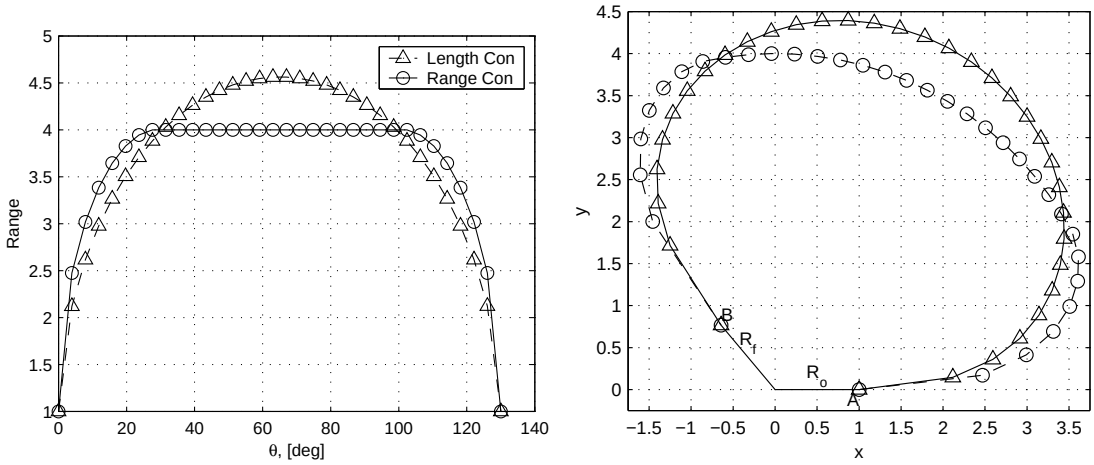

Figure 5.4 Comparison of Constrained Numerical Optimizations for $R_o = R_f$, $\theta_f = 130°$

5.3 Shooting Method

The Euler equation is a necessary condition for a functional of the form

$$J[y] = \int_a^b F(x, y, y')\, dx \tag{5.3}$$

to be extremized, assuming $J[y]$ is defined on the set of functions with continuous first derivatives on $[a, b]$ and satisfy the boundary conditions $y(a) = A$, $y(b) = B$. Solving the Euler equation for the function(s) that extremize(s) the functional in Eq. (5.3) results in a two point boundary value problem. Often these problems are non-linear and closed form solutions are rare.

The shooting method is a numerical technique used to solve boundary value problems. Essentially the shooting method involves searching for the missing initial conditions and once they are found, proceeds as if the problem were an initial value problem. The algorithm is as follows:

1. Develop guesses for the missing initial conditions.

2. Numerically integrate the differential equation over the range $[a, b]$ and save the values of the function at the end points.
3. Determine the difference between the computed end points and the desired end points.
4. Modify the guesses for the missing initial conditions based upon the discrepancy.
5. Iterate until the computed and desired end points agree to some user defined tolerance.

This algorithm describes a "forward" shooting method. It is possible to integrate the equations backwards from guesses of the missing final conditions. Similarly, "multi-shooting" methods exist to integrate from both sides simultaneously, requiring the solutions to meet somewhere in the middle.

Obtaining good guesses for the initial condition in step 1 is essential for obtaining valid solutions from the integrator in step 2. Clearly, a poor guess for the initial condition can result in numerical instability and failure of the differential equation integration process. A robust root finding method is required to cope with failures in the integration process as well as the sensitivity of the problem to small changes in initial conditions (i.e. stiffness). Although there are challenges involved with the shooting method, it is an important and practical method for solving non-linear boundary value problems. Additional information on shooting methods is available from many sources including [11, 40, 36, 7].

5.3.1 Unconstrained Path Length. Once again, consider the problem as stated in Eqs. (3.1)-(3.3), where we wish to minimize the exposure to a radar. The first integral form of the Euler equation, used in the proof of Theorem 3.3.1, resulted in the non-linear ordinary differential equation given in Eq. (3.9). Taking into account the results of Section 3.7, we can define the following

$$\dot{R}(\theta) = \begin{cases} \frac{\sqrt{1/C^2 - R^6(\theta)}}{R^2(\theta)}\,, & 3\theta + \phi < \frac{\pi}{2} \\ 0\,, & 3\theta + \phi = \frac{\pi}{2} \\ -\frac{\sqrt{1/C^2 - R^6(\theta)}}{R^2(\theta)}\,, & 3\theta + \phi > \frac{\pi}{2} \end{cases} \tag{5.4}$$

where

$$\frac{1}{C^2} > R^6 > 0$$

and C is a constant of integration dependent upon the parameters R_o/R_f and θ_f. The shooting method can be applied to Eq. (5.4), where the constant of integration C is the unknown initial parameter. However, there are several numerical difficulties in this approach. For example, the power of the $R^6(\theta)$ term can present numerical sensitivity issues in relation to the other terms in the expression. Additionally, in the neighborhood of $\dot{R} = 0$, numerical roundoff and truncation errors can result in the term $\sqrt{1/C^2 - R^6(\theta)}$ yielding a complex result. This issue, as well as the sign change at the point $\dot{R} = 0$, can cause numerical integration schemes to fail to converge. Lastly, except for symmetric problems, knowing the value of θ where we have the sign change is not possible without first having the analytic result for ϕ in hand.

If we apply the Euler equation

$$F_R - \frac{d}{d\theta} F_{\dot{R}} = 0$$

rather than the first integral form, we obtain the following second order non-linear ordinary differential equation.

$$\ddot{R}(\theta)R(\theta) + 2\dot{R}(\theta) + 3R^2(\theta) = 0 \tag{5.5}$$

which can be expressed as the following system of first order equations

$$Y_1'(\theta) = Y_2(\theta) \tag{5.6}$$

$$Y_2'(\theta) = 3Y_1(\theta) + \frac{2Y_2^2(\theta)}{Y_1(\theta)} \tag{5.7}$$

with boundary conditions

$$Y_1(0) = R_o \tag{5.8}$$

$$Y_1(\theta_f) = R_f \tag{5.9}$$

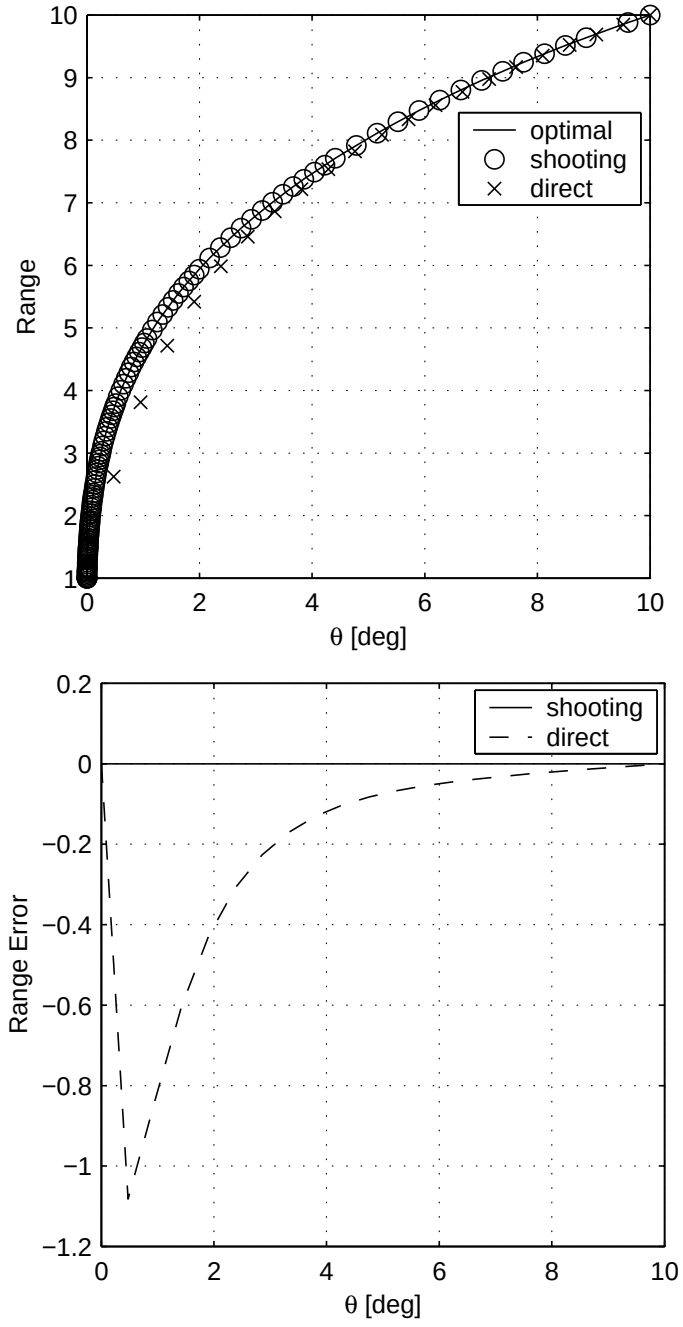

Figure 5.5 Top: Comparison of the Analytic Result, Shooting Method and the Direct Method for $R_f/R_o = 10$ and $\theta_f = 10°$; Bottom: Error in the Two Numerical Methods

Fig. 5.5 is a comparison of the shooting method with the analytic result and the direct method described in the previous section. The problem parameters $R_f/R_o = 10$ and $\theta_f = 10°$. The difficulty the direct method has in matching the results of the analytic solution can be attributed, in part, to the location of the grid points in the mesh. The direct method chosen here employed an initial grid of 20 evenly spaced waypoints, where the number of grid points was adaptively increased until the cost function converged to an acceptable tolerance. A non-evenly spaced grid should be able to capture the shape of the optimal curve more effectively. In comparison, the shooting method uses an adaptive step size Runga-Kutta integrator.

Another difficulty faced by the direct method is the relative flatness of the cost function in the vicinity of the optimal solution. As $\theta_f \to \pi/3$, the direct method experiences increased difficulty in differentiating between the cost of adjacent solutions. The shooting method, on the other hand, is more robust in this regard. The optimal cost, given by Eq. (3.20), the cost of the solution by the shooting method and the cost of the solution by the direct method are as follows:

	Analytic	Direct	Shooting
Cost	0.33304469	0.33306025	0.33304497
Error	-	1.55589E-05	2.77249E-07

It is often useful to employ a technique known as *continuation* when dealing with problems involving stiffness or when having difficulty obtaining good guesses for the initial conditions. Continuation is a technique where solutions are first obtained in an area of the problem space where solutions are easily found. Next, the parameters that causing the stiffness are slowly adjusted in the direction of the desired solution. The results of the successful attempts at the shooting method are then used as the initial guesses for the next attempt.

For complicated problem descriptions, direct methods have an advantage in their flexibility to specify a variety of constraints. Methods based upon variational principles are limited in this regard, however, subsidiary conditions can be readily imposed, i.e., path length constraints.

5.3.2 Constrained Path Length. The constrained path length radar exposure minimization problem is given by

$$\min_{R(\theta)} \int_0^{\theta_f} \frac{\sqrt{\dot{R}^2 + R^2}}{R^4}\, d\theta \tag{5.10a}$$

$$\text{s.t.} \qquad L[R(\theta)] = \int_0^{\theta_f} \sqrt{\dot{R}^2 + R^2}\, d\theta = l \tag{5.10b}$$

$$\text{and} \qquad R(0) = R_o \tag{5.10c}$$

$$R(\theta_f) = R_f, \quad 0 < \theta \leq \theta_f \tag{5.10d}$$

where $L[R(\theta)]$ is a functional representing the isoperimetric constraint.

To solve the constrained path length problem, we will employ the Lagrange multiplier method whereby the constrained problem is formulated as an equivalent unconstrained problem. We can express the augmented cost functional as

$$J_A = \int_0^{\theta_f} \left(\frac{\sqrt{\dot{R}^2 + R^2}}{R^4} + \lambda \sqrt{\dot{R}^2 + R^2} \right) d\theta \tag{5.11}$$

where λ is a real valued constant, i.e., the Lagrange multiplier. The resulting Euler equation yields the non-linear, ordinary differential equation

$$\ddot{R}(\theta)[R(\theta) + \lambda R^5(\theta)] + 3R^2(\theta) - \lambda R^6(\theta) + 2[\dot{R}(\theta)]^2 - 2\lambda R^4(\theta)[\dot{R}(\theta)]^2 = 0$$

which can be expressed as the following system of first order equations

$$Y_1'(\theta) = Y_2(\theta) \tag{5.12}$$

$$Y_2'(\theta) = \frac{3Y_1^2(\theta) - \lambda Y_1^6(\theta) + 2Y_2^2(\theta) - 2\lambda Y_1^4(\theta) Y_2^2(\theta)}{Y_1(\theta) + \lambda Y_1^5(\theta)} \tag{5.13}$$

with boundary conditions

$$Y_1(0) = R_o \tag{5.14}$$

$$Y_1(\theta_f) = R_f \tag{5.15}$$

Since we don't know what value of λ achieves a given path length, we must introduce an additional level of iteration in the shooting method algorithm. That is, we must guess a value of λ, solve the boundary value problem using the shooting method, compute the resulting path length, compare the result to our desired path length, adjust our guess of λ and repeat until the desired path length is achieved.

The numerical integrator employed by the shooting method provides as its output a finite number of points along the curve $R^*(\theta)$. In order to evaluate the path length, the piecewise linear approximation discussed in Sec. 5.2 is made. The number of solution steps the numerical integrator takes is increased until the path length approximation converges within some user defined tolerance. Fig. 5.6 depicts a comparison of an optimal constrained trajectory calculated by the shooting method and by the direct method previously described.

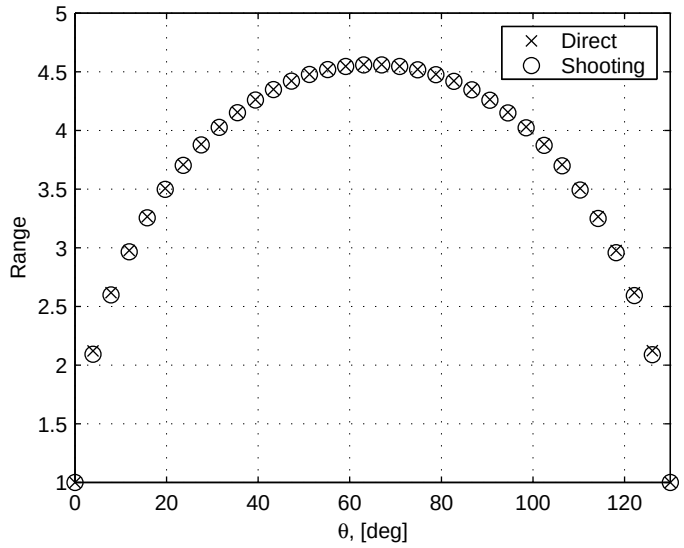

Figure 5.6 Comparison of the Shooting Method and the Direct Method for $R_o = R_f$, $\theta_f = 130^\circ$ and the Path Length $l = 12.667841$

5.3.2.1 Existence Issues for the Variational Constrained Path Length Problem.

We are concerned about the existence of solutions for the constrained radar exposure minimization problem. Specifically, for a given set of initial conditions $(R_f/R_o, \theta_f)$, can an optimal trajectory be determined for any path length l? Equivalently, in the Lagrange

multiplier formulation, what are the restrictions on the choice of λ and how does that effect the range of the path lengths that can be achieved?

Recall that for the completely unconstrained case, Eq. (3.1), there exists an optimal solution with a corresponding optimal path length, l^*. This solution exists iff $\theta_f < \pi/3$. For $\pi/3 \leq \theta_f < \pi$, there does not exist an optimal solution, the cost is bounded from below and is not attained. The path length of the optimizing trajectory approaches infinity.

The constrained problem is solved using the Lagrange multiplier method previously described. There exist restrictions on the selection of λ which will impact the achievable path length l. Similarly, there are restrictions of the range of achievable path length.

Consider the path length constrained problem for the case where $0 < \theta_f < 60^\circ$. Without loss of generality, we have $R_o = 1$ and $R_f \geq R_o$. Furthermore, momentarily [2] assume $R_f = 1$.

Remark 5.3.1. *For the constrained radar exposure minimization problem, an optimal solution does not exist for* $l < 2\sin(\theta_f/2)$.

Proof. The Euclidean distance between the points A and B is given by

$$\sqrt{R_o^2 + R_f^2 - 2\,R_o\,R_f\cos\theta_f}$$

Thus, for $R_o = R_f = 1$, if $l < 2\sin(\theta_f/2)$, the isoperimetric constraint cannot be satisfied and an optimal solution does not exist. □

To achieve the minimum possible path length, $l_{\min} = 2\sin(\theta_f/2)$, allow $\lambda \to \infty$. The optimal path length is achieved by letting $\lambda = 0$. Thus, for $\lambda \in [0, \infty]$, the optimal path length $l \in [2\sin(\theta_f/2), l^*]$., where l^* is given by Eq. (3.6). Fig. 5.7 shows a plot of optimal constrained path length trajectories with $\lambda = 0, 0.1, 1, \to \infty$, for a case where $R_f/R_o = 1$ and $\theta_f = 45^\circ$. For this case, the optimal path length, $l^* = 1.3229$, and the minimum possible path length is 0.7654.

[2] This restriction is imposed for mathematical convenience and can be removed.

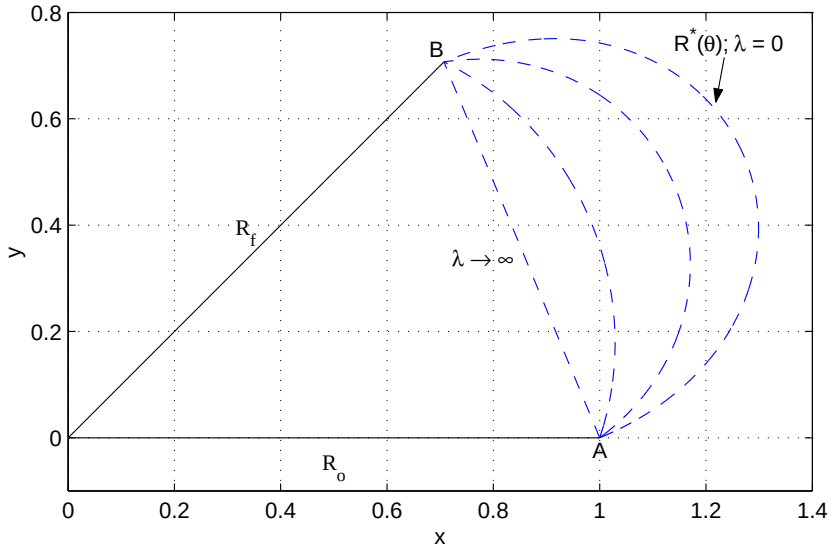

Figure 5.7 Optimal Trajectories for a Class of Path Length Constrained Problems, $\lambda = 0, 0.1, 1, \rightarrow \infty$

Fig. 5.8 depicts the curve of optimal path length versus the Lagrange multiplier λ, for the case $R_f/R_o = 1$ and $\theta_f = 45°$, for $\lambda \geq 0$.

Now we consider achieving a path length *greater* than the optimal path length, viz., we seek $l > l^*(R_f/R_o, \theta_f)$. In aviation parlance, this is the "loitering" case. We again refer to the augmented cost functional, Eq. (5.11), and to achieve a loitering trajectory we must let $\lambda < 0$.

Remark 5.3.2. *Let $0 < \theta_f < 60°$ be given. For $\lambda < 0$, there does not exist a global minimum for the augmented unconstrained radar exposure minimization problem, given by the cost functional, Eq.* (5.11).

Proof. Allow an extremal trajectory to run out to ∞. We know the exposure is bounded, yet the path length is infinite. This implies that the cost goes to $-\infty$, and thus a (global) minimum cannot exist for the augmented unconstrained radar exposure minimization problem. □

Remark 5.3.2 does not preclude the existence of a local minimum in the augmented unconstrained minimization problem. Moreover, this local minimum could be a *global* minimum in the constrained minimization problem given by Eqs. (5.10a)-(5.10d).

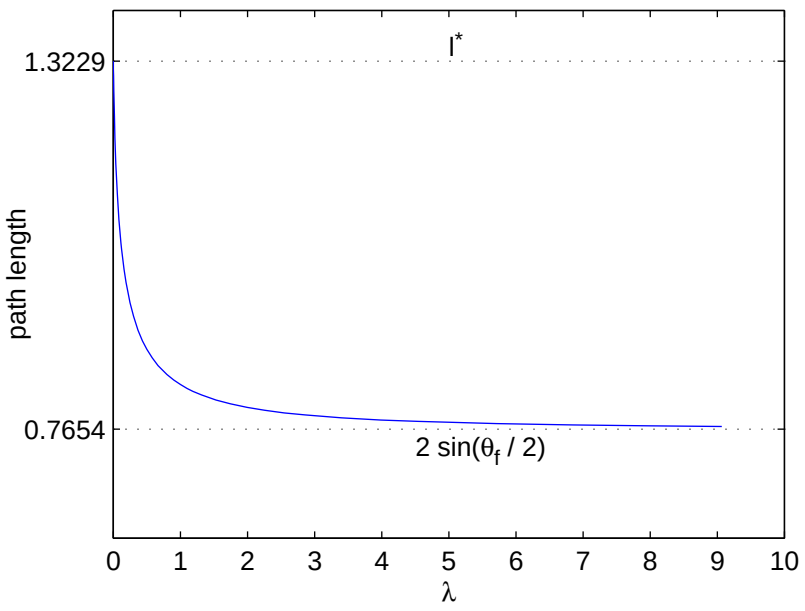

Figure 5.8 Sample Path Length as a Function of λ for $2\sin(\theta_f/2) < l < l^*$

Proposition 5.3.1. *For the functional given in Eq.* (5.11)*, for* $0 < \theta_f < 60°$*, there exists a critical value of the Lagrange multiplier,* $\lambda_c < 0$*, such that for* $\lambda < \lambda_c$*, no extremizing trajectory is a minimum.*

Proof. According to the Legendre condition for a weak (and hence strong) local minimum, it is necessary that the inequality $F_{\dot{R},\dot{R}}[\theta, R(\theta), \dot{R}(\theta)] \geq 0$ be satisfied at every point along the extremal trajectory $R(\theta)$, where $F[\theta, R(\theta), \dot{R}(\theta)]$ is the integrand of the functional given in Eq. (5.11)

$$F_{\dot{R},\dot{R}}[\theta, R(\theta), \dot{R}(\theta)] = \frac{1 + \lambda\, R^4(\theta)}{R^2(\theta)\left[R^2(\theta) + \dot{R}^2(\theta)\right]^{3/2}}$$

$F_{\dot{R},\dot{R}} \geq 0$, as long as the condition $1 + \lambda\, R^4(\theta) \geq 0$ holds, or equivalently

$$\lambda \geq \frac{-1}{R^4(\theta)}, \quad \forall\, 0 \leq \theta \leq \theta_f$$

Under these conditions, Legendre's condition holds. Thus, there exists some $\lambda_c < 0$ such that if $\lambda < \lambda_c$, a minimizing trajectory cannot exist. For $\theta_f \geq 60°$, we require $\lambda > 0$ to

render the problem well posed-see, e.g., Theorem 3.3.1. Thus, this result applies only for $0 < \theta_f < 60°$. □

Summarizing, we see that there are two limitations to the existence of minimizing trajectories; see, e.g., Fig. 5.9: First, the path length cannot be shorter than the Euclidian distance between the points A and B. Secondly, for $\theta_f < 60°$, the Lagrange multiplier is constrained at the point $\lambda < \lambda_c$ and consequently there does not exist a minimizing trajectory when the path length is constrained to be of length $l < l_c$.

It is interesting to note that in the radar exposure minimization problem we introduced the path length constraint in order to deal with the lack of existence of solutions when $\theta_f \geq 60°$. This solved the problem for $\theta_f \geq 60°$, however it introduced a new set of problems when constrained solutions are sought for $\theta_f < 60°$. Similar insights into the radar exposure *maximization* problem are provided in Appendix B.

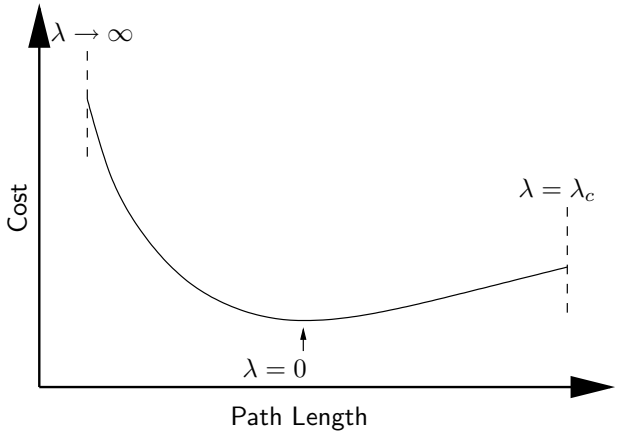

Figure 5.9 Upper and Lower Limits on the Path Lengths of Some Constrained Trajectories

Fig. 5.10 depicts curves of optimal cost versus path length for the situation $R_f/R_o = 1$ and for final angle $\theta_f = 45°, 50°, \ldots, 70°$. Bounding these curves on the left is a plot of the cost and path length of a straight line. Also plotted is the curve of the unconstrained optimal cost versus path length. We notice that for small final angles the optimal cost and path length are essentially the same as the straight line cost cost and path length, viz., there is very little curvature in $R^*(\theta)$ for shallow final angles.

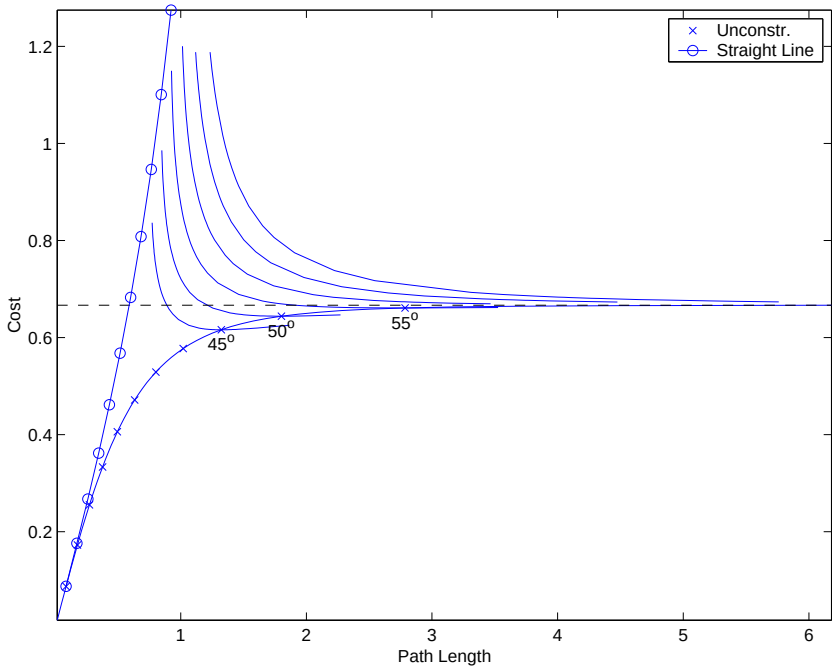

Figure 5.10 Optimal Trajectories of Path Length Constrained Problems for $R_o = R_f$, $\theta_f = 45°, 50°, 55°, 60°, 65°, 70°$

Fig. 5.11 is a zoomed view of Fig. 5.10. Generating the data required for these curves can be numerically intensive. The shooting method using continuation is employed. The constrained path length curves for $\theta_f \geq 60°$, are generated by allowing λ to be very large, such that the optimal trajectory is practically a straight line and the initial conditions are easy to guess. The value of λ is decreased using continuation until $\lambda \to 0$, and the path length increases. For $\theta_f < 60°$, we employ a similar strategy, except we allow λ to reach 0 and continue such that $\lambda < 0$. We see the convex shape of the constrained path length curves in Fig. 5.11, and the lowest cost path is obtained where the Lagrange multiplier, $\lambda = 0$. These curves are bounded on the left by the Euclidean distance limit, and on the right by the existence issues for $\lambda < 0$.

5.4 Summary

In general, it is rare that closed form solutions to optimal control problems are obtained. In this chapter, two numerical methods were developed to address two point boundary value problems. A piecewise linear approximation is developed which converts

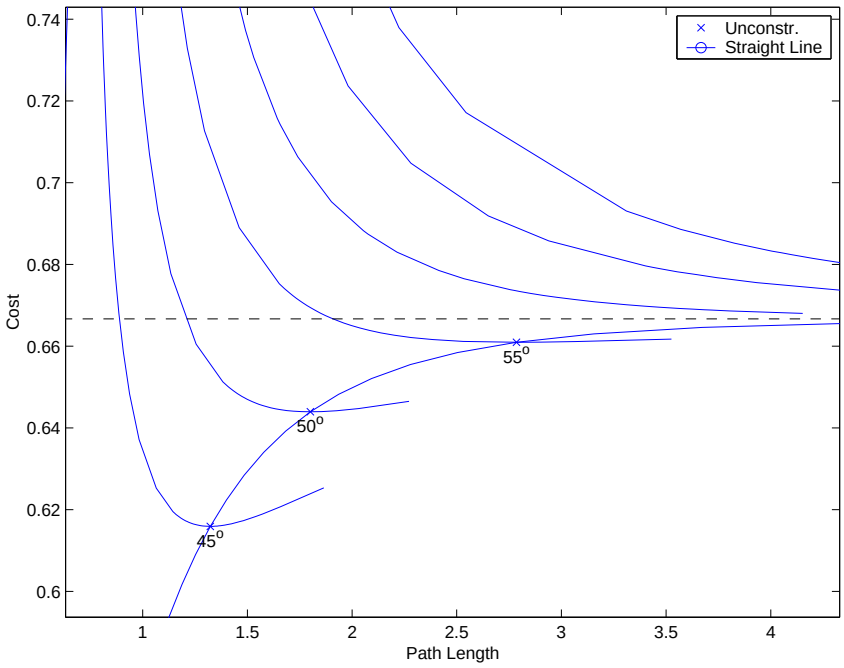

Figure 5.11 Zoomed Image of Optimal Trajectories of Path Length Constrained Problems for $R_o = R_f$, $\theta_f = 45°, 50°, 55°, 60°, 65°, 70°$

the functional optimization problem to a parameter optimization problem. While this method seems more sensitive to numerical issues than the shooting method, it readily handles constraints. The shooting method demonstrates excellent numerical properties for the radar exposure minimization problem and is suitable for the path length constrained problem. The shooting method will be the primary numerical tool employed in the remainder of this dissertation.

In the next chapter, several applications of the methods developed thus far will be presented. First, the cooperative control problem of isochronous rendezvous will be addressed using the path length constrained formulation of the radar exposure minimization problem. Next, the problem of one vehicle minimizing exposure to two radars is addressed numerically and analytically. Finally, a suboptimal method is developed which extends the two radar problem to n-radars.

VI. Radar Exposure Minimization: Application and Extension

6.1 Introduction

In this chapter, we examine the application and extension of the results of the previous chapters on radar exposure minimization. First, we examine the cooperative control problem of multiple vehicle isochronous rendezvous in the context of radar exposure minimization. The solution of a representative two-ship cooperative control problem is presented. Next, the problem of radar exposure minimization is extended to the case of two radars. Numerical and analytical results are sought. Finally, a sub-optimal algorithm is developed which handles the case of radar exposure minimization for n-radars and it's limitations are discussed.

6.2 Multiple Vehicle Isochronous Rendezvous

In order to extend the single vehicle radar exposure minimization problem to multiple vehicles, we must allow for optimal paths of prespecified length. Although a closed form solution of the Euler equation for the path length constrained radar problem is out of reach, numerical methods developed in Chapter V are available to study this problem. The shooting method is employed for solving this class of problems.

Consider the problem of coordinating the isochronous rendezvous of two or more air vehicles such that they reach the target, at the same time, while minimizing their cumulative exposure to a radar. A hierarchical control structure is envisioned. Two decision levels are considered.

At the lower level, for each air vehicle a constrained path length optimal control problem is considered. The costs for various path lengths are separately calculated for each vehicle, from a minimum length path, i.e., a straight line, to some maximum length path. It is envisioned that tables of cost vs. time (path length) are then provided by each vehicle to the higher level, a central decision maker, who determines what time of arrival minimizes a composite cost function; the latter is the cumulative exposure to radar of the (two, or more) air vehicles. The air vehicles are then each provided with an optimal joint time of arrival by the central decision maker, and each air vehicle selects the optimal

(minimum exposure) path to perform the rendezvous, given the joint time of arrival (path length).

For example, consider a ship initially at $(r_1, \theta_1) = (1, 0^\circ)$. Consider a second ship at $(r_2, \theta_2) = (1.5, 10^\circ)$. With a radar located at the origin, the ships must rendezvous at the point $(r_f, \theta_f) = (1, 45^\circ)$; see, e.g., Fig 6.1. For this problem, we assume the vehicles move at the same constant speed, thus time of arrival can be equated to path length.

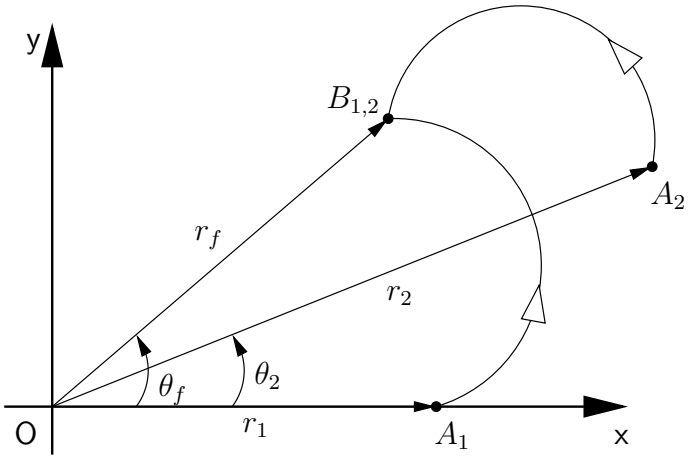

Figure 6.1 Cooperative Isochronous Rendezvous

Determining a series of optimal paths of varying length can be accomplished numerically, in this case by employing the shooting method, with Eqs. (5.12)-(5.15).

Remark 6.2.1. *The problem of the second ship can be solved by transforming to the equivalent problem,* $R_o = 1, R_f = 1.5\cos 10^\circ$ *and* $\theta_f = 35^\circ$. *The path would then be traversed backwards in time and shifted by* 45°, *i.e.,*

$$\theta_i = 45^\circ - \theta_j, \quad i = 1, 2, ..., N, \; j = N, N-1, ..., 1$$

In Fig. 6.2 we see a curve representing optimal path length versus cost for both vehicles. We note that the optimal path length for vehicle 1 is 1.3229. The optimal path length for vehicle 2 is 1.1646. Fig. 6.3 reflects the cumulative exposure cost function $J_1 * + J_2^*$. Each vehicle is commanded by the central decision maker to plan an optimal path of optimal length 1.2556 and the resulting trajectories are shown in Fig. 6.4. The

optimal path length $l^* = 1.2556$ is determined by the central decision maker to minimize the cumulative exposure $J_1^* + J_2^*$.

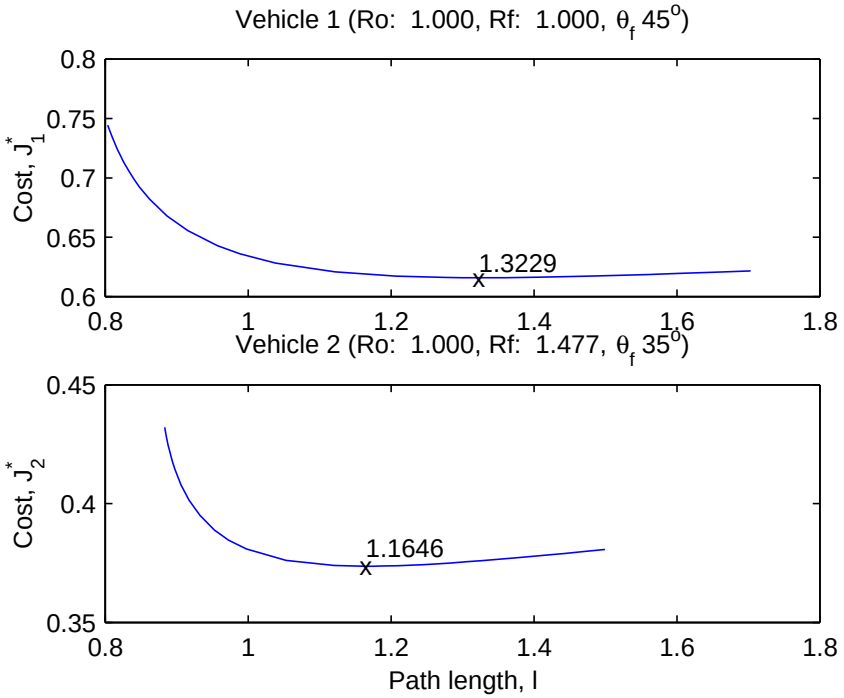

Figure 6.2 Curves of Optimal Cost vs. Path Length for Vehicles 1 and 2

Proposition 6.2.1. *The existence of an optimal solution to the isochronous rendezvous problem is not guaranteed. However, the proposed algorithm constructively settles the existence issue, and when an optimal solution exists, its synthesis is provided.*

Proof. Clearly, if the individual cost curves for vehicles attempting an isochronous rendezvous do not share a common path length, no composite cost curve can be constructed. This occurs when the maximum (minimum) achievable path length for one vehicle is less (greater) than the minimum (maximum) achievable path length of the second vehicle - see, e.g., Proposition 5.3.1 and Remark 5.3.1. □

6.3 Exposure Minimization: Two Radars

In Chapter III, optimal trajectories for radar exposure minimization were derived. The scenario comprised of one radar and one air vehicle (target). In this section, optimal

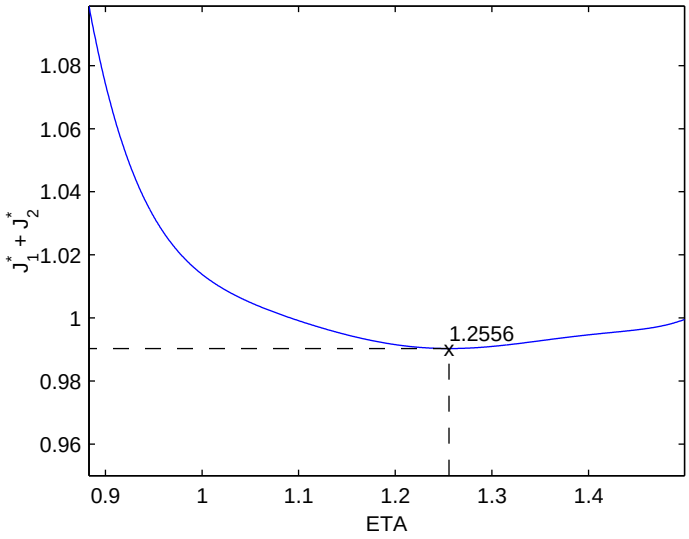

Figure 6.3 Composite Cost Curve Identifying the Optimal Time of Arrival

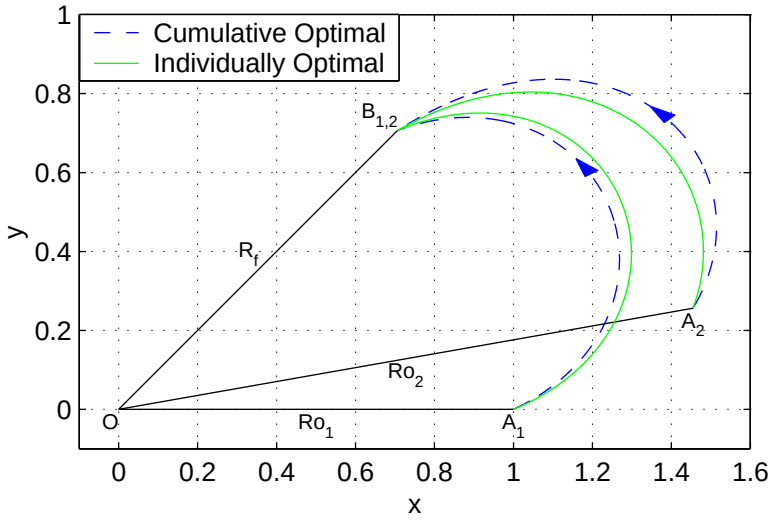

Figure 6.4 Trajectories for the Coordinated Isochronous Rendezvous Example

trajectories for minimizing the exposure to two radars are considered. This is an additional stepping stone in the development of optimal trajectories for multiple threat avoidance. The Voronoi diagram [33], constructed from the positions of the threat radars, has been suggested as a means to plan trajectories for multiple threat radar avoidance [12]. In Fig. 6.5, the Voronoi diagram for a 12 randomly located threats is shown. Path planning involves devising a path onto one of the Voronoi segments, performing a search using the Voronoi edges to build a minimum cost polygonal path, and lastly, exiting the Voronoi segment to arrive at the destination. The "minimum" exposure path connecting points A and B is shown in Fig. 6.5. Understanding the consequences of non-globally optimal solutions for complex optimization problems, such as the control of autonomous air vehicles, is essential.

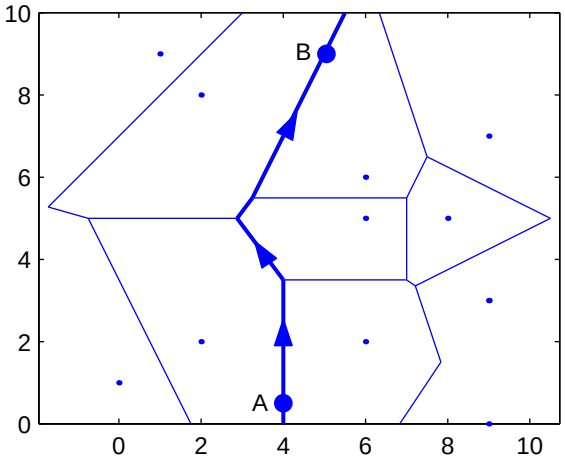

Figure 6.5 Voronoi Diagram for Representative Multiple Threat Avoidance Path Planning Scenario

In our problem, a Voronoi edge is the locus of all points of equal power separating the two radars. Specifically, for the case of two equal power radars, the Voronoi edge is the perpendicular bisector of the line connecting the two radars. When the two radars have unequal power, the Voronoi edge is an Apollonius circle [32, 19]. In this section, we are concerned with the optimality of the Voronoi path for the two radar exposure minimization problem. The question is addressed whether it is optimal to take the Voronoi path between, or go around, the two radars.

Consider an aircraft exposed to illumination by two tracking radars, as depicted in Fig. 6.6. Polar coordinates are used. Without loss of generality, the first radar is located at the origin, O, while the second radar is located at the point $(1, 0°)$. We wish to travel from point A at (R_o, θ_o) to point B at (R_f, θ_f) while minimizing the cumulative exposure to the two radars.

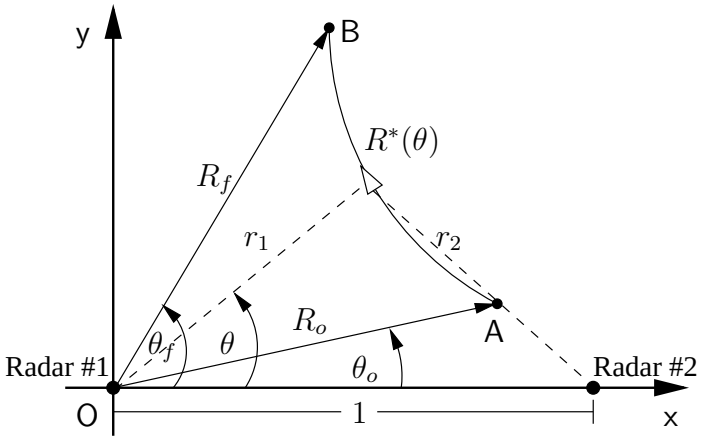

Figure 6.6 Optimal Avoidance of Two Radars

As shown in Fig. 6.6, the distances from the radars to the aircraft are given by

$$r_1 = R(\theta)$$

and

$$r_2 = \sqrt{R^2(\theta) - 2\,R(\theta)\,\cos\theta + 1}$$

Furthermore, if we consider that the two radars have a power ratio of $(\alpha : 1)$ we have the weighted sum

$$\begin{aligned} G[\theta, R(\theta)] &= \frac{\alpha}{{r_1}^4} + \frac{1}{{r_2}^4} \\ &= \frac{\alpha}{R^4(\theta)} + \frac{1}{\left(R^2(\theta) - 2R(\theta)\cos\theta + 1\right)^2} \end{aligned} \tag{6.3}$$

We wish to find $R(\theta)$ which minimizes a cost functional of the form

$$\begin{aligned} J &= \int_{\theta_o}^{\theta_f} F[\theta, R(\theta), \dot{R}(\theta)]\, d\theta \\ &= \int_{\theta_o}^{\theta_f} G[\theta, R(\theta)] \sqrt{\dot{R}^2(\theta) + R^2(\theta)}\, d\theta \end{aligned} \tag{6.4}$$

and satisfies the boundary conditions $R(\theta_o) = R_o$, $R(\theta_f) = R_f$.

A necessary condition for the functional Eq. (6.4) to be extremized, is that the the Euler equation

$$\begin{aligned} F_R - \frac{d}{d\theta} F_{\dot{R}} &= 0 \\ \Rightarrow \quad F_R - F_{\dot{R}\theta} - \dot{R} F_{\dot{R}R} - \ddot{R} F_{\dot{R}\dot{R}} &= 0 \end{aligned} \tag{6.5}$$

be satisfied. We can write

$$\begin{aligned} F_{\dot{R}} &= G_{\dot{R}} \sqrt{\dot{R}^2 + R^2} + G \frac{\dot{R}}{\sqrt{\dot{R}^2 + R^2}} \\ &= G \frac{\dot{R}}{\sqrt{\dot{R}^2 + R^2}} \\ &= \frac{\dot{R}}{\dot{R}^2 + R^2} F \end{aligned}$$

Thus, we obtain the partial derivatives

$$\begin{aligned} F_{\dot{R}\dot{R}} &= \frac{\dot{R}}{\dot{R}^2 + R^2} F_{\dot{R}} + \frac{R^2 - \dot{R}^2}{\left(\dot{R}^2 + R^2\right)^2} F \\ &= \frac{R^2}{\left(\dot{R}^2 + R^2\right)^2} F \end{aligned} \tag{6.6}$$

$$F_{\dot{R}R} = \frac{-2\dot{R}R}{\left(\dot{R}^2 + R^2\right)^2} F + \frac{\dot{R}}{\dot{R}^2 + R^2} F_R \tag{6.7}$$

$$F_{\dot{R}\theta} = \frac{\dot{R}}{\dot{R}^2 + R^2} F_\theta \tag{6.8}$$

We can now substitute Eqs. (6.6)-(6.8) into the Euler Equation, Eq. (6.5), yielding

$$\frac{R^2}{\dot{R}^2+R^2}F_R - \frac{\dot{R}}{\dot{R}^2+R^2}F_\theta - \frac{R\left(\ddot{R}R-2\dot{R}^2\right)}{\left(\dot{R}^2+R^2\right)^2}F = 0 \tag{6.9}$$

From Eq. (6.4) we have

$$F = G\sqrt{\dot{R}^2+R^2} \tag{6.10}$$

and we obtain

$$F_\theta = G_\theta\sqrt{\dot{R}^2+R^2} \tag{6.11}$$

$$F_R = G_R\sqrt{\dot{R}^2+R^2} + G\frac{R}{\sqrt{\dot{R}^2+R^2}} \tag{6.12}$$

Substituting Eqs. (6.10)-(6.12) into Eq. (6.9), and since $R \geq 0$ and $\dot{R}^2 > 0$, we obtain

$$R^2G_R - \dot{R}G_\theta - \frac{R^2\,G}{\dot{R}^2+R^2}\left(\ddot{R}+R\right) + 2RG = 0 \tag{6.13}$$

From Eq. (6.3) we have

$$G_R = \frac{4\left(\cos\theta - R\right)}{\left(R^2-2\,R\,\cos\theta+1\right)^3} - \frac{4\alpha}{R^5} \tag{6.14}$$

$$G_\theta = -\frac{4\,R\,\sin\theta}{\left(R^2-2\,R\,\cos\theta+1\right)^3} \tag{6.15}$$

Eq. (6.13) can be expressed as

$$R\frac{G}{G_\theta}\left(\frac{R}{\dot{R}^2+R^2}\left(\ddot{R}+R\right)-2\right) - R^2\frac{G_R}{G_\theta} + \dot{R} = 0 \tag{6.16}$$

Now,

$$\frac{G}{G_\theta} = -\frac{R^2-2\,R\,\cos\theta+1}{4\,R\sin\theta}\left[1+\frac{\alpha\left(R^2-2\,R\,\cos\theta+1\right)^2}{R^4}\right] \tag{6.17}$$

and

$$\frac{G_R}{G_\theta} = -\frac{1}{R\sin\theta}\left[\cos\theta - R - \alpha\frac{\left(R^2 - 2\,R\,\cos\theta + 1\right)^3}{R^5}\right] \tag{6.18}$$

Substituting Eqs.(6.17) and (6.18) into Eq. (6.16), we obtain

$$\frac{1}{2}\frac{R}{\dot{R}^2 + R^2}\left(\ddot{R} + R\right)\left(R^2 - 2\,R\,\cos\theta + 1 + \alpha\frac{\left(R^2 - 2\,R\,\cos\theta + 1\right)^3}{R^4}\right)$$
$$+ R^2 - 2\,\dot{R}\sin\theta - 1 + \alpha\frac{\left(R^2 - 2\,R\,\cos\theta + 1\right)^3}{R^4} = 0 \tag{6.19}$$

An analytic solution to Eq. (6.19) appears out of reach. Hence, numerical methods must be applied to examine the nature of the extremal trajectories. Solving Eq. (6.19) for $\ddot{R}(\theta)$, we obtain

$$\ddot{R} = -R + \frac{2(\dot{R}^2 + R^2)}{R}\left(\frac{R^4(1 - R^2 + 2\,\dot{R}\sin\theta) - \alpha\left(R^2 - 2\,R\,\cos\theta + 1\right)^3}{R^4\left(R^2 - 2\,R\,\cos\theta + 1\right) + \alpha\left(R^2 - 2\,R\,\cos\theta + 1\right)^3}\right) \tag{6.20}$$

which is numerically integrated using the shooting method.

As an example, let each radar be of equal power, i.e., $\alpha = 1$. Suppose we wish to travel from point A, located at $(-1/2, -1/2)$ to point B, located at $(1/2, 1/2)$, while minimizing the cumulative exposure to both radars. The resulting optimal trajectory is shown in Fig. 6.7; we see that while a swerve maneuver is initially performed, the solution of the Euler equation is essentially "attracted" to the Voronoi edge, i.e., the perpendicular bisector of the line joining the two radars.

Several scenarios were useful in validating the algorithm used to generate trajectories for the two radar case. First, both radars were placed at the origin and the start and endpoints were configured such that $\theta_f - \theta_o < 60^\circ$. The results of the numerical integration were compared to the analytic result from Eq. (3.4). Several cases were generated and the trajectories and path lengths agreed with the analytic results to the numerical precision specified. The cost calculated by the numerical scheme was twice that of the one radar case. Additionally, several cases were examined where the line segments connecting the two

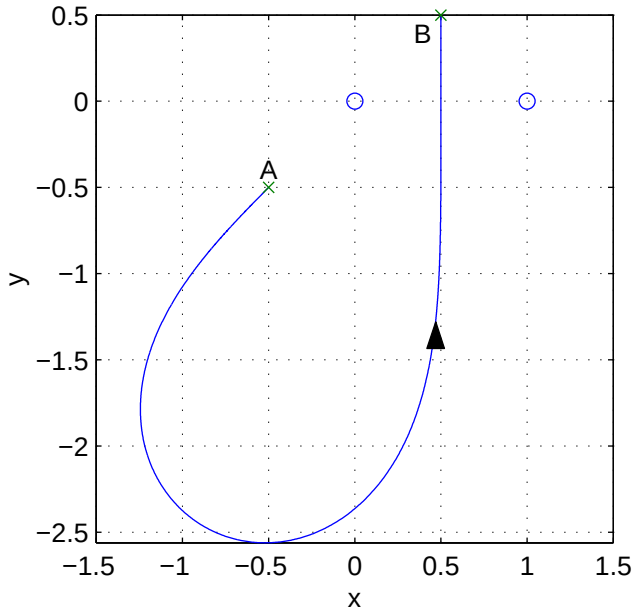

Figure 6.7 Trajectory for Two Radar Exposure Minimization, Obtained by the Shooting Method, Radars Located at $(0,0)$ and $(1,0)$

radars and the points A and B lay on the Voronoi edge. As expected, Fig. 6.8 shows that the extremizing curve obtained by the shooting method is a straight line. The optimality of the Voronoi edge is discussed in the next section.

From the analytical results obtained in the one radar exposure minimization problem in Chapter III, it is also evident that for the case of multiple radars, a path length constraint would be required to make *some* problems well posed. For example, if we move the second radar in Fig. 6.7 from $(1,0)$ to $(0,0)$, we recover the one radar exposure minimization problem with the angle θ_f included between the radials to points A and B, $180^\circ \geq \theta_f \geq 60^\circ$. We already know, for this case, the unconstrained problem is not well posed. Other geometries could also be ill posed.

For the constrained formulation, we wish to find the optimal trajectory $R^*(\theta)$ which minimizes exposure to both radars, connecting points A and B while the subsidiary condition

$$L[R(\theta)] = \sqrt{\dot{R}^2(\theta) + R^2(\theta)} = l$$

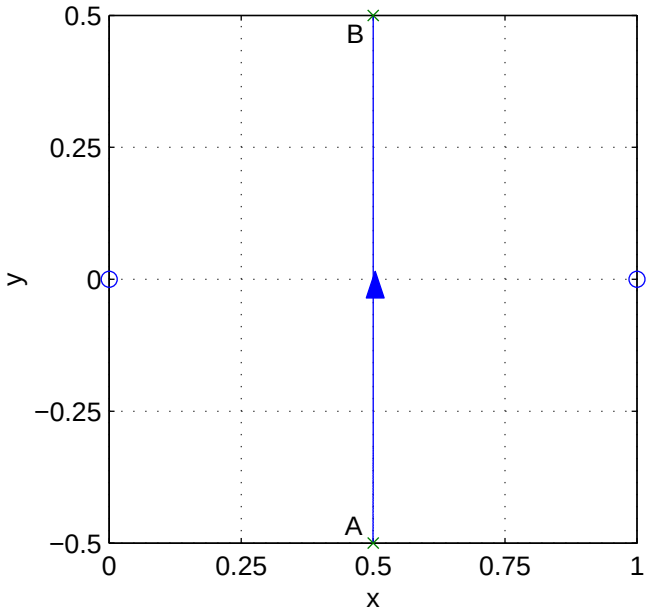

Figure 6.8 Trajectory for Two Radar Exposure Minimization, Obtained by the Shooting Method, Radars Located at $(0,0)$ and $(1,0)$

applies. Thus, we wish to find $R^*(\theta)$, which minimizes the augmented functional

$$J[R(\theta)] = \int_{\theta_o}^{\theta_f} \left(\frac{\alpha}{R^4(\theta)} + \frac{1}{{r_2}^4\,[\theta, R(\theta)]} + \lambda \right) \sqrt{\dot{R}^2(\theta) + R^2(\theta)}\; d\theta \tag{6.21}$$

where λ is a Lagrange multiplier. Thus,

$$G[\theta, R(\theta)] = \frac{\alpha}{R^4(\theta)} + \frac{1}{\left(R^2(\theta) - 2\,R(\theta)\cos\theta + 1\right)^2} + \lambda \tag{6.22}$$

depends only on θ and $R(\theta)$, and Eqs. (6.16) applies. The partial derivatives G_R and G_θ remain unchanged. Hence the ratio $\frac{G_R}{G_\theta}$ given in Eq. (6.18) applies and

$$\frac{G}{G_\theta} = -\frac{R^2 - 2\,R\,\cos\theta + 1}{4\,R\sin\theta} \left[1 + \left(\frac{\alpha}{R^4} + \lambda \right) \left(R^2 - 2\,R\,\cos\theta + 1 \right)^2 \right] \tag{6.23}$$

Substituting Eqs.(6.23) and (6.18) into Eq. (6.16), we obtain

$$\frac{1}{2}\frac{R}{\dot{R}^2+R^2}\left(\ddot{R}+R\right)\left(R^2-2\,R\,\cos\theta+1+\left(\frac{\alpha}{R^4}+\lambda\right)\left(R^2-2\,R\,\cos\theta+1\right)^3\right)$$
$$+R^2-2\,\dot{R}\sin\theta-1+\left(\frac{\alpha}{R^4}-\lambda\right)\left(R^2-2\,R\,\cos\theta+1\right)^3=0 \quad (6.24)$$

Solving Eq. (6.19) for $\ddot{R}(\theta)$, we obtain

$$\ddot{R}=-R+\frac{2(\dot{R}^2+R^2)}{R}\left(\frac{R^4(1-R^2+2\,\dot{R}\sin\theta)+(R^4\lambda-\alpha)\left(R^2-2\,R\,\cos\theta+1\right)^3}{R^4\left(R^2-2\,R\,\cos\theta+1\right)+(\alpha+R^4\lambda)\left(R^2-2\,R\,\cos\theta+1\right)^3}\right) \quad (6.25)$$

Eq. (6.25) is evaluated using constrained shooting technique described in Sec. 5.3.2.

6.3.1 Local vs. Global Optimality of Solutions. A fundamental question in the two radar exposure minimization problem is whether the best policy is to travel on the Voronoi edge, or around, the two radars. Insights into this question are obtained by examining the relationship between locally and globally optimal solutions.

6.3.1.1 Equal Power Radars. Consider the symmetric exposure minimization problem for two equal-power radars, when the points, A and B, lie on the perpendicular bisector of the line joining the two radars. Cartesian coordinates are now used, and the two radars are located on the y-axis, each a distance $a = 1/2$ from the origin - see, e.g., Fig. 6.9. In Appendix C, it is shown that the perpendicular bisector is a local minimizer of the functional, defined by Eqs. (6.3) and (6.4), given that the points A and B lie on the bisector.

The cost incurred in travelling along this line from point A to point B is

$$J_A^B = 2\int_{\tilde{R}_o}^{\tilde{R}_f}\frac{\sqrt{1+y'(x)^2}}{\left(a^2+x^2\right)^2}\,dx$$
$$= 2\int_{\tilde{R}_o}^{\tilde{R}_f}\frac{1}{\left(a^2+x^2\right)^2}\,dx$$

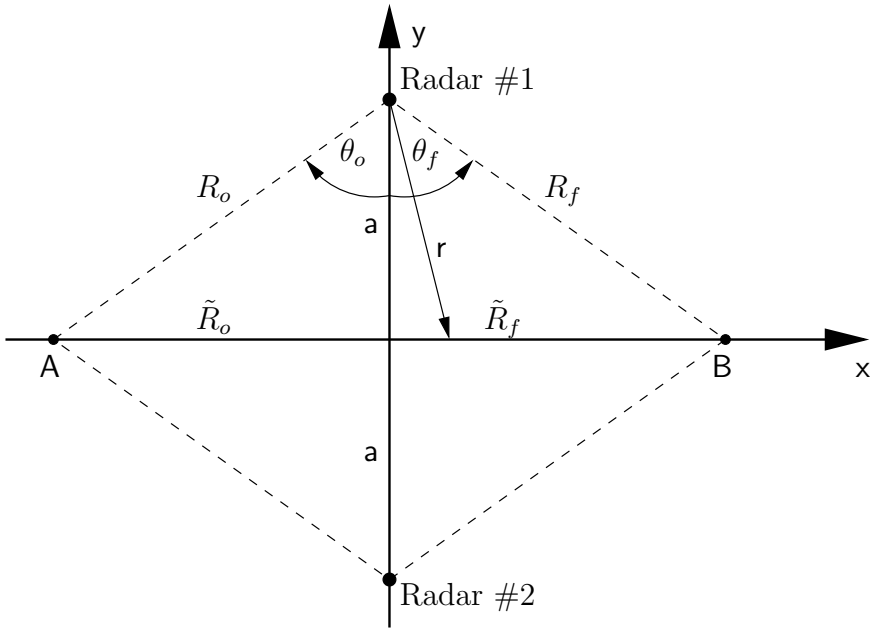

Figure 6.9 Two Equal-Power Radars: Perpendicular Bisector Path

since $y'(x) = 0$ along the perpendicular bisector in our chosen coordinate frame. Let

$$x = a \tan\theta \quad \Longrightarrow \; dx = a \sec^2\theta \; d\theta \tag{6.26}$$

Thus, the integral

$$\begin{aligned} J_A^B &= \frac{2}{a^3} \int_{-\operatorname{Arctan}\left(\tilde{R}_o/a\right)}^{\operatorname{Arctan}\left(\tilde{R}_f/a\right)} \cos^2\theta \; d\theta \\ &= \frac{1}{a^3} \int_{-\theta_o}^{\theta_f} (1 + \cos 2\theta) \; d\theta \\ &= \frac{1}{a^3} \left(\theta_f + \theta_o + \frac{1}{2}\sin 2\theta_f + \frac{1}{2}\sin 2\theta_o \right) \end{aligned} \tag{6.27}$$

is the total cost of traversing the path from point A to point B.

Now take an alternate route "around" the radars by following the path from point A to $-\infty$ to ∞ to B. The cost is obtained by

$$J_A^{-\infty} + J_\infty^B = 2 \left[\int_{\tilde{R}_f}^{\infty} \frac{1}{\left(a^2 + x^2\right)^2} \, dx + \int_{\tilde{R}_o}^{\infty} \frac{1}{\left(a^2 + x^2\right)^2} \, dx \right]$$

Using the transformation (6.26), we evaluate

$$\begin{aligned} J_A^{-\infty} + J_\infty^B &= \frac{1}{a^3}\left[\int_{\theta_f}^{\pi/2} (1+\cos 2\theta)\ d\theta + \int_{\theta_o}^{\pi/2} (1+\cos 2\theta)\ d\theta\right] \\ &= \frac{1}{a^3}\left(\pi - \theta_f - \theta_o - \frac{1}{2}\sin 2\theta_f - \frac{1}{2}\sin 2\theta_o\right) \\ &= \frac{\pi}{a^3} - J_A^B \end{aligned} \tag{6.28}$$

Hence,the cost of traversing the entire perpendicular bisector, i.e., from $-\infty$ to ∞, is

$$J_A^B + \left(J_A^{-\infty} + J_\infty^B\right) = \frac{\pi}{a^3}$$

Given $a = 1/2$, if the cost of a segment between any points A and B along the perpendicular bisector exceeds 4π, the segment cannot be globally optimal.

Lemma 6.3.1. *Consider the fully symmetric case: $\theta_o = \theta_f = \theta$. There exists a critical angle of separation, $\theta_c = 2\theta \approx 47.6535°$, beyond which the path AB between the two radars is no longer globally optimal.*

Proof. Given $\theta_o = \theta_f = \theta$, the cost to take the path between the two radars, is

$$J_A^B = \frac{1}{a^3}\left(2\theta + \sin 2\theta\right)$$

Similarly, the cost to "go around" the radars is

$$J_A^{-\infty} + J_\infty^B = \frac{1}{a^3}\left(\pi - 2\theta - \sin 2\theta\right)$$

Equating J_A^B and $J_A^{-\infty} + J_\infty^B$ yields

$$2\theta + \sin 2\theta = \pi/2 \tag{6.29}$$

Solving the transcendental Eq. (6.29) for θ is accomplished numerically, and results in the unique solution

$$\theta \approx 23.8268°$$

to four significant digits. Thus, the critical angle of separation is

$$\theta_c = 2\theta \approx 47.6535^\circ$$

When $\theta > \theta_c$, we have $J_A^{-\infty} + J_\infty^B < J_A^B$, thus the path *between* the radars cannot be globally optimal. □

Moreover, the following holds.

Theorem 6.3.1. *For minimizing the exposure to two equal power radars, where the start and end points of the trajectory lie upon the perpendicular bisector separating the two radars, define the ratio*

$$\begin{aligned} \mathcal{D} &= \frac{J_A^B}{J_A^{-\infty} + J_\infty^B} \\ &= \frac{\theta_f + \theta_o + \frac{1}{2}\sin 2\theta_f + \frac{1}{2}\sin 2\theta_o}{\pi - \theta_f - \theta_o - \frac{1}{2}\sin 2\theta_f - \frac{1}{2}\sin 2\theta_o} \end{aligned} \tag{6.30}$$

where $\mathcal{D}(\theta_o, \theta_f)$, $\theta_o, \theta_f \in [0, \pi/2]$, is a decision variable. If $\mathcal{D}(\theta_o, \theta_f) > 1$, then the globally optimal policy is to go around the two radars and if $\mathcal{D}(\theta_o, \theta_f) < 1$, then the globally optimal policy is to go between the two radars.

Proof. For the case where the start and end points lie on the perpendicular bisector, viz., the line which is the locus of all equal power points, the trajectory that minimizes the radar exposure cannot deviate from that line. The only two candidate minimizers involve following the path from A to B, i.e., "between" the two radars, or the path from A to ∞ and from $-\infty$ to B, i.e., "around" the two radars. Thus, by definition, the function $\mathcal{D}$ discriminates between the globally optimal trajectory and a locally optimal trajectory. □

Corollary 6.3.1. *For the problem of Theorem 6.3.1,*

$$\mathcal{D} < 1 \Leftrightarrow J_A^B < 4\pi$$

Proof. This follows from the previous discussion. □

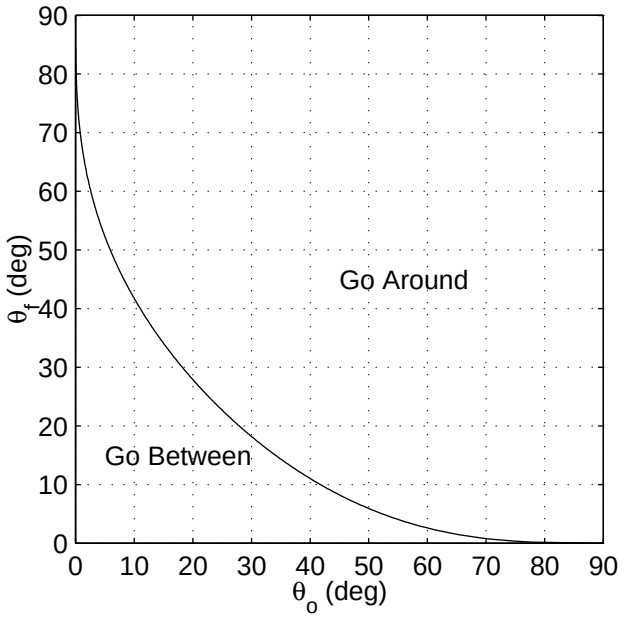

Figure 6.10 Go Around or Go Between Decision Boundary for the Case of Equal Power Radars and Endpoints on the Perpendicular Bisector

Evaluating Eq. (6.30) over the entire domain of θ_o and θ_f yields a boundary curve that separates the 'space' defined by (θ_o, θ_f) into two distinct regions. *For any* (θ_o, θ_f) *pair, the decision to "go around" or "go between" the two radars can be made by referring to the curve* $\mathcal{D}(\theta_o, \theta_f)$*, as depicted in Fig. 6.10.* As can be seen, for the majority of problem geometries, it is better to go around the radars than between them. Theoretically, going around the two radars involves following a path of infinite length. In practical terms air vehicle paths are limited by mission, fuel and time constraints. The go-around path is still very useful, as it provides a lower bound of the best achievable cost.

Endpoints Off the Voronoi Edge. It is also of interest to examine the relationship between the "go around" and "go between" paths for cases where one or both of the endpoints do not lie on the perpendicular bisector. Analytic results are difficult to obtain without a closed form solution for the extremizing trajectory.

Instead, a study of curves obtained from the Euler equation (6.25) is performed. We consider the following geometry expressed in Cartesian coordinates:

- Points A: $(-0.5, 0^{\pm})$, B: $(0.5, 0.5)$

- Radars : $(0, 0)$ and $(1, 0)$

It was observed that this geometry provides a means to control whether the solution of the Euler equation (obtained numerically by a shooting technique), went "around" or "between" the two radars. When the y-axis coordinate of the point A is positive, albeit infinitesimally small, viz. 0^+, the solution to the Euler equation will result in a path "around" the two radars. Conversely, if the y-axis coordinate of the point A is negative, yet albeit infinitesimally small, viz. 0^-, the solution to the Euler equation will result in a path "between" the two radars. In order to make the optimization problem well posed, a constraint is required to bound the path length, viz., $\lambda > 0$ in Eq. (6.25).

Fig. 6.11 shows some of the paths "around" and "between" the radars, beginning with the shortest possible distance $\lambda \to \infty$ and then relaxing the path length constraint. For the "go around" case, when $\lambda \to \infty$ we obtain a straight line connecting the points A and B. For the geometry described above, this results in a cost approaching 145.782 and a path length of $\sqrt{2}/2$. Alternatively, for the "go between" case, as $\lambda \to \infty$, we obtain two straight line segments connecting the point A with the point B while going through the radar at the origin. While the cost in this case becomes infinite, the path length approaches $(1 + \sqrt{2})/2$.

As with the one radar exposure minimization problem, although the path length grows without bounds, the cost appears to be bounded. Fig. 6.12 depicts the curves of cost vs. path length for the "go around" and "go between" trajectories. While it may seem obvious from the geometry alone, the analysis clearly shows that going around the two radars always results in the lower cost, for the given geometry. It is easy to imagine that for other geometries, the two curves may intersect, that is, there may be cases when the decision to "go around" or "go between" is not as obvious.

6.3.1.2 Unequal Power Radars. Consider the radar exposure minimization problem for two unequal power radars. The radars are located at (x_i, y_i), for $i = 1, 2$, in the xy-plane. The power ratio is $\alpha > 0$. The locus of all points of equal power, viz.,

$$\frac{\alpha}{{R_1}^4(\theta)} = \frac{1}{{R_2}^4(\theta)}$$

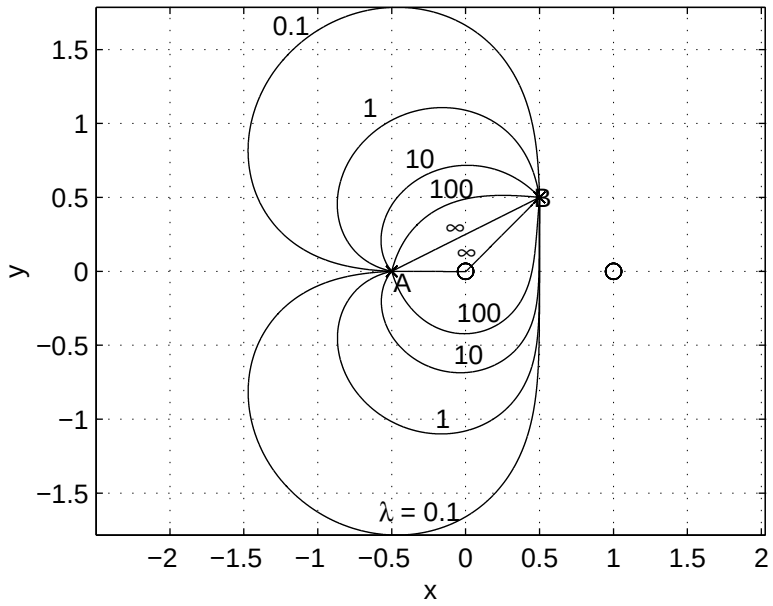

Figure 6.11 Path Length Constrained Trajectories Around and Between Two Radars for $\lambda = \{0.1, 1, 10, 100, \rightarrow \infty\}$

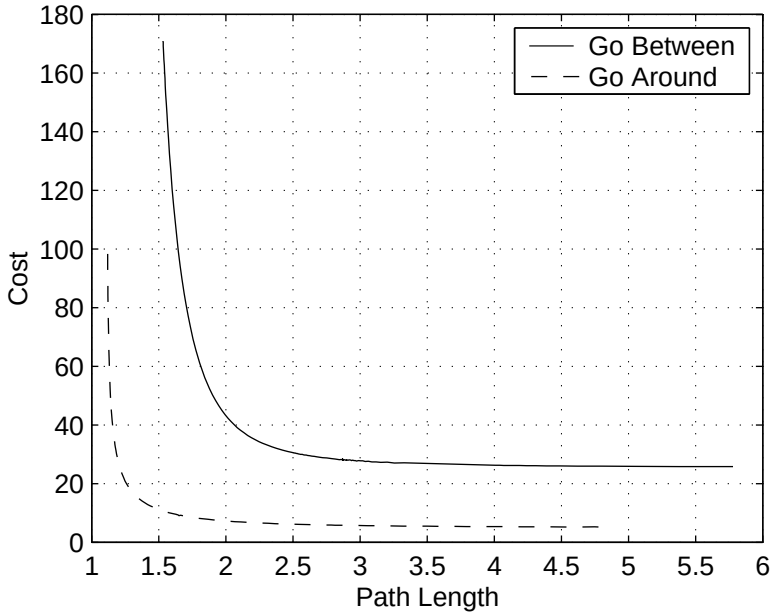

Figure 6.12 Comparison of Cost vs. Path Length for Constrained Trajectories Around and Between Two Radars

from the two radars is an Apollonius circle, centered at (x_a, y_a), with

$$x_a = \frac{x_2 - c\,x_1}{1-c} \tag{6.31}$$

$$y_a = \frac{y_2 - c\,y_1}{1-c} \tag{6.32}$$

and radius r,

$$r = \frac{\sqrt{c}}{1-c}\,d \tag{6.33}$$

where

$$d = \sqrt{(x_1 - x_2)^2 + (y_1 - y_2)^2}$$

is the distance between the two radars and

$$c = \frac{1}{\sqrt{\alpha}}$$

is determined by the two radar's power ratio.

We wish to traverse a segment of the Apollonius circle, from point A to point B as shown in Fig. 6.13. The cost can be expressed as the summation of the cost from the first radar with the cost from the second radar, i.e.,

$$J = \int_{\theta_A}^{\theta_B} \frac{\sqrt{{R_1}^2(\theta) + \dot{R_1}^2(\theta)}}{{R_1}^4(\theta)}\,d\theta + \int_{\theta_A}^{\theta_B} \frac{\sqrt{{R_2}^2(\theta) + \dot{R_2}^2(\theta)}}{{R_2}^4(\theta)}\,d\theta$$

However, our chosen path from A to B lies on the locus of equal power points. That is, the cost to traverse the path from A to B due to the first radar is equivalent to the cost imposed by the second radar. Thus, we let $R(\theta) = R_2(\theta)$ and write

$$J = 2\int_{\theta_A}^{\theta_B} \frac{\sqrt{R^2(\theta) + \dot{R}^2(\theta)}}{R^4(\theta)}\,d\theta \tag{6.34}$$

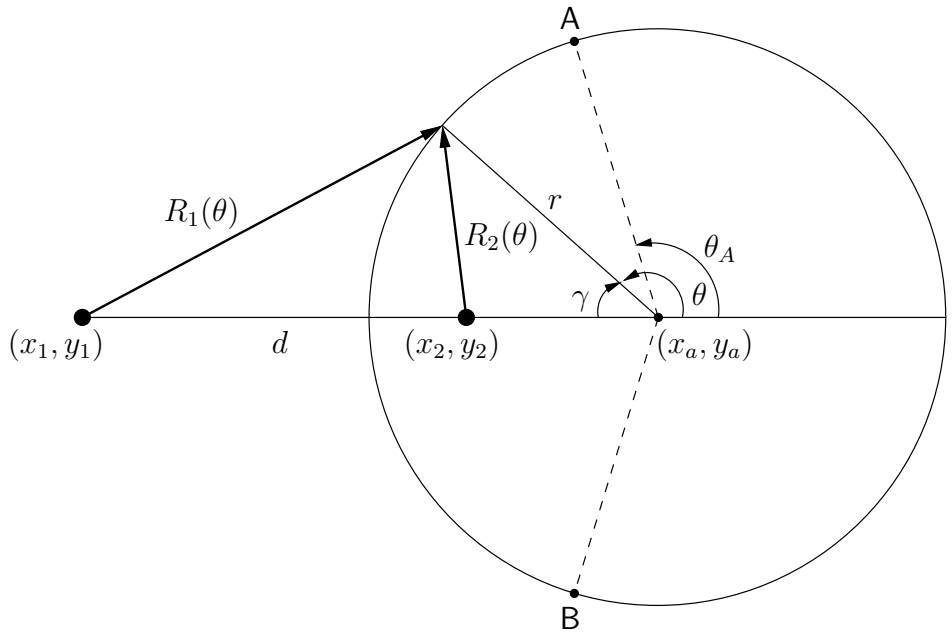

Figure 6.13 Apollonius Circle for the Case of Two Unequal Power Radars

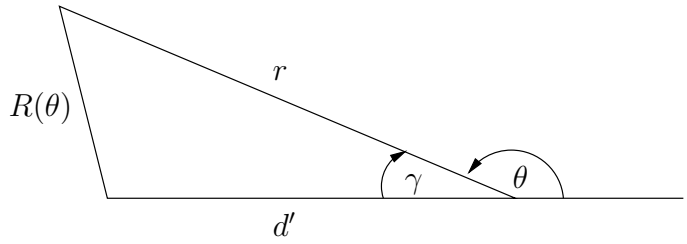

Figure 6.14 Solution Triangle

To calculate $R(\theta)$, we evaluate the solution triangle in Fig. 6.14 where

$$\gamma = |\pi - \theta|$$

and the distance between the center of the Apollonius circle and the second radar is

$$d' = \sqrt{(x_a - x_2)^2 + (y_a - y_2)^2} \tag{6.35}$$

We have

$$
\begin{aligned}
R^2(\theta) &= d'^2 + r^2 - 2\,r\,d'\cos\gamma \\
&= d'^2 + r^2 - 2\,r\,d'\cos|\pi-\theta| \\
&= d'^2 + r^2 - 2\,r\,d'\cos(\pi-\theta) \\
&= d'^2 + r^2 + 2\,r\,d'\cos\theta
\end{aligned} \tag{6.36}
$$

Substituting Eqs. (6.31) and (6.32) into Eq. (6.35) yields

$$
\begin{aligned}
d' &= \sqrt{\left(\frac{x_2 - c\,x_1}{1-c} - x_2\right)^2 + \left(\frac{y_2 - c\,y_1}{1-c} - y_2\right)^2} \\
&= \sqrt{\left(\frac{x_2 - c\,x_1 - x_2 + c\,x_2}{1-c}\right)^2 + \left(\frac{y_2 - c\,y_1 - y_2 + c\,y_2}{1-c}\right)^2} \\
&= \sqrt{\left(\frac{c}{1-c}\right)^2 (x_2-x_1)^2 + \left(\frac{c}{1-c}\right)^2 (y_2-y_1)^2} \\
&= \left(\frac{c}{1-c}\right)\sqrt{(x_2-x_1)^2 + (y_2-y_1)^2} \\
&= \left(\frac{c}{1-c}\right) d
\end{aligned} \tag{6.37}
$$

Substituting Eq. (6.37) into Eq. (6.36) we obtain

$$
R^2(\theta) = \left(\frac{c}{1-c}\right)^2 d^2 + r^2 + 2\left(\frac{c}{1-c}\right) r\,d\cos\theta \tag{6.38}
$$

Subsituting Eq. (6.33) into Eq. (6.38) yields

$$
\begin{aligned}
R^2(\theta) &= \left(\frac{c}{1-c}\right)^2 d^2 + \frac{c}{(1-c)^2}\,d^2 + \frac{2}{\sqrt{c}}\left(\frac{c}{1-c}\right)^2 d^2\cos\theta \\
&= \left(\frac{c}{1-c}\right)^2 d^2\left[1 + \frac{1}{c} + \frac{2}{\sqrt{c}}\cos\theta\right]
\end{aligned} \tag{6.39}
$$

Thus, we obtain the following expression for $R(\theta)$,

$$
R(\theta) = \left(\frac{c}{1-c}\right) d\sqrt{1 + \frac{1}{c} + \frac{2}{\sqrt{c}}\cos\theta} \tag{6.40}
$$

Differentiating yields

$$\begin{aligned}\dot{R}(\theta) &= -\left(\frac{c}{1-c}\right) d \frac{\frac{1}{\sqrt{c}}\sin\theta}{\sqrt{1+\frac{1}{c}+\frac{2}{\sqrt{c}}\cos\theta}} \\ &= -R(\theta)\frac{\frac{1}{\sqrt{c}}\sin\theta}{1+\frac{1}{c}+\frac{2}{\sqrt{c}}\cos\theta} \end{aligned} \tag{6.41}$$

Substituting Eqs.(6.40) and (6.41) into the cost function, Eq. (6.34)

$$\begin{aligned} J_A^B &= 2\int_{\theta_A}^{\theta_B} \frac{\sqrt{R^2(\theta) + R^2(\theta)\left(\frac{\frac{1}{\sqrt{c}}\sin\theta}{1+\frac{1}{c}+\frac{2}{\sqrt{c}}\cos\theta}\right)}}{R^4(\theta)}\, d\theta \\ &= 2\int_{\theta_A}^{\theta_B} \frac{\sqrt{1+\frac{\frac{1}{\sqrt{c}}\sin\theta}{1+\frac{1}{c}+\frac{2}{\sqrt{c}}\cos\theta}}}{R^3(\theta)}\, d\theta \\ &= 2\int_{\theta_A}^{\theta_B} \frac{\sqrt{\frac{1+\frac{1}{c}+\frac{2}{\sqrt{c}}\cos\theta+\frac{1}{\sqrt{c}}\sin\theta}{1+\frac{1}{c}+\frac{2}{\sqrt{c}}\cos\theta}}}{\left[\left(\frac{c}{1-c}\right) d\sqrt{1+\frac{1}{c}+\frac{2}{\sqrt{c}}\cos\theta}\right]^3}\, d\theta \\ &= 2\left(\frac{1-c}{c\,d}\right)^3 \int_{\theta_A}^{\theta_B} \frac{\sqrt{1+\frac{1}{c}+\frac{2}{\sqrt{c}}\cos\theta+\frac{1}{\sqrt{c}}\sin\theta}}{\left(1+\frac{1}{c}+\frac{2}{\sqrt{c}}\cos\theta\right)^2}\, d\theta \end{aligned}$$

yields an expression for the cost to traverse an arc AB of the Apollonius circle.

Without loss of generality, let $d = 1$ and consider $\theta_A \in [0, \pi)$ and $\theta_B \in (\pi, 2\pi)$. We define the decision variable

$$\begin{aligned}\mathcal{D} &= \frac{J_A^B}{J_B^A} \\ &= \frac{J_A^B}{J_0^{2\pi} - J_A^B}\end{aligned}$$

such that if $\mathcal{D} < 1$, then the optimal strategy is to travel from A to B in a counterclockwise fashion, going between the two radars. Conversely, if $\mathcal{D} > 1$, then the optimal strategy is to go around the two radars clockwise.

Fig. 6.15 depicts sample curves of the decision variable $\mathcal{D}$ vs. θ_A, for the case where $\theta_B = 13\pi/12$ and $c = \{2, 3, 4, 10\}$. We notice the curves of the decision variable $\mathcal{D}$ appear to be monotonic, and the break even point, viz., where $\mathcal{D} = 1$, is unique.

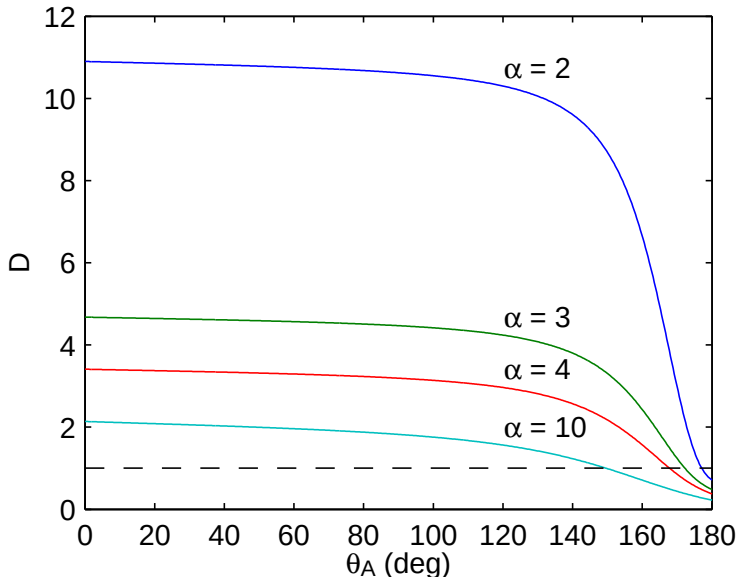

Figure 6.15 Decision Variable for Two Radars of Unequal Power, $\alpha = 2, 3, 4, 10$ and $\theta_B = 13\pi/12$

Consider a fully symmetric problem, depicted in Fig. 6.16, where we require $\pi - \theta_A = \theta_B - \pi$. For a given α, we wish to find some critical angle θ_C such that the cost to go between the two radars is equivalent to the cost to go around the radars, viz., $\mathcal{D} = 1$. The results are shown in Table. 6.1. It is important to note that the angle θ_c is measured from the center of the Apollonius circle. For the case of equal power radars mentioned previously, the critical angle was measured from the origin.

Table 6.1 Critical Angles for the Fully Symmetric Problem: Unequal Power Radars

α	Critical Angle, θ_C
2	14.37°
3	21.91°
4	27.05°
10	43.40°

By employing a root finding algorithm, the break even points are calculated for various values of the power ratio parameter α, as θ_A and θ_B are allowed to vary over their

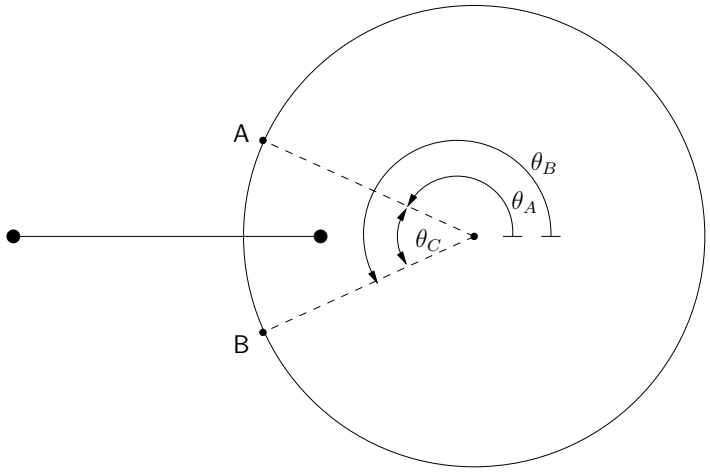

Figure 6.16 Depiction of a Symmetric Problem where $\mathcal{D} = 1$

domains. Fig. 6.17 depicts such a locus of break even points for $\alpha = 2, 3, 4, 10$. From studying Figs. 6.15 and 6.17, we see that the strategy of going between the two radars is generally only favored when θ_A is close to 180°. Values of θ_A significantly smaller than 180° requires θ_B to approach 180° as well, viz., the points A and B are close to each other. As expected, as $\theta_b \to 360°$, the break even point occurs when $\theta_A \to 180°$. Similarly, as $\theta_A \to 0°$ the break even point is found as $\theta_B \to 180°$.

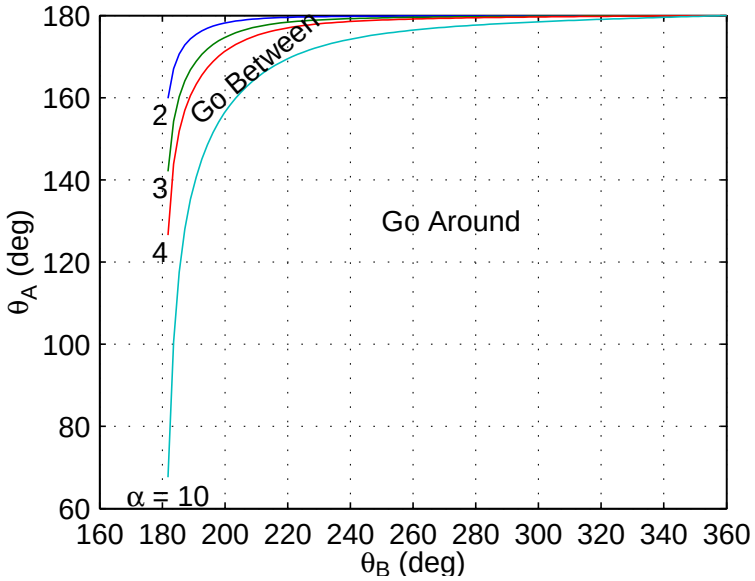

Figure 6.17 Locus of Break Even Points for Two Radars of Unequal Power, $\alpha = 2, 3, 4, 10$

6.4 Suboptimal Technique for Multiple Radar Avoidance

In the previous section, the optimal radar exposure minimization trajectory for the two radar case was developed. Extending this approach to more than two radars would be impractical. In this section, an alternative, albeit suboptimal, method is explored for multiple radar exposure minimization.

One approach to the multiple radar exposure minimization problem is to minimize exposure to the strongest (maximum) single source of radar energy. We consider the multiple radar problem to be a series of single radar exposure problems, viz.,

$$\min_{R(\theta)} \max_{J_i[R(\theta)]} \{J_i[R(\theta)]\}$$

such that

$$L[R(\theta)] = \int_0^{\theta_f} \sqrt{\dot{R}^2 + R^2}\, d\theta \leq l$$

where $J_i[R(\theta)]$ is the cost of the trajectory to avoid the i^{th} radar and the appropriate boundary conditions are satisfied.

Consider the following algorithm:

1. Identify the radar with the highest individual cost
2. Plan a path to avoid the radar which meets the path length constraint
3. Progress along the planned trajectory some distance Δl
4. Repeat until the terminal point is reached

This algorithm, while suboptimal, is easily implemented and can scale to any number of radars. However, for most problems, a path length constraint will need to be imposed to keep the single radar problems feasible.

Fig. 6.18 depicts the first three iterations of the minimax algorithm. We have two equivalent radars, one at the origin and the second at (1,0). The start point is (1/2,-1/2) and the end point is (1/2,1/2). The algorithm begins by planning a path to avoid the radar at the origin. The aircraft traverses a distance, $\Delta l = 0.2$, denoted by a solid

line. The dotted lines indicate the remainder of the planned trajectory. The aircraft then determines that the second radar has greater intensity and plans a new route around it. Fig. 6.18 depicts the first three segments of the trajectory generated by the minimax technique. The Δl parameter is chosen to be extremely coarse to illustrate the algorithm.

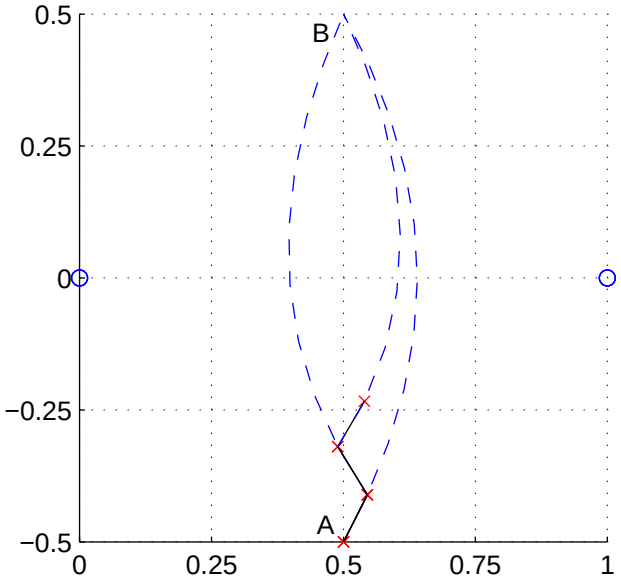

Figure 6.18 Portion of a Minimax Generated Trajectory for Two Radar Exposure Minimization, Radars Located at $(0, 0)$ and $(1, 0)$, $\Delta l = 0.2$

Fig. 6.19 shows the same problem solved by the minimax algorithm using a $\Delta l = 0.01$. We see that the minimax algorithm converges to the Voronoi edge separating the two radars, as expected.

While the minimax approach provides a simple means to deal with a complex problem, there are drawbacks to this suboptimal approach. In the minimax approach, solutions that lie on the Voronoi edges are often preferred. Consider the minimax algorithm under the scenario depicted in Fig. 6.20. Under this scenario, travelling from point A to point B would place the aircraft in between a sequence of two radars where the distance separating the two continues to decrease. By making sequential locally optimal decisions, the globally optimal decision is not considered. The preferred strategy would be to avoid such a trap.

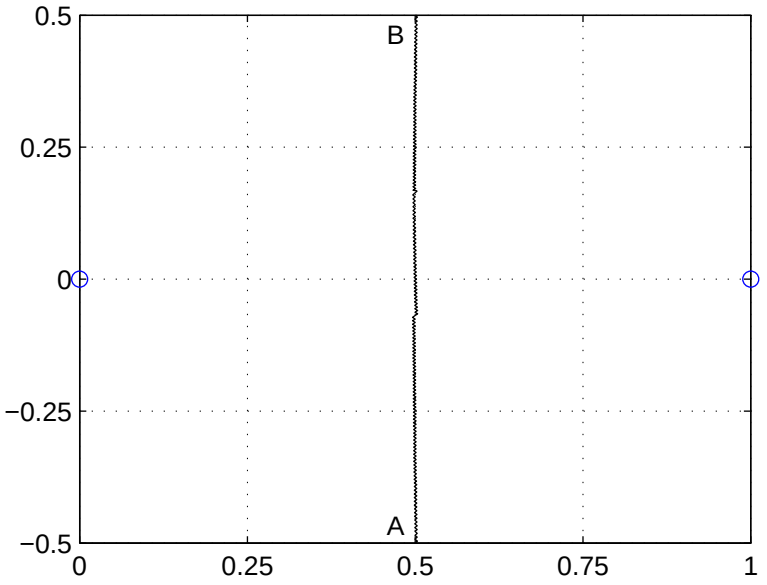

Figure 6.19 Minimax Generated Trajectory for Two Radar Exposure Minimization, Radars Located at $(0, 0)$ and $(1, 0)$, $\Delta l = 0.01$

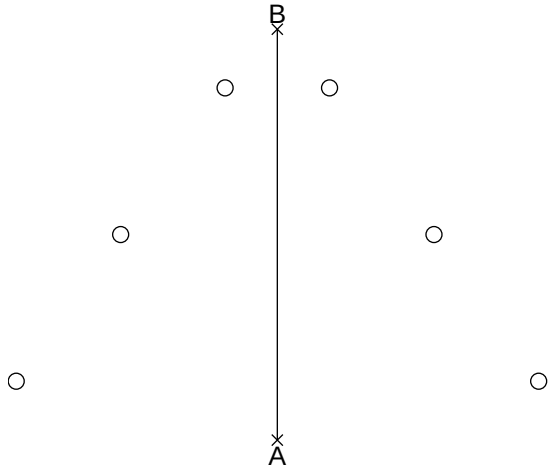

Figure 6.20 Trapping the Minimax Algorithm

6.5 Summary

In this chapter, several applications and extensions of the fundamental results obtained in earlier chapters were presented. A hierarchical cooperative control law was developed for the problem of multiple vehicle isochronous rendezvous for radar exposure minimization. The algorithm was applied to a representative two-ship problem. The constructive nature of the algorithm renders the existence of these solutions readily verifiable.

The optimality of the Voronoi edge, for the problem of an aircraft exposed to illumination by two threat radars, has been investigated. An analytic solution to the two radar problem is presented for the case where the end points of the trajectory lie upon the Voronoi edge. The issue of local versus global optimality is investigated and a decision criterion is identified for when going around the two radars is preferable than going between the two radars. This decision criterion is developed for the cases of equal and unequal power radars. We have shown that while the Voronoi edge is locally optimal, the globally optimal decision, in most cases, is *not* to go between the two threats. Thus, an awareness of the consequences of embracing non-globally optimal solutions for large scale optimization problems such as the cooperative control of UAVs is essential.

Finally, a suboptimal technique is presented which is scalable to address the n-radar exposure minimization problem. The next chapter develops optimal trajectories for target identification and classification missions performed by autonomous air vehicles.

VII. Optimal Trajectories for Autonomous Target Classification

7.1 Introduction

A projected role for autonomous uninhabited air vehicles is to classify and subsequently attack time critical targets, as well as perform battle damage assessment after an attack [21, 25]. Thus, the problem of determining optimal look angles for automatic target recognition/classification is addressed first. Next, minimum time trajectories for this mission, for a vehicle with a minimum turning radius are constructed. Lastly, an algorithm for performing cooperative classification and/or battle damage assessment involving more than one air vehicle, is presented.

7.2 Optimal Look Angles for ATR

The targets' universe of discourse is stipulated to consist of rectangles located in a plane and with an arbitrary orientation. We assume that the probability of successfully classifying a rectangular target with sides a and b, using an Automatic Target Recognition (ATR) algorithm, is directly proportional to the projection of the visible sides of the rectangular object onto a line perpendicular to the aspect angle θ of the viewing sensor, as shown in Fig. 7.1.

Without loss of generality assume $a \geq b$. The probability of classification $\rho(\theta)$ is then calculated as follows:

$$\rho(\theta) = \begin{cases} \frac{a\cos\theta + b\sin\theta}{a+b} & 0 \leq \theta \leq \frac{\pi}{2} \\ \frac{-a\cos\theta + b\sin\theta}{a+b} & \frac{\pi}{2} \leq \theta \leq \pi \\ \frac{-a\cos\theta - b\sin\theta}{a+b} & \pi \leq \theta \leq \frac{3\pi}{2} \\ \frac{a\cos\theta - b\sin\theta}{a+b} & \frac{3\pi}{2} \leq \theta \leq 2\pi \end{cases} \tag{7.1}$$

A plot of $\rho(\theta)$ for $-\pi < \theta < \pi$ is provided in Fig. 7.2.

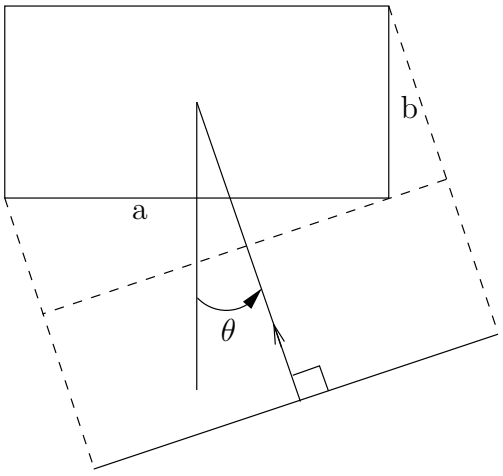

Figure 7.1 Geometry for the Optimal Look Angle ATR Problem

Consider the function $\rho(\theta)$ where $\theta \in (0, \pi/2)$. The first and second derivatives of $\rho(\theta)$ are

$$\rho'(\theta) = \frac{-a\sin\theta + b\cos\theta}{a+b} \tag{7.2}$$

$$\rho''(\theta) = \frac{-a\cos\theta - b\sin\theta}{a+b} \tag{7.3}$$

Evidently, we have an extreme value of ρ at the aspect angle

$$\theta^* = \text{Arctan}\left(\frac{b}{a}\right) \tag{7.4}$$

Substituting Eq. (7.4) into Eq. (7.3) yields the result

$$\rho''(\theta^*) = -\frac{\sqrt{a^2+b^2}}{a+b} < 0$$

i.e., we have a relative maximum at the extreme point $\theta = \theta^*$. Substituting Eq. (7.4) into Eq. (7.1) finally yields

$$\rho(\theta^*) = \frac{\sqrt{a^2+b^2}}{a+b}$$

This maximum probability is repeated at the aspect angles

$$\theta^* = \left\{\frac{\pi}{2} + \text{Arctan}\left(\frac{b}{a}\right), -\text{Arctan}\left(\frac{b}{a}\right), -\frac{\pi}{2} - \text{Arctan}\left(\frac{b}{a}\right)\right\}$$

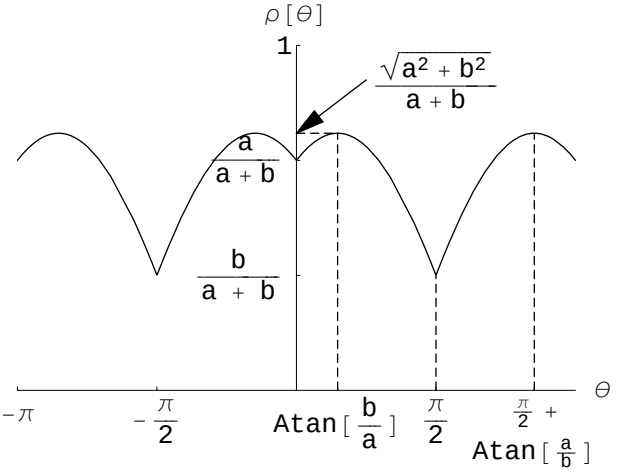

Figure 7.2 Parametric Plot of Probability of Classification for $-\pi \leq \theta \leq \pi$

At $\theta = \pi/2$, we have $\rho = \frac{b}{a+b}$. However, $\rho'(\pi/2)$ does not exist. Since

$$\rho'(\theta) < 0 \quad \text{for Arctan}\left(\frac{b}{a}\right) < \theta < \frac{\pi}{2}$$

and

$$\rho'(\theta) > 0 \quad \text{for } \frac{\pi}{2} < \theta < \frac{\pi}{2} + \text{Arctan}\left(\frac{b}{a}\right)$$

we conclude $\rho(\pi/2)$ is a relative minimum. Similarly, we find that $\rho(-\pi/2)$ is a relative minimum. Lastly, we note that

$$\rho(0) = \frac{a}{a+b}$$

7.2.1 Multiple Look Classification. For multiple-look classification, where a predetermined probability of correct classification threshold needs to be achieved for a target to be classified, possibly employing more than one air vehicle, we consider the probability of correct classification, $\rho(\theta_i)$ for a look i, where the aspect angle is θ_i, to be an independent event. Thus, the probability ρ of correctly identifying a target after n independent snapshots have been taken is

$$\rho = 1 - \prod_{i=1}^{n} [1 - \rho(\theta_i)] \tag{7.5}$$

and for the special case of two looks, $n = 2$, we have the probability of correctly having classified the target

$$\rho = \rho(\theta_1) + \rho(\theta_2) - \rho(\theta_1)\rho(\theta_2) \tag{7.6}$$

The function $\rho(\theta)$ is the probability of being able to classify the target when a snapshot of the target is taken from an aspect angle of θ. Strictly speaking, a snapshot of the target is taken and is being reviewed, after which a binary (yes/no) decision is made:

- The target can be identified/classified
- The target cannot be identified/classified

Then, if n snapshots of the target are taken from aspect angles $\theta_1, \theta_2, \ldots, \theta_n$, the probability that the target has been correctly identified/classified, is given by Eq. (7.5). Here, the n snapshots are taken, and only thereafter, are they examined.

7.3 Optimal Angular Separation for Second Look

Consider the scenario where an initial snapshot of the target has been taken at an unknown aspect angle, θ. We wish to find the optimal change in aspect angle Δ that maximizes the average probability of identifying the target in two passes. Δ directly translates into a change in the vector of approach to the target. Without loss of generality, assume $\theta \in [0, \pi/2]$, $\Delta \in [0, \pi/2]$ and $0 \leq |\Delta - \theta| \leq \frac{\pi}{2}$. Thus, the optimization problem is posed

$$\max_{\Delta} \frac{1}{\pi/2} \left[\int_0^{\frac{\pi}{2}} \left(\rho(\theta) + \rho(\theta + \Delta) - \rho(\theta)\rho(\theta + \Delta) \right) \, d\theta \right] \tag{7.7}$$

Substituting Eq. (7.6) into Eq. (7.7), we define the following cost function

$$J = \int_0^{\frac{\pi}{2}} \left[\frac{a\cos\theta + b\sin\theta}{a+b} + \frac{a\cos(\Delta+\theta) + b\sin(\Delta+\theta)}{a+b} - \frac{(a\cos\theta + b\sin\theta)\ (a\cos(\Delta+\theta) + b\sin(\Delta+\theta))}{(a+b)^2} \right] d\theta$$

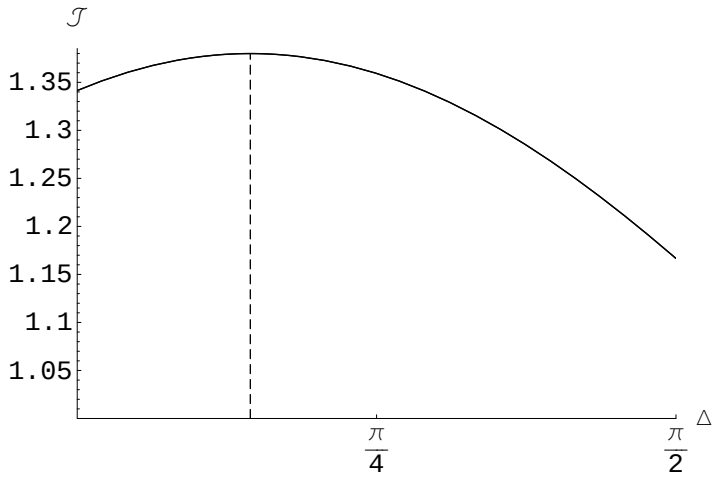

Figure 7.3 Example Cost Function for Second Target Identification Attempt

Integration yields

$$J(\Delta) = \frac{-\left(a^2+b^2\right)\,\pi\,\cos\Delta}{4\,(a+b)^2} - \frac{2\,\cos\frac{\Delta}{2}}{a+b}\left((a+b)\sin\frac{\Delta}{2} + (a-b)\cos\frac{\Delta}{2}\right) + \frac{a^2\,\sin\Delta - 2\,a\,b\,\cos\Delta - b^2\,\sin\Delta}{2\,(a+b)^2}$$

Equivalently,

$$J(\Delta) = \frac{\left[4\,a\,b - (a^2+b^2)\,(\pi-4)\right]\,\cos\Delta + 4\,(a+b)\,\left[(a+b) - \frac{1}{2}\,(a-b)\,\sin\Delta\right]}{4\,(a+b)^2}$$

This function is plotted in Fig. 7.3 for the aspect ratio $a/b = 1/2$, and $0 \le \Delta \le \frac{\pi}{2}$.

We can find the extreme value for this function by setting

$$\frac{\partial J}{\partial \Delta} = 0$$

which yields

$$\frac{-2\,\left(a^2-b^2\right)\,\cos\Delta + \left(a^2\,(\pi-4) + b^2\,(\pi-4) - 4\,a\,b\right)\,\sin\Delta}{4\,(a+b)^2} = 0$$

Table 7.1 Optimal Change in Aspect Angle (degrees) for the Second Target Identification Pass for Various Aspect Ratios

$\frac{b}{a}$	Δ^* (deg)
1	0
2	26.0180
3	37.8579
4	44.4394
5	48.5994
6	57.3850

We have an extreme value of J at

$$\Delta^* = \text{Arctan}\left(\frac{2\left(a^2-b^2\right)}{\left(a^2+b^2\right)(\pi-4)-4\,a\,b}\right) \tag{7.8}$$

Substituting Eq. (7.8) into the second derivative of J yields

$$\left.\frac{\partial^2 J}{\partial \Delta^2}\right|_{\Delta^*} = \frac{\sqrt{1+\frac{4\left(a^2-b^2\right)^2}{\left(a^2+b^2\right)(\pi-4)-4\,a\,b^2}}\left[\left(a^2+b^2\right)(\pi-4)-4\,a\,b\right]}{4\left(a+b\right)^2} < 0$$

which holds for all $a, b > 0$. Thus, the extreme value obtained at Δ^* is a relative maximum. As an example, for the case shown in Fig. 7.3 where the aspect ratio $a/b = 1/2$, the maximum value of J is achieved at

$$\begin{aligned}\Delta^* &= \text{Arctan}\left(\frac{6}{28-5\pi}\right)\\ &= 26.018^\circ\end{aligned}$$

It is important to note that Δ^* exists in the first quadrant, i.e., $0 \le \Delta^* \le \pi/2$, only if $b \ge a$. For all $a > b$, $J(\Delta)$ is maximized on the interval $[0, \pi/2]$ at the boundary $\Delta^* = 0$. Thus, for any rectangular object with $a > b$, the optimal change in aspect angle for the second look, given an unknown aspect angle θ, is zero - see, e.g., the illustration in Fig. 7.4. Furthermore, for a square object, i.e., $a = b$, the optimal change in aspect angle is zero. Table 7.3 presents the optimal change in aspect angle for varying aspect ratios for the case $b > a$.

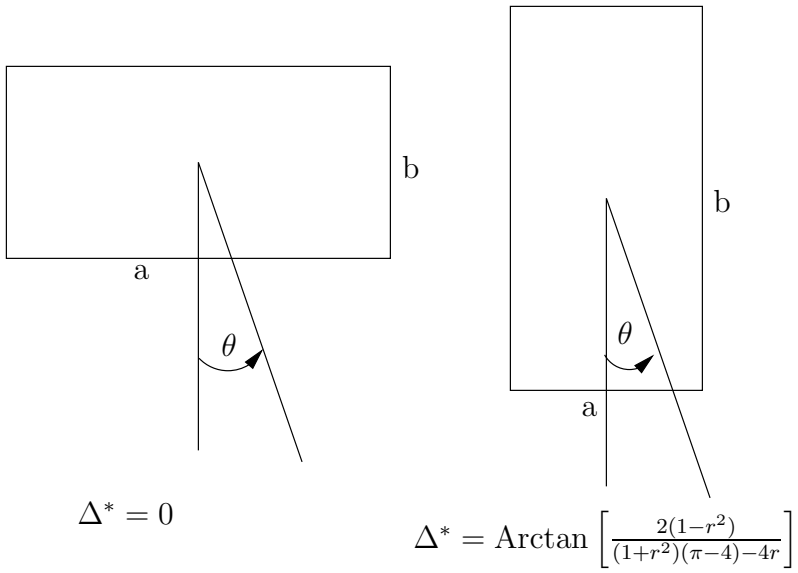

Figure 7.4 Geometry for the Optimal Look Angle ATR Problem

7.3.1 Feedback Control. If the ATR algorithm can provide an estimate of the aspect angle, θ, then the second pass should be flown such that the probability of classification of the second pass will be maximized, i.e.,

$$\theta^* = \text{Arctan}\left(\frac{b}{a}\right)$$

Thus, invariably, the target identification probability after the second look is given by Eq. (7.4). Let the aspect ratio $r = b/a$. We have

$$\rho(\theta^*) = \frac{\sqrt{r^2+1}}{r+1}$$

The probability of classification after two looks is

$$\begin{aligned} p(\theta) &= \rho(\theta) + \frac{\sqrt{r^2+1}}{r+1} - \rho(\theta)\frac{\sqrt{r^2+1}}{r+1} \\ &= \frac{\sqrt{r^2+1}}{r+1} + \left(1 - \frac{\sqrt{r^2+1}}{r+1}\right)\rho(\theta) \end{aligned}$$

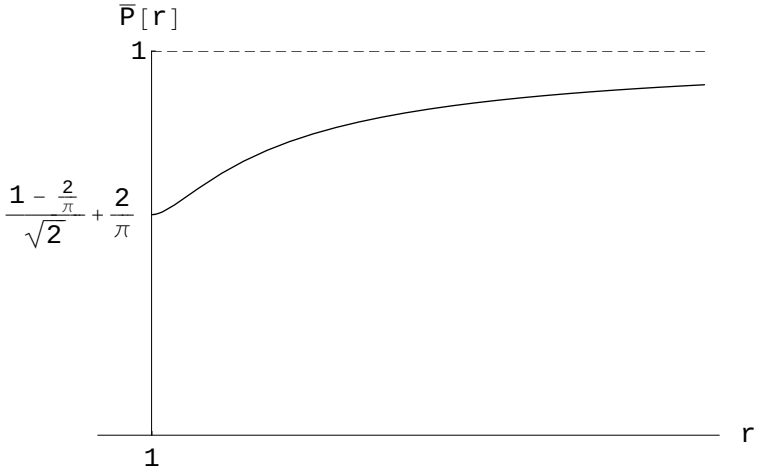

Figure 7.5 Average Classification Probability after Two Looks when First Pass Aspect Angle is Known

Thus, the average classification probability according to the feedback strategy is

$$\begin{aligned}\bar{P}(r) &= \frac{1}{\frac{\pi}{2}} \left\{ \int_0^{\frac{\pi}{2}} \left[\frac{\sqrt{r^2+1}}{r+1} + \left(1 - \frac{\sqrt{r^2+1}}{r+1} \right) \rho(\theta) \right] \, d\theta \right\} \\ &= \frac{\sqrt{r^2+1}}{r+1} + \frac{1}{\frac{\pi}{2}} \left(1 - \frac{\sqrt{r^2+1}}{r+1} \right) \int_0^{\frac{\pi}{2}} \frac{a\cos\theta + b\sin\theta}{a+b} \, d\theta \end{aligned}$$

Hence, the average probability of classification after two looks, as a function of the aspect ratio, is

$$\bar{P}(r) = \frac{2}{\pi} + \left(1 - \frac{2}{\pi} \right) \frac{\sqrt{r^2+1}}{r+1}$$

A plot of $\bar{P}(r)$ is shown in Fig. 7.5. Note that $\bar{P}(\infty) = 1$.

7.4 Minimum Time Trajectories with a Minimum Turning Radius Constraint

In this section we consider minimum time optimal trajectories where an air vehicle travelling in the plane with a constant velocity is constrained to have a minimum turning radius, R.

7.4.1 Specified Terminal Point. The first case examined entails a specified terminal point. The vehicle is initially at the origin, O with some initial heading angle and

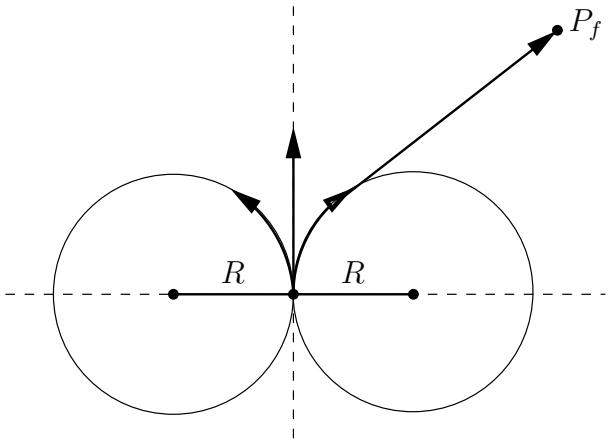

Figure 7.6 Minimum Time Trajectory Problem with Specified Terminal Point Outside the Minimum Turning Radius

the terminal point, P_f, is outside the minimum turning radius. Without loss of generality, assume $P_f \in RH$ plane, see, e.g., Fig. 7.6.

Proposition 7.4.1. *The minimum time trajectory, for the case where the specified terminal point P_f lies outside the minimum turning radius circle, consists of a hard turn into P_f until the bearing to P_f is 0°, followed by a straight line dash to P_f.*

Proof. This problem can be viewed as a special case of a two player differential game, where the second player is considered stationary and the first player is restricted to move at constant velocity with a limited maximum turning radius. The problem described is a special case of the Homicidal Chauffeur Game, and the minimum time trajectory of a hard turn into P_f until the bearing to P_f is 0°, followed by a straight line dash to P_f is the optimal strategy for the first player - see, e.g., [22]. □

The second case considered is the situation where the final point, P_f, is inside the minimum turning radius circle. The position of P_f is specified by the distance, d, from the center of the left minimum turning radius circle, and by the angle φ - see, e.g., Fig. 7.7.

The parameters d and φ are constrained as follows. The equation of the right minimum turning radius circle is

$$(x - 2R)^2 + y^2 = R^2$$

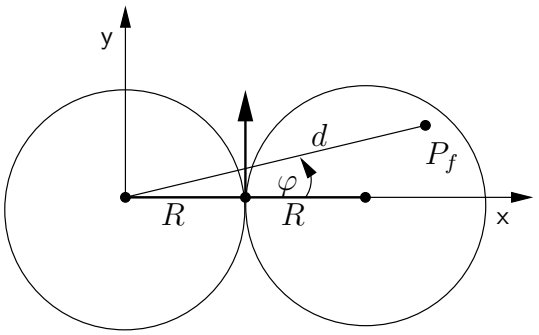

Figure 7.7 Minimum Time Trajectory Problem with Specified Terminal Point Inside the Minimum Turning Radius

The final point P_f has coordinates $(x, y) = (d\cos\varphi, d\sin\varphi)$. Since P_f is inside the right minimum turning radius circle, we have

$$\begin{aligned} & (d\,\cos\varphi - 2\,R)^2 + d^2\sin^2\varphi \leq R^2 \\ \Rightarrow \qquad & d^2 - 4\,R\,d\,\cos\varphi + 3\,R^2 \leq 0 \end{aligned}$$

Solving for the parameter $\frac{d}{R}$, yields the constraint

$$\max(0, 2\,\cos\varphi - \sqrt{4\cos^2\varphi - 3}) < \frac{d}{R} < 2\,\cos\varphi + \sqrt{4\cos^2\varphi - 3} \tag{7.9}$$

Given P_f is contained within the right minimum turning radius circle, the angle φ is constrained by the two lines tangent to the right minimum radius turning circle which pass through the origin. By constructing right triangles with the following three points: the origin, the center of the right minimum turning radius circle, and each of the points of tangency, it is evident that

$$-\frac{\pi}{6} \leq \varphi \leq \frac{\pi}{6} \tag{7.10}$$

In Fig. 7.8 we plot the constraints (7.9) as a function of φ.

The solution of the optimal control problem entails the construction of a circle of radius R which is tangent to the left minimum turning radius circle and which passes through the point P_f. This requires construction of a triangle, given three sides: d, R and $2\,R$. The construction is illustrated in Fig. 7.9(a).

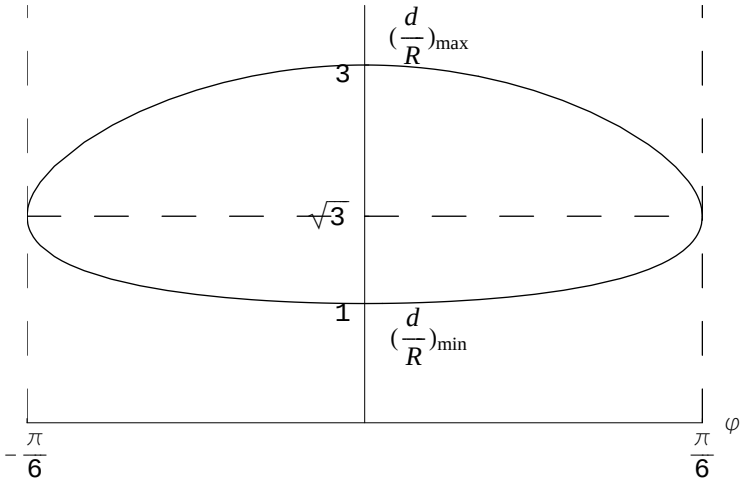

Figure 7.8 Plot of $\frac{d}{R}$ vs φ

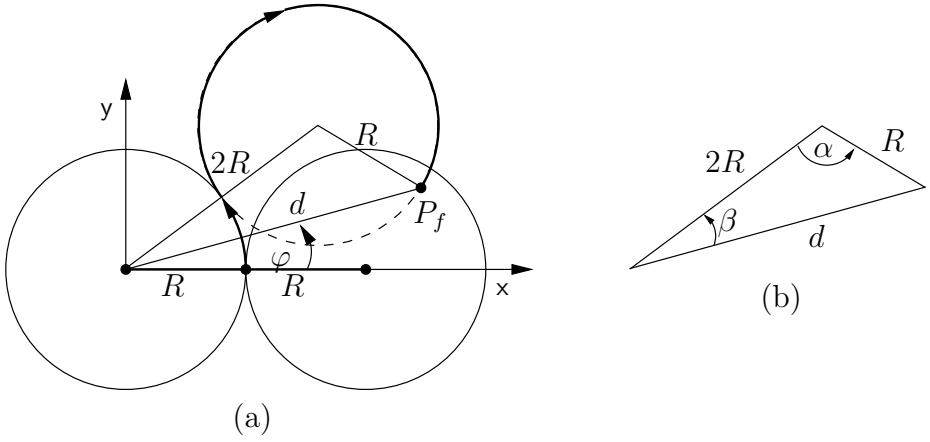

Figure 7.9 Construction of Circle Required to Solve the Minimum Time Trajectory Problem with Specified Terminal Point Inside the Minimum Turning Radius

The shown trajectory entails a hard turn to the left followed by a hard turn to the right, viz., a swerve maneuver. The length of the trajectory is determined by the angles of the constructed triangle, which is shown in Fig. 7.9(b). Note: Since $d < 3\,R$, the solution triangle can always be constructed. From the law of cosines we have

$$d^2 = 4\,R^2 + R^2 - 4\,R^2 \cos\alpha$$
$$\Rightarrow \quad \alpha = \text{Arccos}\left(\frac{1}{4}\left[5 - \left(\frac{d}{R}\right)^2\right]\right)$$

Similarly

$$R^2 = 4\,R^2 + d^2 - 4\,R\,d\,\cos\beta$$
$$\Rightarrow \quad \beta = \text{Arccos}\left(\frac{1}{4}\left[\frac{3}{\left(\frac{d}{R}\right)} + \left(\frac{d}{R}\right)\right]\right)$$

The path length, l, for the swerve maneuver is

$$\frac{l}{R} = \beta + \varphi + 2\pi - \alpha$$

Hence,

$$\frac{l}{R} = 2\pi + \varphi + \text{Arccos}\left(\frac{1}{4}\left[\frac{3}{\left(\frac{d}{R}\right)} + \left(\frac{d}{R}\right)\right]\right) - \text{Arccos}\left(\frac{1}{4}\left[5 - \left(\frac{d}{R}\right)^2\right]\right) \qquad (7.11)$$

The construction shown in Fig. 7.9(b) will "fail", viz., the point at which the right hand constructed circle is tangent to the left hand minimum radius circle will fall below the initial position, if

$$\varphi < 0$$

Similarly, if

$$\varphi > 30^\circ$$

the constructed circle cannot simultaneously contain points inside the right minimum turning radius circle and have a point tangent to the left minimum turning radius circle. However, these conditions need never occur.

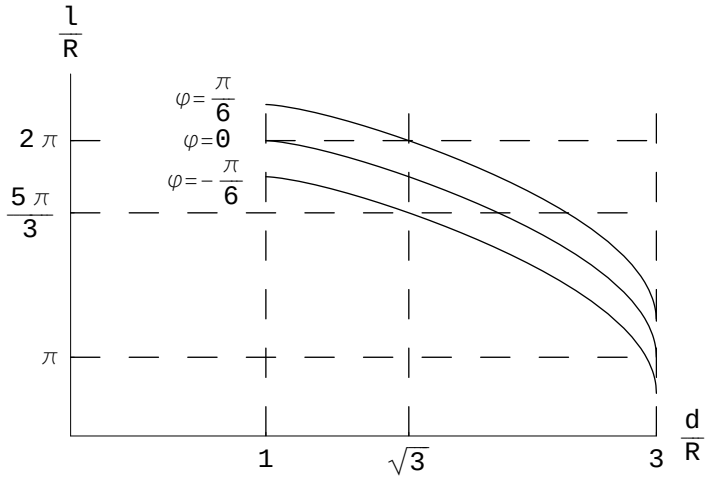

Figure 7.10 Plot of $\frac{l}{R}$

Proposition 7.4.2. *All final points, P_f, in the interior of the right hand minimum radius circle can be reached by the constructed circle if the inequalities, $0 < \varphi < \pi/6$ and $\beta > 0$ are satisfied.*

Proof. Let $0 < \varphi < \pi/6$ such that A is any point in the interior of the right minimum turning radius circle, some distance, d, from the center of the left minimum turning radius circle, O - see, e.g., Fig. 7.11. $\exists$ a pair of triangles, each with a common side OA a side of length $2R$ and a side of length R. Let the points of the triangles opposite OA be C and C'. Construct two circles of radius R at C and C'. Both circles will be tangent to the left minimum radius circle at one point. The angle between the point of tangency and center of the left turning radius circle is β. Associate the circle at C with $\beta > 0$ and the circle at C' with $\beta < 0$. The circle for which $\beta < 0$ must be disregarded since this requires movement in the opposite direction of the initial heading angle. Thus, the constructed circle with $\beta > 0$, is the only solution which intersects point A and permits movement in the direction of the initial heading vector.

□

We also must investigate the possibility of a hard turn to the left followed by a straight line dash, as shown in Fig. 7.12. Now,

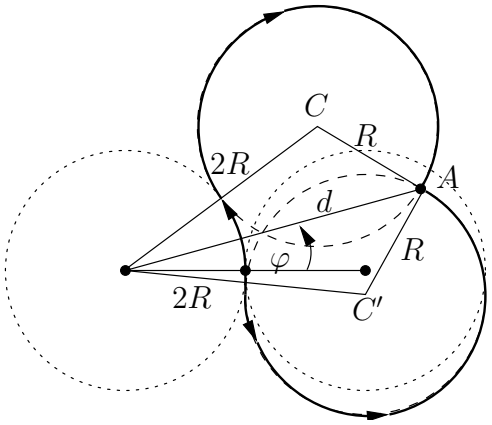

Figure 7.11 Two Candidate Minimum Time Paths

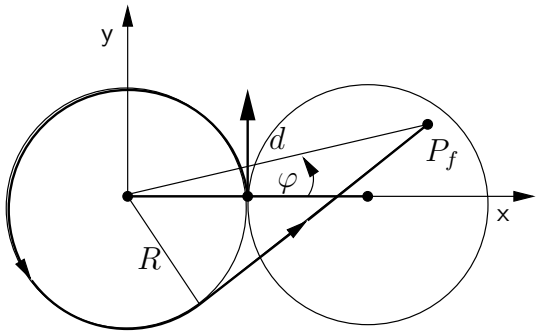

Figure 7.12 Hard Turn to Left Followed By a Straight Line Dash

$$l = 2\pi R - \left(\text{Arccos}\left[\frac{1}{\left(\frac{d}{R}\right)} \right] - \varphi \right) R + \sqrt{d^2 + R^2} \quad \Rightarrow$$

$$\frac{l}{R} = 2\pi + \varphi - \text{Arccos}\left[\frac{1}{\left(\frac{d}{R}\right)} \right] + \sqrt{\left(\frac{d}{R}\right)^2 - 1} \tag{7.12}$$

Equating Eqs. (7.11) and (7.12) yields the following transcendental equation, in terms of a single parameter, $\frac{d}{R}$

$$\text{Arccos}\left(\frac{1}{4}\left[\frac{3}{\left(\frac{d}{R}\right)} + \left(\frac{d}{R}\right) \right] \right) - \text{Arccos}\left(\frac{1}{4}\left[5 - \left(\frac{d}{R}\right)^2 \right] \right) = \text{Arccos}\left[\frac{1}{\left(\frac{d}{R}\right)} \right] + \sqrt{\left(\frac{d}{R}\right)^2 - 1} \tag{7.13}$$

A solution, $\frac{d}{R}$, of Eq. (7.13) must also satisfy the inequality (7.9). Obviously, $1 \leq \frac{d}{R} \leq 3$. Further, if P_f is restricted to the interior of the right minimum turning radius circle, then $1 < \frac{d}{R} < 3$ holds.

Proposition 7.4.3. *The transcendental equation* (7.13) *does not have a solution which satisfies*

$$1 < \frac{d}{R} < 3$$

Proof. Suppose $\frac{d}{R}$ is a solution of the transcendental equation (7.13). Evidently, φ must satisfy $\varphi + \beta \leq 0$, which implies

$$\varphi \leq \bar{\varphi} = \text{Arccos}\left(\frac{1}{4}\left[\left(\frac{d}{R}\right) + \frac{3}{\left(\frac{d}{R}\right)} \right] \right)$$

Should a solution of Eq. (7.13) exist, there would be a boundary in the right minimum turning radius circle separating the optimal policies of two circular turns and one circular turn with a straight line dash - see, e.g., Fig. 7.13. Consider that the final point, P_f, lies in the unshaded areas of the right minimum turning radius circle shown in Fig. 7.13. The question arises, what would then be the optimal policy in those unshaded areas? If no

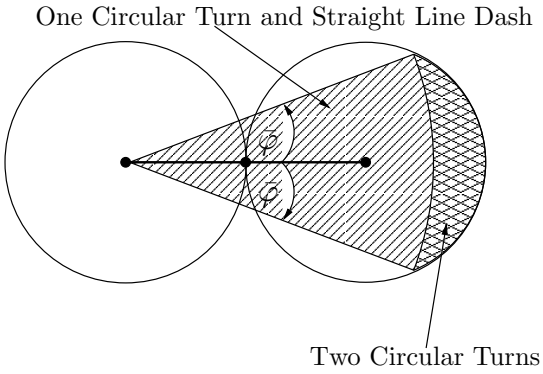

Figure 7.13 Hypothetical Boundary Separating Two Optimal Policies

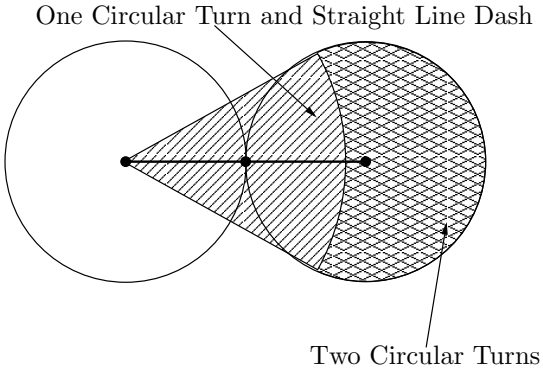

Figure 7.14 Hypothetical Boundary Separating Two Optimal Policies

unshaded areas exist, e.g., see Fig. 7.14, then we have the case where

$$\frac{d}{R} = \sqrt{3}$$

Inserting $\frac{d}{R} = \sqrt{3}$ into Eq. (7.13), we can check to see if this can be a solution. For the left hand side we have

$$\text{Arccos}\left(\frac{\sqrt{3}}{2}\right) + \text{Arccos}\left(\frac{1}{\sqrt{3}}\right)$$

For the right hand side we have

$$\text{Arccos}\left(\frac{1}{2}\right) + \sqrt{2}$$

Since

$$\text{Arccos}\left(\frac{1}{2}\right) > \text{Arccos}\left(\frac{1}{\sqrt{3}}\right)$$

and

$$\sqrt{2} > \frac{\pi}{6} = \text{Arccos}\left(\frac{\sqrt{3}}{2}\right)$$

we see that $\frac{d}{R} = \sqrt{3}$ is *not* a solution of the transcendental Eq. (7.13). □

Theorem 7.4.1. *The minimum time trajectory, for the case where the final point, P_f, is inside the minimum turning radius circle, entails a swerve maneuver which consists of a hard turn to the left of*

$$\varphi + \text{Arccos}\left(\frac{1}{4}\left[\frac{3}{\left(\frac{d}{R}\right)} + \left(\frac{d}{R}\right)\right]\right)$$

followed by a hard turn to the right of

$$2\pi - \text{Arccos}\left(\frac{1}{4}\left[\frac{3}{\left(\frac{d}{R}\right)} + \left(\frac{d}{R}\right)\right]\right)$$

Proof. This result proceeds from the previous discussion. □

7.5 Minimum Time Trajectories for Target Classification

Consider a target classification problem where the sensor footprint is circular, of radius r, and it is offset from the sensor platform by a distance d. The sensor platform moves at a constant velocity and has a minimum turning radius of R. We define the distance

$$\nu = d + r$$

and stipulate that the target circle defined by a target at the center, P_f, with radius ν, be approached orthogonally from the outside. See, e.g., Fig. 7.15.

7.5.1 Type 1 Problems. Consider the case where P_f is outside the circle of radius ν', which is concentric with the right minimum turning radius circle.

$$\nu' \doteq \sqrt{\nu^2 + R^2}$$

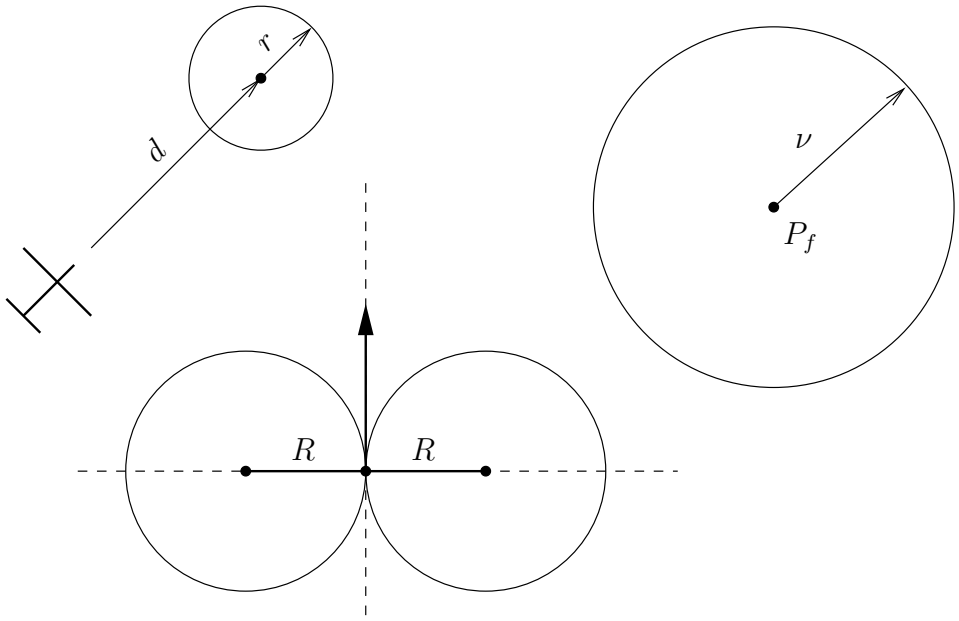

Figure 7.15 Minimum Time Trajectories for Target Classification

The critical circle is shown in Fig. 7.16.

Proposition 7.5.1. *When P_f is outside the critical circle the minimum time trajectory entails a hard turn into P_f until a bearing of 0° to P_f is established. Thereafter, a straight line path is followed until the target circle is met, as shown in Fig. 7.17.*

Proof. See proof of Proposition 7.4.1. □

7.5.2 Type 2 Problems. Next we consider the case where P_f is inside the circle of radius ν' which is concentric with the right minimum turning radius circle, see, e.g., Fig. 7.18. This yields the following condition

If $\nu' > 2R$, i.e., $\nu^2 + R^2 > 4R^2$, i.e., $\nu > \sqrt{3}R$, then

$$-\frac{\pi}{2} < \varphi \leq \frac{\pi}{2}$$

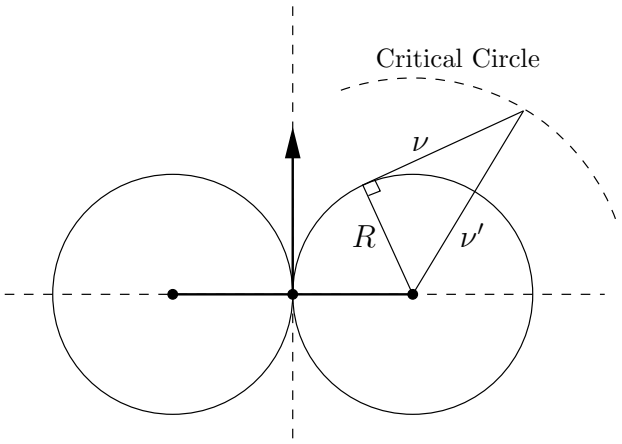

Figure 7.16 Critical Circle

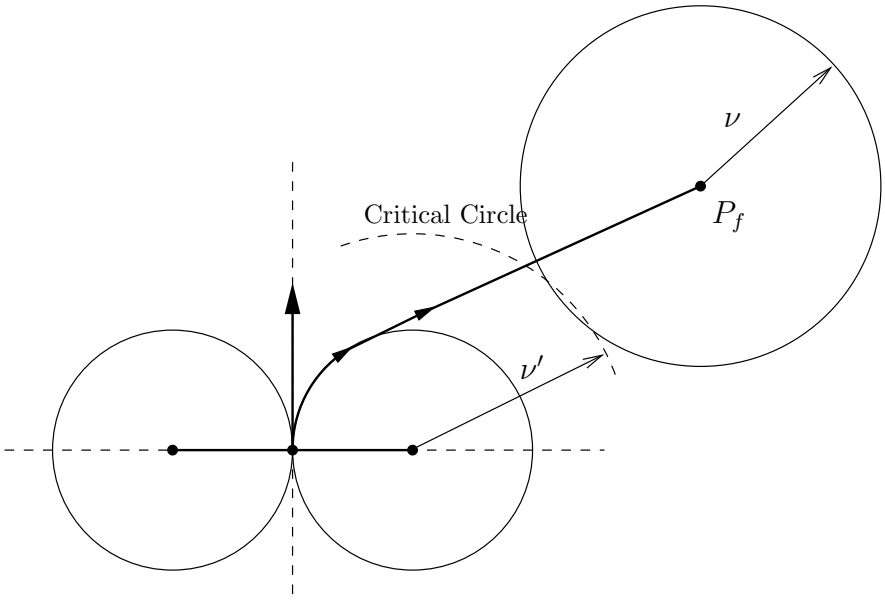

Figure 7.17 Minimum Time Trajectory for P_f Outside Critical Circle

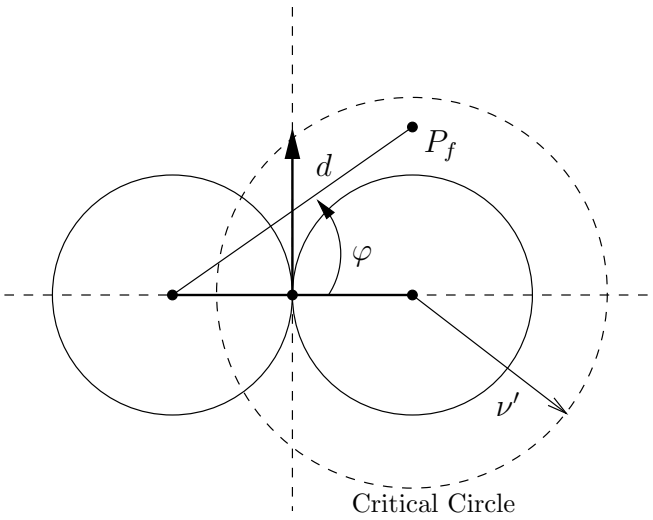

Figure 7.18 P_f Inside Critical Circle

If $\nu' < 2R$, i.e., $\nu < \sqrt{3}R$, then

$$
\begin{aligned}
& -\operatorname{Arccos}\left(\frac{\nu'}{2R}\right) \le \varphi \le \operatorname{Arccos}\left(\frac{\nu'}{2R}\right) \\
\Rightarrow \quad & -\operatorname{Arccos}\left(\frac{\sqrt{\nu^2+R^2}}{2R}\right) \le \varphi \le \operatorname{Arccos}\left(\frac{\sqrt{\nu^2+R^2}}{2R}\right) \\
\Rightarrow \quad & -\operatorname{Arccos}\left(\frac{1}{2}\sqrt{\left(\frac{\nu}{R}\right)^2+1}\right) \le \varphi \le \operatorname{Arccos}\left(\frac{1}{2}\sqrt{\left(\frac{\nu}{R}\right)^2+1}\right)
\end{aligned}
$$

For P_f to be inside the critical circle, we have

$$(x-2R)^2 + y^2 \le \nu'^2 = \nu^2 + R^2$$

with $x = d\cos\varphi$, $y = d\sin\varphi$, thus

$$
\begin{aligned}
& (d\cos\varphi - 2R)^2 + d^2\sin^2\varphi \le \nu^2 + R^2 \\
\Rightarrow \quad & d^2 - 4\,R\,d\cos\varphi + 3\,R^2 - \nu^2 \le 0
\end{aligned}
$$

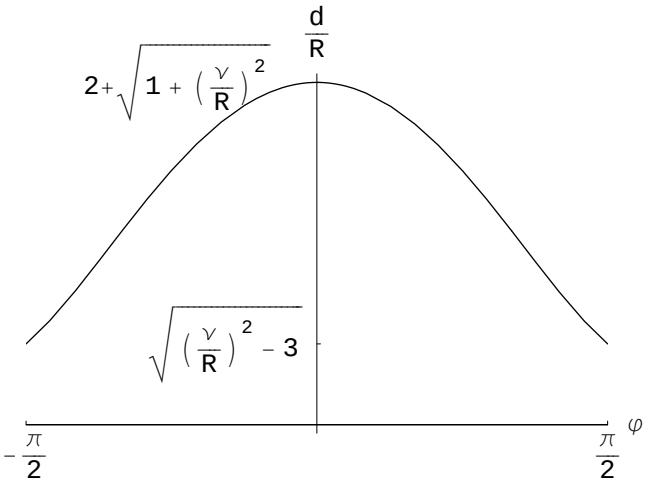

Figure 7.19 Plot of $\frac{d}{R}$ vs φ

We have the following inequality

$$\max\left(0, 2\cos\varphi - \sqrt{4\cos^2\varphi + \left(\frac{\nu}{R}\right)^2 - 3}\right) < \frac{d}{R} < 2\cos\varphi + \sqrt{4\cos^2\varphi + \left(\frac{\nu}{R}\right)^2 - 3} \tag{7.14}$$

Since

$$2\cos\varphi - \sqrt{4\cos^2\varphi + \left(\frac{\nu}{R}\right)^2 - 3} < 0, \qquad \forall\, \nu < \sqrt{3}R$$

and

$$2\cos\varphi - \sqrt{4\cos^2\varphi + \left(\frac{\nu}{R}\right)^2 - 3} > 0, \qquad \forall\, \nu > \sqrt{3}R$$

Eq. (7.14) becomes

$$\begin{cases} 0 < \frac{d}{R} < 2\cos\varphi + \sqrt{4\cos^2\varphi + \left(\frac{\nu}{R}\right)^2 - 3}, & \nu < \sqrt{3}R \\ 2\cos\varphi - \sqrt{4\cos^2\varphi + \left(\frac{\nu}{R}\right)^2 - 3} < \frac{d}{R} < 2\cos\varphi + \sqrt{4\cos^2\varphi + \left(\frac{\nu}{R}\right)^2 - 3}, & \nu > \sqrt{3}R \end{cases}$$

In Fig. 7.19 we plot the constraint (7.14) as a function of φ.

Consider the situation where P_f is inside the circle of radius ν', which is concentric with the right minimum turning radius circle, the minimum time trajectory involves a swerve maneuver. The swerve is just enough for P_f to be reached by the boundary of a new critical circle of radius ν', concentric with a new right minimum turning radius circle.

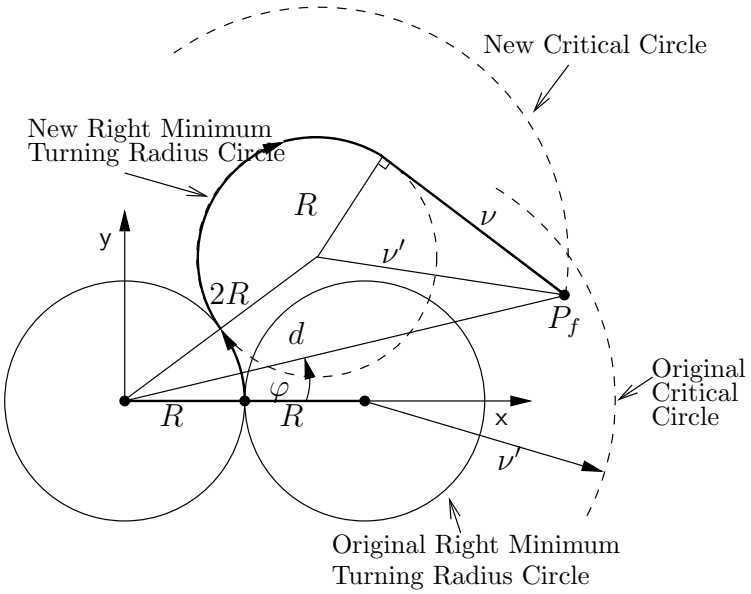

Figure 7.20 Construction of New Critical Circle

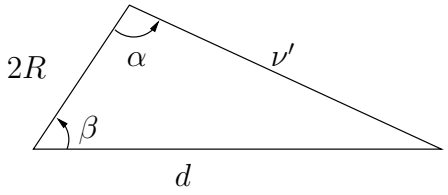

Figure 7.21 Solution Triangle

This is depicted in Fig. 7.20. We need to construct a solution triangle, e.g., see Fig. 7.21, given its three sides d, $2R$ and ν'. We calculate

$$\nu'^2 = d^2 + 4\,R^2 - 4\,R\,d\cos\beta$$

Thus,

$$\begin{aligned}\cos\beta &= \frac{d^2 + 4\,R^2 - \nu'^2}{4\,R\,d} \\ &= \frac{3R^2 + d^2 - \nu^2}{4\,R\,d} \quad \Rightarrow \\ \beta &= \text{Arccos}\left(\frac{1}{4}\left[\frac{3}{\left(\frac{d}{R}\right)} + \left(\frac{d}{R}\right) - \frac{\left(\frac{\nu}{R}\right)^2}{\left(\frac{d}{R}\right)}\right]\right)\end{aligned}$$

Similarly,

$$d^2 = \nu'^2 + 4\,R^2 - 4\,R\,\nu'\cos\beta$$

Thus,

$$\begin{aligned}
\cos\alpha &= \frac{\nu'^2 + 4\,R^2 - d^2}{4\,R\,\nu'} \\
&= \frac{5R^2 + \nu^2 - d^2}{4\,R\,\nu'} \\
&= \frac{1}{4}\left[\frac{5 - \left(\frac{d}{R}\right)^2 + \left(\frac{\nu}{R}\right)^2}{\sqrt{1 + \left(\frac{\nu}{R}\right)^2}}\right] \quad \Rightarrow \\
\beta &= \text{Arccos}\left(\frac{1}{4}\left[\frac{5 - \left(\frac{d}{R}\right)^2 + \left(\frac{\nu}{R}\right)^2}{\sqrt{1 + \left(\frac{\nu}{R}\right)^2}}\right]\right)
\end{aligned}$$

For the turn to the left, the change in heading is

$$\varphi + \beta$$

For the turn to the right, the change in heading is

$$2\pi - \alpha - \text{Arctan}\left(\frac{\nu}{R}\right)$$

The path length is then expressed as

$$\frac{l}{R} = \beta + \varphi + 2\pi\left[\alpha + \text{Arctan}\left(\frac{\nu}{R}\right)\right]$$

Equivalently,

$$\begin{aligned}
\frac{l}{R} = 2\pi + \varphi - \text{Arctan}\left(\frac{\nu}{R}\right) &+ \text{Arccos}\left(\frac{1}{4}\left[\frac{3}{\left(\frac{d}{R}\right)} + \left(\frac{d}{R}\right) - \frac{\left(\frac{\nu}{R}\right)^2}{\left(\frac{d}{R}\right)}\right]\right) \\
&- \text{Arccos}\left(\frac{1}{4}\left[\frac{5 - \left(\frac{d}{R}\right)^2 + \left(\frac{\nu}{R}\right)^2}{\sqrt{1 + \left(\frac{\nu}{R}\right)^2}}\right]\right) \qquad (7.15)
\end{aligned}$$

Remark 7.5.1. *The target circle is penetrated orthogonally by construction.*

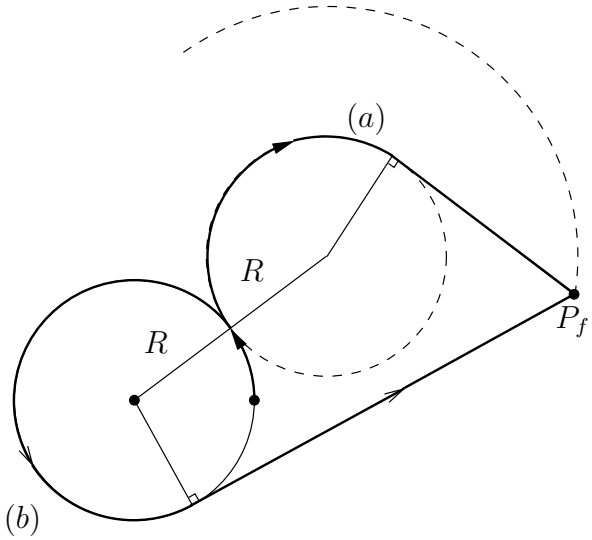

Figure 7.22 Two Candidate Minimum Time Trajectories After An Initial Swerve

Theorem 7.5.1. *When P_f is inside the circle of radius ν', which is concentric with the right minimum turning radius circle, the minimum time trajectory involves a swerve maneuver. The swerve is just enough for P_f to be reached by the boundary of a new critical circle of radius ν', concentric with a new right minimum turning radius circle.*

Proof. Consider the situation after an initial swerve which puts P_f on the boundary of a circle of radius ν', centered at the new position of the right minimum turning radius circle.

From this time onward, the "optimal" trajectories, (a) and (b), are indicated in Fig. 7.22. Similarly to the proof in Proposition 7.4.1, we realize that the optimal trajectory is (a). □

7.6 Cooperative Target Classification

Lastly, consider the problem of cooperative target classification. As in Section 7.5, the sensor footprint is circular, of radius r, and offset from the sensor platform by a distance d. Additionally, there is a commanded approach angle ξ, which corresponds, for instance, to an optimal second look at the target directed by the results of Sec. 7.3. Since our target is assumed rectangular, symmetry provides four candidate angles of approach, as shown in Fig. 7.23.

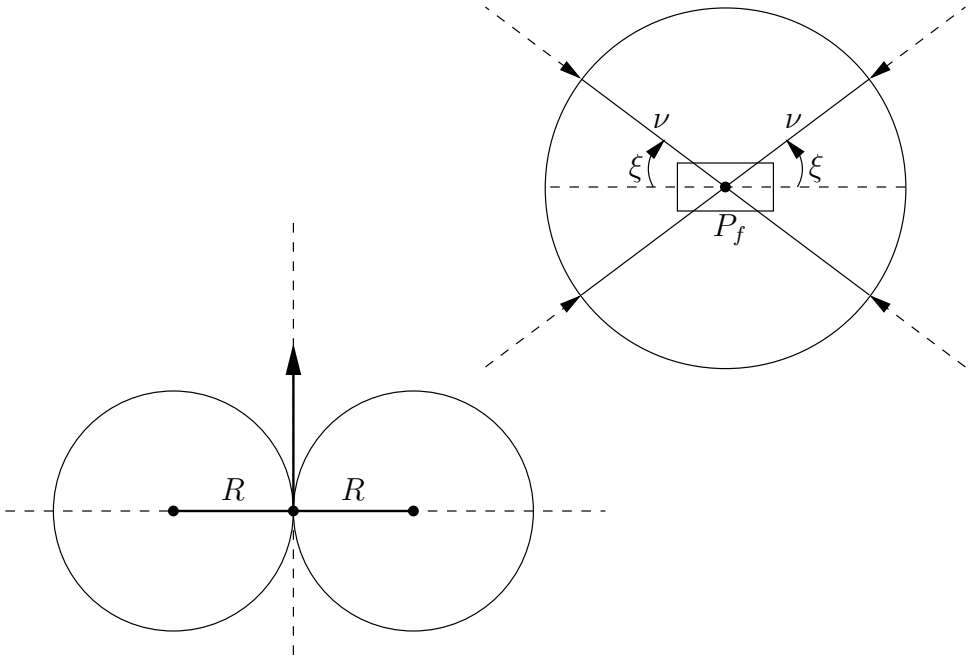

Figure 7.23 Cooperative Target Classification Problem

The first step in developing the optimal trajectory to perform the cooperative target classification is to construct minimum turning radius circles such that the entry into the target circle is orthogonal. Eight circles are constructed, see, e.g., Fig. 7.24.

All candidate trajectories consist of a hard turn, a straight line dash and a hard turn. The straight line dash is to be constructed tangent to the two minimum turning radius circles. Depending on the location of P_f and the sizes of the target circle and the minimum turning radii circles, a swerve maneuver may be considered as a portion of a candidate trajectory. Fig. 7.25 depicts several candidate minimum time trajectories.

Lastly, the candidate trajectories are ranked according to path length, and the minimum length trajectory is selected as optimal.

7.7 Summary

In this chapter, a cost function was developed for enhancing the probability of automatic target recognition and the corresponding optimization problem was solved. This requires approaching the target from specified directions and making sure that the air

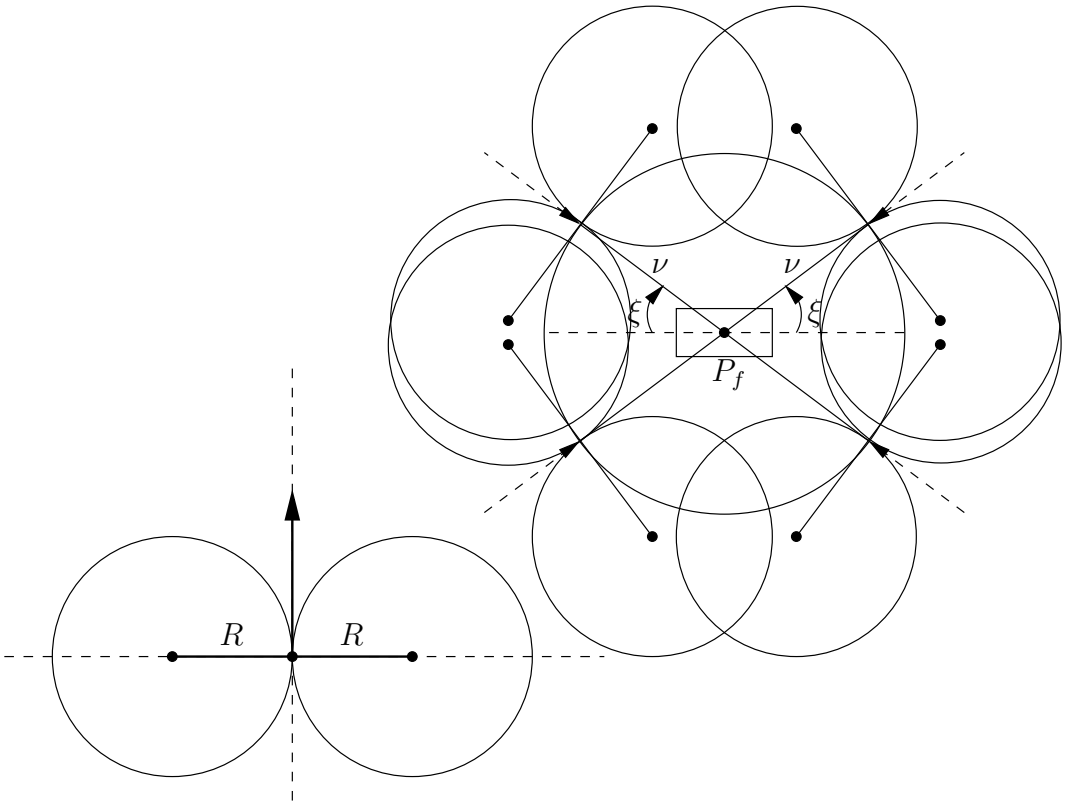

Figure 7.24 Construction of the Minimum Turning Radius Circles for Orthogonal Entry into the Target Circle

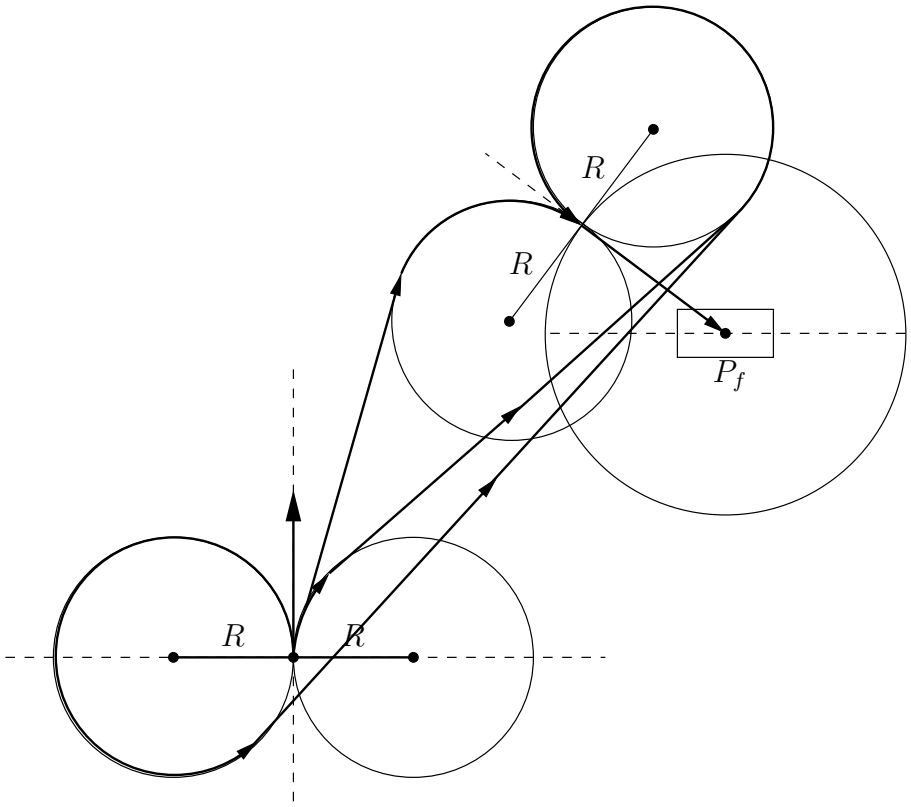

Figure 7.25 Construction of Some Candidate Minimum Time Trajectories for Cooperative Target Classification

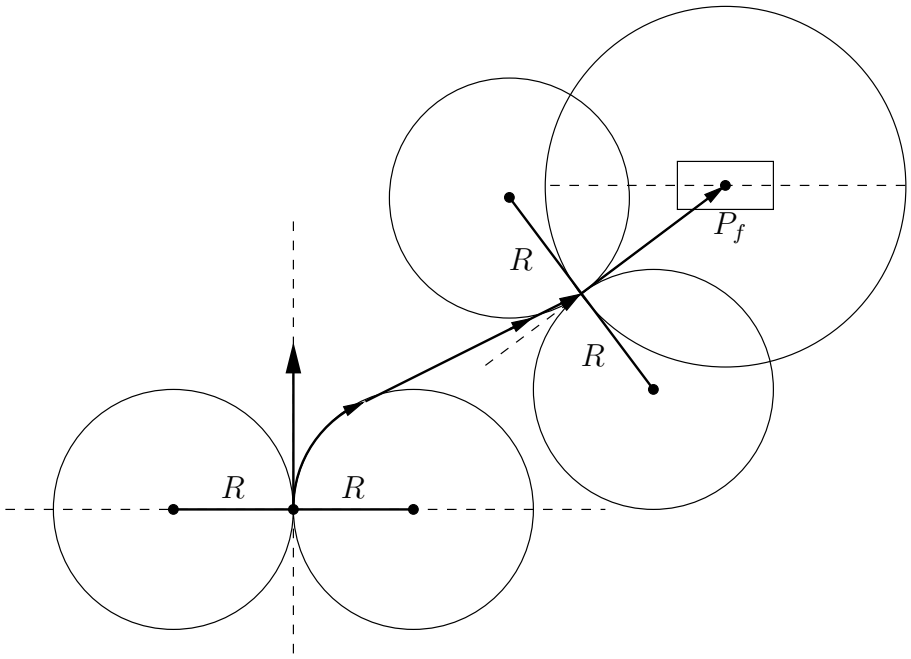

Figure 7.26 Characterization of the Minimum Time Cooperative Classification Trajectory

vehicle's sensor covers the target. Minimum time trajectories for air vehicles with a minimum turning radius were constructed for these tasks, and also for target attack and battle damage assessment. Lastly, the single vehicle results are encapsulated in a methodology addressing cooperative target classification and attack.

VIII. Conclusion and Recommendations

8.1 Introduction

The objective of this research was to develop a mathematically rigorous approach to a problem in air vehicle path planning, seeking fundamental truths concerning autonomous air vehicles and their cooperative control. The objective was motivated by the intention to develop a significant military force consisting of UAVs, UCAVs and autonomous munitions and the desire for this technology to make an effective contribution to air power. Specifically, this research considered the air vehicle path planning problem in the context of radar exposure minimization.

In Chapter 1 of this dissertation, an overview of air vehicle path planning was presented, along with historical background, problem statement and key results. Chapter 2 provided the essential elements of radar technology and optimization theory utilized in this research. In Chapter 3, the single vehicle radar exposure minimization problem was addressed, including derivations of the optimal trajectory, it's cost and path length. A similar analysis of the passive sensor exposure minimization problem was delineated in Chapter 4. Chapter 5 presented a description of the numerical methods developed and employed in this research. Applications and extensions of the work in the previous chapters were presented in Chapter 6. A hierarchical cooperative control algorithm was formulated for the problem of isochronous rendezvous of multiple air vehicles. Furthermore, the problem of a single vehicle minimizing exposure to two radars was studied. In Chapter 7, the process of automatic target recognition was modelled. An optimal minimum time control law was developed for the problem of autonomous target classification and was extended to address cooperative target classification. In the present chapter, the significant advances of this research are summarized and and suggestions for further research are provided.

8.2 Summary of Results

The analysis conducted in this research has led to the following key results:

- The problem of determining the flight path connecting the point of departure and the point of arrival, such that the exposure of an aircraft to illumination by a tracking

radar located at the origin is minimized, has been solved, *in closed form*, using the Calculus of Variations.

  - The solution is shown to satisfy necessary and sufficient conditions for a weak local minimum as well as the Weierstrass necessary conditions for a strong local minimum.
  - The solution is shown to exist if, and only if, the angle included between the departure and destination points is less than 60°.
  - A closed form expression for the optimal heading angle control law is obtained.
  - A closed form expression for the optimal cost is obtained.
  - An expression for the optimal path length, not available in closed form, is derived using elliptic integrals.
  - A method for determining optimal path length constrained solutions to the single vehicle radar exposure minimization problem is presented and conditions for the existence of these solutions are identified.

- A similar analysis is conducted for the single vehicle passive sensor exposure minimization problem to include a closed form solution and closed form expressions for the optimal path length and cost. A comparison between the solutions to the passive sensor and radar exposure minimization problems is made.
- It is verified that the Voronoi edge is the locally optimal solution for exposure minimization against two radars. The issues of global versus local optimality are explored yielding analytic results identifying the conditions where going around (between) two radars is preferable to going between (around) two radars.
  - A suboptimal algorithm for n-radar exposure minimization is developed and examined.
- A hierarchical cooperative control algorithm is formulated to determine optimal trajectories minimizing radar exposure for two (or more) air vehicles performing isochronous rendezvous. The constructive nature of the algorithm renders the existence of these solutions readily verifiable.

- A methodology for designing optimal trajectories for an autonomous air vehicle is presented. The automatic target recognition process is formulated as a novel optimization problem and solved. Minimum time trajectories for air vehicles with a minimum turning radius were covered. Finally, the problem of target classification was formulated using these concepts and a solution to the autonomous air vehicle search problem is presented.

8.3 Recommendations for Future Research

The research in this dissertation has revealed several mathematical facts concerning the radar exposure minimization problem. While this research has answered many important questions, many other challenges have been uncovered or remain unanswered. These issues are outlined in the following paragraphs.

- In this work, a particular deterministic metric was utilized to measure radar exposure. Future work could consider other radar metrics.
  - Probability based radar metrics such as probability of detection and probability of tracking could be developed.
  - A radar cross section model could be added to the cost functional in Eq. (3.1) such that radar cross section becomes a function of the air vehicle attitude. A rigorous mathematical analysis would complement previous work in this area by Pendelton [34].
- Consider the problem of minimizing exposure to a radar where the final point is not fixed but lies on some curve γ. For example, one may wish to flee from "hostile" territory into "friendly" territory where the border is defined by a line segment - see, e.g., Fig. 8.1. Alternatively, one may consider the lethality zone of an air defense radar to be a circle and it is desired to escape from inside the circle while minimizing exposure to the radar.

  Similarly, one might consider the variable end point problem as a means to address the multiple radar exposure minimization problem. In this case, the target curve, γ,

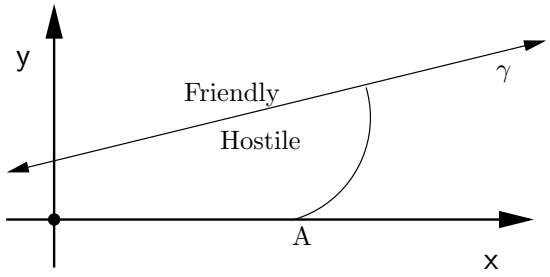

Figure 8.1 Application of Single Radar Exposure Minimization with Variable End Point

is a Voronoi edge, and the problem is to minimize exposure to a single radar. Both McLain [28] and Novy [30] presented ad-hoc methods of getting onto the Voronoi edge and transitioning between Voronoi edges. An open question remains as to what is a computationally efficient, possibly suboptimal, approach to multiple radar exposure minimization. Using a variational approach and applying a transversality condition may result in a closed form solution, thus being extremely computationally efficient. However, satisfying the transversality condition may result in the extremal curve and the Voronoi edge meeting orthogonally. In this case, an inequality constraint imposed with slack variables could result in a solution that approaches the Voronoi edge tangentially as opposed to orthogonally - see, e.g., Fig. 8.2. In the end, a comparison could be made between these ad-hoc methods and the optimal method presented in this dissertation.

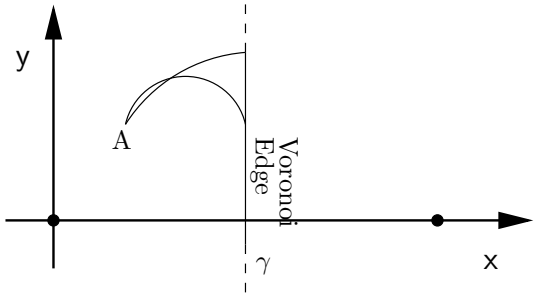

Figure 8.2 Variable End Point Problems as a Means to Address Multiple Radar Exposure Minimization

- It is possible that a solution for the path length constrained radar exposure minimization problem can be obtained, i.e., in terms of elliptic integrals, similar to what was accomplished for the constrained passive sensor problem in Sec. 4.6. Such a

formulation would be a great improvement over the numerically challenging shooting method employed in this research.

- A numerical study could be undertaken to determine the "go-around" versus "go-between" decision boundary for the two radar exposure minimization problem for the case where the start (end) point is not on the Voronoi edge.

Appendix A. Characterizing the Radar Exposure Minimization Extremal

In this Appendix we show that the extremal identified in (3.4) satisfies the necessary and sufficient conditions for a weak local minimum. Recall that our cost function is of the form

$$J = \int_0^{\theta_f} F(\theta, R, \dot{R})\, d\theta$$

where

$$F(\theta, R, \dot{R}) = \frac{\sqrt{\dot{R}^2 + R^2}}{R^4} \tag{A.1}$$

We define the partial derivatives we will need to evaluate the conditions for weak and strong extrema:

$$F_R(\theta, R, \dot{R}) = \frac{-3R^2 - 4\dot{R}^2}{R^5\sqrt{\dot{R}^2 + R^2}} \tag{A.2a}$$

$$F_{\dot{R}}(\theta, R, \dot{R}) = \frac{\dot{R}}{R^4\sqrt{\dot{R}^2 + R^2}} \tag{A.2b}$$

$$F_{\dot{R}\dot{R}}(\theta, R, \dot{R}) = \frac{1}{R^2(\dot{R}^2 + R^2)^{\frac{3}{2}}} \tag{A.2c}$$

$$F_{R\dot{R}}(\theta, R, \dot{R}) = \frac{12R^4 + 33R^2\dot{R}^2 + 20\dot{R}^4}{R^6(\dot{R}^2 + R^2)^{\frac{3}{2}}} \tag{A.2d}$$

$$F_{R\dot{R}}(\theta, R, \dot{R}) = \frac{-5R^2\dot{R} - 4\dot{R}^3}{R^5(\dot{R}^2 + R^2)^{\frac{3}{2}}} \tag{A.2e}$$

The following conditions are sufficient for the cost functional (A.1) to have a weak local minimum for $R = R(\theta)$ [16].

1. The curve $R = R(\theta)$ is an extremal, i.e., it satisfies the Euler equation.
2. The strengthened Legendre condition

$$P(\theta) \equiv \frac{1}{2}F_{\dot{R}\dot{R}}(\theta, R, \dot{R}) > 0 \tag{A.3}$$

   holds along the curve $R = R(\theta)$.
3. The strengthened Jacobi condition holds, i.e., the interval $[a, b]$ contains no points conjugate to a.

We will show these three sufficient conditions are met by examining the second variation of J, which can be expressed as

$$\delta^2 J(h) = \int_a^b (P\dot{h}^2 + Qh^2)\, d\theta \tag{A.4}$$

where $h(\theta)$ is an increment of $R(\theta)$ satisfying $h(a) = h(b) = 0$ and

$$\begin{aligned} P(\theta) &\equiv \frac{1}{2} F_{\dot{R}\dot{R}} \\ &= \frac{1}{2R^2(\dot{R}^2 + R^2)^{\frac{3}{2}}} \end{aligned} \tag{A.5}$$

$$\begin{aligned} Q(\theta) &\equiv \frac{1}{2}\left(F_{RR} - \frac{d}{d\theta} F_{R\dot{R}}\right) \\ &= \frac{12R^4 + 15R^2\dot{R}^2 + 6\dot{R}^4 + 5R^3\ddot{R} + 2R\dot{R}^2\ddot{R}}{2R^4(\dot{R}^2 + R^2)^{\frac{5}{2}}} \\ &= \frac{12R^4 + 15R^2\dot{R}^2 + 6\dot{R}^4 + \ddot{R}R(5R^2 + 2\dot{R}^2)}{2R^4(\dot{R}^2 + R^2)^{\frac{5}{2}}} \end{aligned} \tag{A.6}$$

In section 3.3 we showed that $R(\theta)$ extremizes our cost functional. Thus we have met the first sufficient condition for a weak local minimum.

The Legendre necessary condition for a weak minimum is that $P(\theta) \geq 0$. Clearly this is satisfied in (A.5) for any extremal satisfying the Euler equation since $R^2 > 0$ and $\dot{R}^2 \geq 0$. Furthermore, the strengthened Legendre condition $P(\theta) > 0$ is met.

Now we examine the Jacobi condition to show there are no points conjugate to 0 in the interval $[0, \theta_f]$. If we can show that the quadratic functional (A.4) is nonnegative for all $h(\theta)$ where $P(\theta) > 0$, then the interval $[a, b]$ contains no points conjugate to a [16]. It is then sufficient (albeit conservative) for the second variation to be nonnegative, if $Q(\theta) \geq 0$.

We wish to show that $Q(\theta) \geq 0$. Clearly, the denominator of $Q(\theta)$ is strictly positive, since $R^4 > 0$ and $\dot{R}^2 + R^2 > 0$. Similarly the first three terms of the numerator of $Q(\theta)$ are positive, that is $12R^4 + 15R^2\dot{R}^2 + 6\dot{R}^4 > 0$. Thus, for $Q(\theta) \geq 0$ we need only show

$$12R^4 + 15R^2\dot{R}^2 + 6\dot{R}^4 \geq \ddot{R}R(5R^2 + 2\dot{R}^2)$$

Proof.

$$
\begin{aligned}
& {R_o}^6(4-\cos(2(3\theta+\phi)) \geq 0 \\
\Rightarrow \quad & \frac{{R_o}^6(4-\cos(2(3\theta+\phi))}{R^4} \geq 0 \\
& \frac{{R_o}^6(4-\cos(2(3\theta+\phi))}{R^4} = \frac{{R_o}^6(4-\cos(2(3\theta+\phi))}{({R_o}^3\frac{\sin(3\theta+\phi)}{\sin\phi})^{\frac{4}{3}}} \\
\Rightarrow \quad & \frac{{R_o}^6(4-\cos(2(3\theta+\phi))}{({R_o}^3\frac{\sin(3\theta+\phi)}{\sin\phi})^{\frac{4}{3}}} \geq 0 \\
\Rightarrow \quad & \frac{{R_o}^6(4-\cos(2(3\theta+\phi))}{\sin^2\phi({R_o}^3\frac{\sin(3\theta+\phi)}{\sin\phi})^{\frac{4}{3}}} \geq 0 \\
& \frac{{R_o}^6(4-\cos(2(3\theta+\phi))}{\sin^2\phi({R_o}^3\frac{\sin(3\theta+\phi)}{\sin\phi})^{\frac{4}{3}}} = 2R^2+\dot{R}^2-R\ddot{R} \\
\Rightarrow \quad & 2R^2+\dot{R}^2-R\ddot{R} \geq 0 \\
\Rightarrow \quad & 2R^2+\dot{R}^2 \geq R\ddot{R} \\
\Rightarrow \quad & (2R^2+\dot{R}^2)(6R^2+\dot{R}^2) \geq R\ddot{R}(6R^2+\dot{R}^2) \\
\Rightarrow \quad & 12R^4+10\dot{R}^2R^2+4\dot{R}^4 \geq R\ddot{R}(6R^2+\dot{R}^2) \\
\Rightarrow \quad & 12R^4+15R^2\dot{R}^2+6\dot{R}^4 \geq R\ddot{R}(6R^2+\dot{R}^2) \\
\Rightarrow \quad & 12R^4+15R^2\dot{R}^2+6\dot{R}^4 \geq R\ddot{R}(5R^2+\dot{R}^2)
\end{aligned}
$$

Since $Q(\theta) \geq 0$ we have demonstrated all sufficient conditions for our extremal (3.4) to be a weak local minimum. □

To be considered a strong local minimum, it is necessary that the Weierstrass E-function condition be satisfied, that is

$$F(\theta, R, \dot{R}^*) - F(\theta, R, \dot{R}) - F_{\dot{R}}(\theta, R, \dot{R})(\dot{R}^* - \dot{R}) \geq 0 \tag{A.7}$$

For our cost functional, the Weierstrass E-function (A.7) becomes

$$\frac{\sqrt{\dot{R}^{*2}+R^2}}{R^4} - \frac{\sqrt{\dot{R}^2+R^2}}{R^4} - \frac{\dot{R}(\dot{R}^*-\dot{R})}{R^4\sqrt{\dot{R}^2+R^2}}$$

Obtaining a common denominator

$$\frac{\sqrt{(\dot{R}\dot{R}^*)^2 + (\dot{R}R)^2 + (\dot{R}^*R)^2 + R^4} - (\dot{R}\dot{R}^* + R^2)}{R^4\sqrt{\dot{R}^2 + R^2}} \tag{A.8}$$

Notice that the quantities $(\dot{R}\dot{R}^*)^2$,$(\dot{R}R)^2$,$(\dot{R}^*R)^2$,$\dot{R}^2$,R^2 and R^4 are all guaranteed to be non-negative. In fact, the only quantity that could be negative in (A.8) is $\dot{R}\dot{R}^*$. Thus we can neglect the denominator of (A.8) and to show that the condition (A.7) holds, we need only show that the numerator of (A.8) is greater than or equal to zero. That is, we wish to show

$$\sqrt{(\dot{R}\dot{R}^*)^2 + (\dot{R}R)^2 + (\dot{R}^*R)^2 + R^4} \geq \dot{R}\dot{R}^* + R^2$$

Proof.

$$\begin{aligned}
& (\dot{R} - \dot{R}^*)^2 \geq 0 \\
\Rightarrow \quad & \dot{R}^2 + \dot{R}^{*2} - 2\dot{R}\dot{R}^* \geq 0 \\
\Rightarrow \quad & \dot{R}^2 + \dot{R}^{*2} \geq 2\dot{R}\dot{R}^* \\
\Rightarrow \quad & R^2(\dot{R}^2 + \dot{R}^{*2}) \geq 2R^2\dot{R}\dot{R}^* \\
\Rightarrow \quad & (\dot{R}R)^2 + (\dot{R}^*R)^2 \geq 2R^2\dot{R}\dot{R}^* \\
\Rightarrow \quad & (\dot{R}R)^2 + (\dot{R}^*R)^2 + R^4 \geq 2R^2\dot{R}\dot{R}^* + R^4 \\
\Rightarrow \quad & (\dot{R}R)^2 + (\dot{R}^*R)^2 + (\dot{R}\dot{R}^*)^2 + R^4 \geq (\dot{R}\dot{R}^*)^2 + 2R^2\dot{R}\dot{R}^* + R^4 \\
\Rightarrow \quad & (\dot{R}\dot{R}^*)^2 + (\dot{R}R)^2 + (\dot{R}^*R)^2 + R^4 \geq (R^2 + \dot{R}\dot{R}^*)^2 \\
\Rightarrow \quad & \sqrt{(\dot{R}\dot{R}^*)^2 + (\dot{R}R)^2 + (\dot{R}^*R)^2 + R^4} \geq \dot{R}\dot{R}^* + R^2
\end{aligned}$$

Thus we have satisfied the Weierstrass E-function condition, a necessary condition for the extremal (3.4) to have a strong local minimum. □

Appendix B. Radar Exposure Maximization

B.1 Introduction

In this Appendix, the problem of maximizing exposure to radar is examined. From an operational standpoint, the idea is nonsensical. However, analysis of the maximization problem provides insight into the dual problem of radar exposure minimization.

Given a radar at the origin, we wish to find the planar trajectory, $R^*(\theta)$, that maximizes the reflected RF energy reflected from the target. The trajectory connects two prespecified points A and B, respectively located a distance R_o and R_f from the origin, and separated by an included angle θ_f - see, e.g., Fig. B.1.

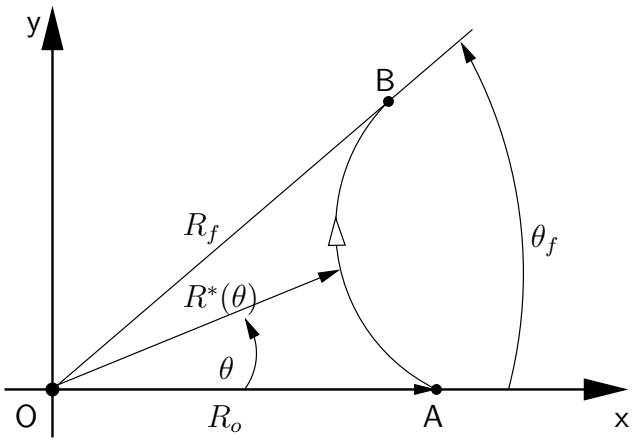

Figure B.1 Radar Exposure Maximization

B.2 Unconstrained Radar Exposure Maximization

As in Chapter III, the problem is posed in the Calculus of Variations. We wish to maximize the cost functional

$$J = \int_0^{\theta_f} \frac{\sqrt{\dot{R}^2 + R^2}}{R^4}\, d\theta \tag{B.1}$$

Without loss of generality, we can write the boundary conditions as

$$R(0) = R_o = 1 \tag{B.2}$$

$$R(\theta_f) = R_f \geq 1, \quad 0 < \theta \leq \theta_f. \tag{B.3}$$

Remark B.2.1. *For the unconstrained radar exposure maximization problem, an optimal solution does not exist.*

Proof. Starting at point A, any trajectory that maximizes J will run to the origin O, and then to the point B. Hence, $J^* \to \infty$ and there does not exist an optimal solution to the unconstrained radar exposure maximization problem. □

B.3 Constrained Radar Exposure Maximization

Assume[1] $R_f = 1$. In order to render the maximization problem well posed, we introduce the isoperimetric constraint

$$\int_0^{\theta_f} \sqrt{\dot{R}^2 + R^2}\, d\theta = l \tag{B.4}$$

Remark B.3.1. *For the constrained radar exposure maximization problem, an optimal solution does not exist for $l > 2$ or $l < 2\sin(\theta_f/2)$.*

Proof. If $l > 2$, maximizing J requires running to the origin O. Hence, as in Remark B.2.1, an optimal solution does not exist.

The Euclidean distance between the points A and B is given by

$$\sqrt{R_o^2 + R_f^2 - 2\, R_o\, R_f \cos\theta_f}$$

Thus, for $R_o = R_f = 1$, if $l < 2\sin(\theta_f/2)$, the isoperimetric constraint cannot be satisfied and an optimal solution does not exist. □

[1] This restriction is for mathematical convenience and can be relaxed.

Now consider the case where $2\sin(\theta_f/2) < l < 2$. The constrained maximization problem described by Eqs. (B.1) and (B.4), can be reformulated as an unconstrained problem using the Lagrange multiplier method. That is, we form the augmented cost functional

$$J_A = \int_0^{\theta_f} \sqrt{\dot{R}^2 + R^2} \left(\frac{1}{R^4} - \lambda \right) \, d\theta \tag{B.5}$$

and choose a value for λ that results in the desired path length l. Clearly, if we choose a value of λ such that the trajectory runs to the origin and $J_A \to \infty$, there does not exist an optimal solution. Thus, questions arise as to whether the Lagrange multiplier method can be used at all in this maximization problem and how should one solve the constrained maximization problem given by

$$\max_{R(\theta)} \int_0^{\theta_f} \frac{\sqrt{\dot{R}^2 + R^2}}{R^4} \, d\theta \tag{B.6a}$$

$$\text{s.t.} \qquad \int_0^{\theta_f} \sqrt{\dot{R}^2 + R^2} \, d\theta = l \tag{B.6b}$$

$$\text{and} \qquad R(0) = R(\theta_f) = 1 \tag{B.6c}$$

$$\text{where} \qquad 2\sin\left(\frac{\theta_f}{2}\right) < l < 2 \tag{B.6d}$$

We note that there does not exist a global maximum in the unconstrained optimization problem with the Lagrange multiplier, e.g., Eq. (B.5). This does not forego the possibility of a local maximum. Interestingly, it is precisely such a local maximum in the unconstrained maximization problem with a Lagrange multiplier that provides a globally optimal solution to the constrained maximization problem, Eqs. (B.6a)-(B.6d).

Furthermore, a range of $\lambda_c > \lambda > 0$ can exist where a local maximizing solution to the unconstrained maximization problem with Lagrange multipliers does not exist. Here $lambda_c$ will be determined by the Legendre necessary condition for a local maximum

$$F_{\dot{R},\dot{R}} \leq 0$$

Thus we require the condition

$$\frac{1}{R^4(\theta)} - \lambda \leq 0$$

be satisfied in addition to our restrictions on l for a maximizing solution to exist. As these are necessary conditions, there may exist additional constraints on λ and thus l as well.

Fig. B.2 is a radar exposure maximizing trajectory obtained using the Lagrange multiplier method for $R_f/R_o = 1$, $\theta_f = 45°$ and $\lambda = -8.9$. The resultant path length is approximately 0.8418.

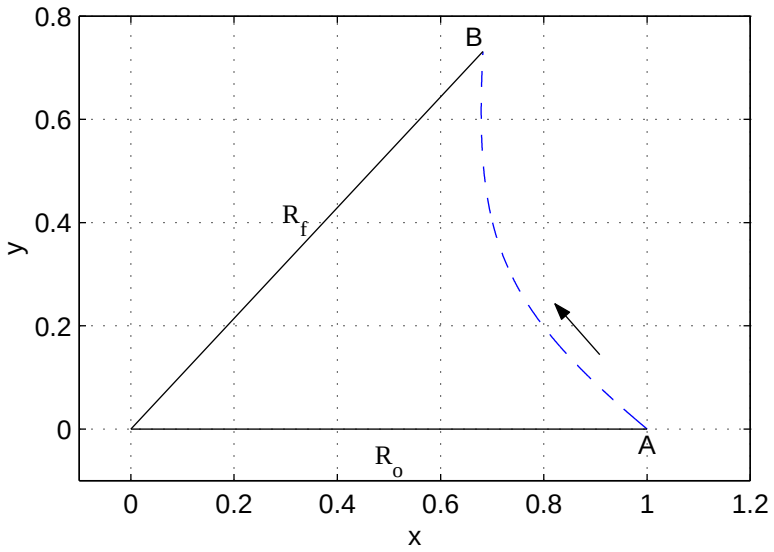

Figure B.2 Example Trajectory for Radar Exposure Maximization

B.4 Summary

We see that the radar exposure maximization problem is somewhat simpler than the radar exposure minimization problem of Chapter III. In the radar exposure minimization problem, an unconstrained solution exists for $0 < \theta_f < \pi/3$ and a path length constraint must be imposed for $\theta_f \geq \pi/3$. In the maximization problem, an unconstrained solution does not exist and only constrained solutions are sought. In addition to the Legendre necessary condition condition on the Lagrange multiplier, the path length constraint $2\sin(\theta_f/2) < l < 2$ may further constrain the range of λ we can choose.

Appendix C. Local Optimality of the Voronoi Edge in Two Radar Exposure Minimization Problems

C.1 Introduction

We are concerned with demonstrating the local optimality of a segment of the Voronoi edge in the two radar exposure minimization problem. The Voronoi edge, for this problem, is the locus of all points of equal power separating the two radars. Specifically, for the case of two equal power radars, the Voronoi edge is a straight line. In this Appendix, we show that the Voronoi edge is an extremizing, and locally minimizing[1], path for the two radar exposure minimization cost functional.

C.2 Equal Power Radars

Consider the two radar exposure minimization problem where the radars are located, without loss of generality, on the x-axis at $(0,0)$ and $(1,0)$. Polar coordinates are used. For the case of equal power radars, the Voronoi edge is the perpendicular bisector of the line connecting these two radars - see, e.g., Fig. C.1.

Let the initial point A on the Voronoi edge be at a distance R_o from the origin, such that

$$R_o = R(\theta_o) = \frac{1}{2}\sec\theta_o \tag{C.1}$$

Similarly for the final point B we have

$$R_f = R(\theta_f) = \frac{1}{2}\sec\theta_f \tag{C.2}$$

Thus, for $\theta \in (-\pi/2, \pi/2)$, the equation of the candidate extremal trajectory connecting A and B, viz., a segment of the Voronoi edge, is

$$R(\theta) = \frac{1}{2}\sec\theta, \quad \theta_o \le \theta \le \theta_f \tag{C.3}$$

[1] Conditions concerning the global optimality of segments of the Voronoi edge are addressed in Sec. 6.3.

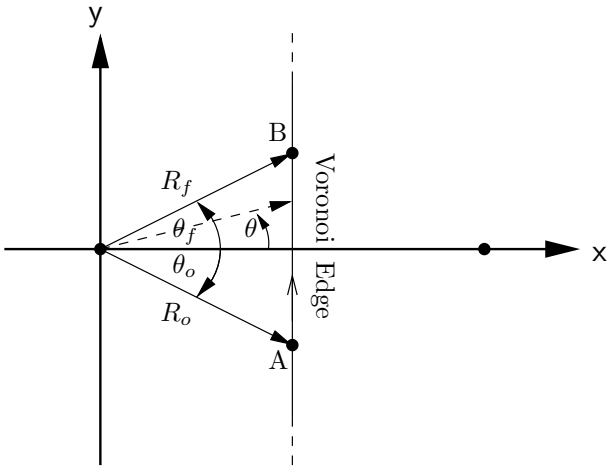

Figure C.1 Two Radar Exposure Minimization and the Voronoi Edge

Lemma C.2.1. *Any segment of the Voronoi edge extremizes the cost functional associated with the (equal power) two radar exposure minimization problem.*

Proof. Let AB be any segment of the Voronoi edge, Eq. (C.3) with endpoints given by Eqs. (C.1) and (C.2). From Sec. 6.3, the Euler equation for the unconstrained two radar exposure minimization problem is

$$\frac{1}{2}\frac{R}{\dot{R}^2+R^2}\left(\ddot{R}+R\right)\left(R^2+a^2-2\,a\,R\,\cos\theta+\alpha\frac{\left(R^2+a^2-2\,a\,R\,\cos\theta\right)^3}{R^4}\right)$$
$$+R^2-a^2-2a\dot{R}\sin\theta+\alpha\frac{\left(R^2+a^2-2\,a\,R\,\cos\theta\right)^3}{R^4}=0 \quad \text{(C.4)}$$

Let $a=1$ and $\alpha=1$. Differentiating Eq. (C.3), we have

$$\dot{R}(\theta)=\frac{1}{2}\sec\theta\tan\theta \quad \text{(C.5)}$$
$$\ddot{R}(\theta)=\frac{1}{4}\left(3-\cos 2\theta\right)\sec^3\theta \quad \text{(C.6)}$$

Substituting the candidate extremal, Eq. (C.3), and its derivatives, Eqs. (C.5) and (C.6), into Eq. (C.4) satisfies the Euler equation. Thus, any segment of the Voronoi edge is an extremizing path. □

Lemma C.2.2. *Any segment of the Voronoi edge satisfies the Legendre necessary condition for a weak local minimum, viz.,*

$$P(\theta) \equiv \frac{1}{2} F_{\dot{R}\dot{R}} \geq 0 \tag{C.7}$$

holds at every point along the trajectory $R(\theta)$ given by Eq. (C.3)*.*

Proof. From Sec. 6.3, we have the following:

$$F_{\dot{R}\dot{R}} = \frac{R^2}{\left(\dot{R}^2 + R^2\right)^2} F$$

where the integrand of the cost functional is given by

$$F = G\sqrt{\dot{R}^2 + R^2} \tag{C.9}$$

and

$$G = \frac{\alpha}{R^4(\theta)} + \frac{1}{\left(R^2(\theta) + a^2 - 2aR(\theta)\cos\theta\right)^2} \tag{C.10}$$

Substituting Eqs. (C.3) and (C.5) into Eq. (C.10) and Eq. (C.9), letting $a = 1$ and $\alpha = 1$, we have

$$G = 32\cos^4\theta$$

$$F = 16\cos^2\theta$$

Similarly, we find

$$P = 32\cos^8\theta \tag{C.11}$$

Thus, the Legendre necessary condition $\frac{1}{2}F_{\dot{R}\dot{R}} \geq 0$ is satisfied. □

Indeed, for any closed interval $\theta \in [\theta_o, \theta_f]$, where $\theta_o > -\pi/2$ and $\theta_f < \pi/2$, the strengthened Legendre condition $\frac{1}{2}F_{\dot{R}\dot{R}} > 0$ is satisfied.

Lastly, we show that the strengthened Jacobi condition holds, namely, that the interval $[\theta_o, \theta_f]$, where $\theta_o > -\pi/2$ and $\theta_f < \pi/2$, contains no points conjugate to the point θ_o.

The Jacobi equation, Eq. (2.7), is

$$-\frac{d}{d\theta}\left(Ph'\right) + Qh = 0 \tag{C.12}$$

where the function $P(\theta) > 0$ is given by Eq. (C.7) and

$$Q = Q(\theta) = \frac{1}{2}\left(F_{RR} - \frac{d}{d\theta}F_{R\dot{R}}\right) \tag{C.13}$$

Evaluating the partial derivatives and substituting Eqs. (C.3), (C.5) and (C.6) into Eq. (C.13), yields

$$Q = 16\cos^6\theta\ (11 + 31\ \cos 2\theta) \tag{C.14}$$

Substituting Eqs. (C.11) and (C.14) into the Jacobi equation, we have

$$\begin{aligned}
& -16\cos^6\theta\ \left[2\cos^2\theta\, h''(\theta) - 8\ \sin 2\theta\, h'(\theta) - (11 + 31\ \cos 2\theta)\ h(\theta)\right] = 0 \\
\Rightarrow\quad & 2\cos^2\theta\, h''(\theta) - 8\ \sin 2\theta\, h'(\theta) - (11 + 31\ \cos 2\theta)\ h(\theta) = 0 \\
\Rightarrow\quad & h''(\theta) - \frac{8\ \sin 2\theta}{2\cos^2\theta}\, h'(\theta) - \frac{11 + 31\ \cos 2\theta}{2\cos^2\theta}\, h(\theta) = 0 \\
\Rightarrow\quad & h''(\theta) - \frac{8\ \sin\theta\ \cos\theta}{\cos^2\theta}\, h'(\theta) - \frac{11 + 31\left(2\ \cos^2\theta - 1\right)}{2\cos^2\theta}\, h(\theta) = 0 \\
\Rightarrow\quad & h''(\theta) - 8\ \tan\theta\, h'(\theta) - \left(31 - 10\sec^2\theta\right)\ h(\theta) = 0 \\
\Rightarrow\quad & h''(\theta) - 8\ \tan\theta\, h'(\theta) + \left(10\tan^2\theta - 21\right)\ h(\theta) = 0
\end{aligned} \tag{C.15}$$

This second order linear differential equation is of the form

$$h'' + a\tan\theta\, h' + \left(\alpha\tan^2\theta + \gamma\right)\ h = 0$$

which is a special case of the equation

$$h'' + (a\tan\theta + b\cot\theta)\ h' + \left(\alpha\tan^2\theta + \beta\cot^2\theta + \gamma\right)\ h = 0 \tag{C.16}$$

where

$$a = -8$$

$$b = 0$$

$$\alpha = 10$$

$$\beta = 0$$

$$\gamma = -21$$

Also, $h(\theta_o) = h(\theta_f) = 0$. According to [35], Eq. (C.16) has an exact solution. Following the methodology in [35], pp. 188, Sec. 2.1.6, Eq. (55), we employ the transformation

$$\xi = \sin^2\theta$$

$$h = w\,\tan\theta\,\sec^4\theta$$

Applying the transformation above leads to the equation:

$$\xi\,(\xi-1)\;w''(\xi) + \left(\xi - \frac{3}{2}\right)\;w'(\xi) + \frac{15}{4}\,w(\xi) = 0$$

with boundary conditions $w(\xi_1) = 0, w(\xi_2) = 0,\ \xi_i \in (0,1)$. Note: we assumed that $x_1 = \sin^2\theta_o$ and $x_2 = \sin^2\theta_f$. Hence, this transformation lead to the Gauss hypergeometric equation given in [35], pp. 152, Sec. 2.1.2, Eq. (158),

$$x\,(x-1)\,y'' + [(\alpha+\beta+1)\,x - \gamma]\,y' + \alpha\,\beta\,y = 0 \tag{C.17}$$

with the boundary conditions $y(x_1) = y(x_2) = 0$ and the parameters

$$\alpha = \pm\imath\frac{\sqrt{15}}{2}$$

$$\beta = \mp\imath\frac{\sqrt{15}}{2} = \bar{\alpha}$$

$$\gamma = \frac{3}{2}$$

Since γ is not an integer, the general solution of the Gauss hypergeometric equation, Eq. (C.17), is [35]

$$y = C_1 F(\alpha, \beta, \gamma; x) + C_2\, x^{1-\gamma} F(\alpha - \gamma + 1, \beta - \gamma + 1, 2 - \gamma; x) \tag{C.18}$$

where

$$\begin{aligned} F(\alpha, \beta, \gamma; x) &= \frac{\Gamma(\gamma)}{\Gamma(\beta)\Gamma(\gamma - \beta)} \int_0^1 t^{\beta-1} \, (1-t)^{\gamma-\beta-1} \, (1 - t\, x)^{-\alpha} \, dt \\ &= 1 + \sum_{k=1}^{\infty} \frac{(\alpha)_k \, (\beta)_k}{(\gamma)_k} \frac{x^k}{k!}, \qquad (\alpha)_k = \alpha \, (\alpha + 1) \ldots (\alpha + k - 1) \end{aligned}$$

is a hypergeometric function and $\Gamma(\beta)$ is the gamma function. Without loss of generality[2], let $\alpha = \imath\frac{\sqrt{15}}{2}$, and $\beta = -\imath\frac{\sqrt{15}}{2}$. We have

$$y = C_1 F(\imath\frac{\sqrt{15}}{2}, -\imath\frac{\sqrt{15}}{2}, \frac{3}{2}; x) + C_2\, x^{-\frac{1}{2}} F(-\frac{1}{2} + \imath\frac{\sqrt{15}}{2}, -\frac{1}{2} - \imath\frac{\sqrt{15}}{2}, \frac{1}{2}; x) \tag{C.19}$$

Applying the first boundary condition $y(x_1) = 0$ and solving Eq. (C.19) for the constant C_1, yields

$$C_1 = -\frac{C_2\, F(-\frac{1}{2} + \imath\frac{\sqrt{15}}{2}, -\frac{1}{2} - \imath\frac{\sqrt{15}}{2}, \frac{1}{2}; x_1)}{\sqrt{x_1}\, F(\imath\frac{\sqrt{15}}{2}, -\imath\frac{\sqrt{15}}{2}, \frac{3}{2}; x_1)} \tag{C.20}$$

Substituting Eq. (C.20) into Eq. (C.19), and imposing the second boundary condition $y(x_2) = 0$, yields the equation in C_2

$$\begin{aligned} C_2 \Bigg(& \frac{F(-\frac{1}{2} + \imath\frac{\sqrt{15}}{2}, -\frac{1}{2} - \imath\frac{\sqrt{15}}{2}, \frac{1}{2}; x_2)}{\sqrt{x_2}} \\ & - \frac{F(\imath\frac{\sqrt{15}}{2}, -\imath\frac{\sqrt{15}}{2}, \frac{3}{2}; x_2)\, F(-\frac{1}{2} + \imath\frac{\sqrt{15}}{2}, -\frac{1}{2} - \imath\frac{\sqrt{15}}{2}, \frac{1}{2}; x_1)}{\sqrt{x_1}\, F(\imath\frac{\sqrt{15}}{2}, -\imath\frac{\sqrt{15}}{2}, \frac{3}{2}; x_1)} \Bigg) = 0 \end{aligned} \tag{C.21}$$

[2] We have two solutions for the parameters α and β. However, $\beta = \bar{\alpha}$, the complex conjugate of α. Hypergeometric functions have the property $F(\alpha, \beta, \gamma; x) = F(\beta, \alpha, \gamma; x)$ - see, e.g., [31]. Thus, we need only consider one of the two solutions for α and β.

Proposition C.2.1. *For any $x_2 \neq x_1$, $x_1, x_2 \in (0,1)$, the expression*

$$\frac{F(-\frac{1}{2}+\imath\frac{\sqrt{15}}{2}, -\frac{1}{2}-\imath\frac{\sqrt{15}}{2}, \frac{1}{2}; x_2)}{\sqrt{x_2}} - \frac{F(\imath\frac{\sqrt{15}}{2}, -\imath\frac{\sqrt{15}}{2}, \frac{3}{2}; x_2)\, F(-\frac{1}{2}+\imath\frac{\sqrt{15}}{2}, -\frac{1}{2}-\imath\frac{\sqrt{15}}{2}, \frac{1}{2}; x_1)}{\sqrt{x_1}\, F(\imath\frac{\sqrt{15}}{2}, -\imath\frac{\sqrt{15}}{2}, \frac{3}{2}; x_1)}$$

is not zero.

Proof. Momentarily let $x_2 > x_1$. Define

$$\begin{aligned} f_1(x) &= F(\imath\frac{\sqrt{15}}{2}, -\imath\frac{\sqrt{15}}{2}, \frac{3}{2}; x) \\ f_2(x) &= F(-\frac{1}{2}+\imath\frac{\sqrt{15}}{2}, -\frac{1}{2}-\imath\frac{\sqrt{15}}{2}, \frac{1}{2}; x) \\ f_3(x) &= \sqrt{x}\, F(\imath\frac{\sqrt{15}}{2}, -\imath\frac{\sqrt{15}}{2}, \frac{3}{2}; x) \\ &= \sqrt{x}\, f_1(x) \end{aligned}$$

It can be shown that the series representations of the hypergeometric functions $f_1(x)$, $f_2(x)$ and $f_3(x)$ are absolutely convergent - see, e.g., [31]. Furthermore, the functions $f_1(x)$, $f_2(x)$ and $f_3(x)$ are continuous and monotonically increasing on the interval $(0,1)$ - see, e.g. Fig. C.2. Evidently, the functions have many properties, including

$$\begin{gathered} f_1(x) > 0 \\ f_2(x) > 0 \\ f_3(x) \geq 0 \\ f_2(x_1) > f_3(x_1) \\ f_2(x_2) > f_3(x_2) \\ f_2(x_2) > f_2(x_1) \\ f_2(x_2) > f_3(x_1) \\ f_3(x_2) > f_3(x_1) \end{gathered}$$

Define

$$g(x) = \frac{f_3(x)}{f_2(x)}$$

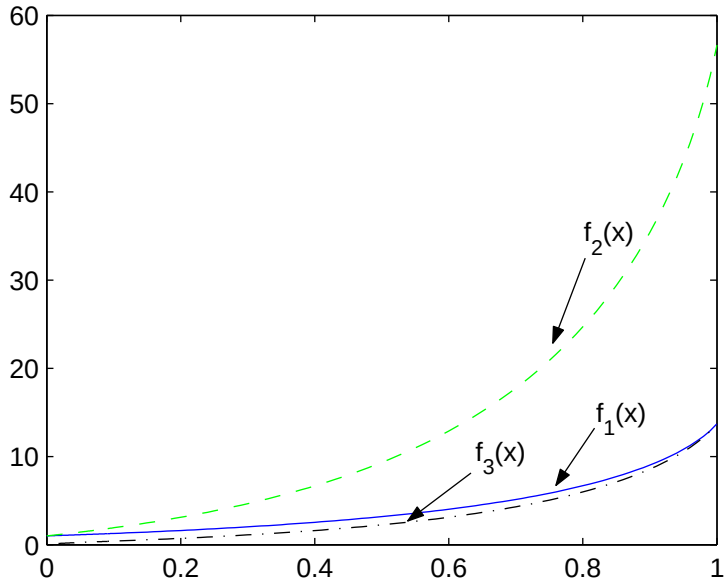

Figure C.2 The Hypergeometric Functions $f_1(x), f_2(x)$ and $f_3(x)$

Clearly,

$$0 \leq g(x) < 1$$

Furthermore, $g(x)$ is monotonically increasing, see, e.g., Fig. C.3, so that

$$g(x_2) > g(x_1)$$

for all $x_2 > x_1$. Thus,

$$\begin{aligned}
& \frac{f_3(x_2)}{f_2(x_2)} > \frac{f_3(x_1)}{f_2(x_1)} \\
\Rightarrow \quad & f_3(x_2)\, f_2(x_1) > f_3(x_1)\, f_2(x_2) \\
\Rightarrow \quad & \sqrt{x_2}\, f_1(x_2)\, f_2(x_1) > \sqrt{x_1}\, f_1(x_1)\, f_2(x_2) \\
\Rightarrow \quad & \frac{f_1(x_2)\, f_2(x_1)}{\sqrt{x_1}\, f_1(x_1)} > \frac{f_2(x_2)}{\sqrt{x_2}} \\
\Rightarrow \quad & \frac{f_2(x_2)}{\sqrt{x_2}} - \frac{f_1(x_2)\, f_2(x_1)}{\sqrt{x_1}\, f_1(x_1)} < 0, \quad \forall\, x_i \in (0,1)
\end{aligned} \tag{C.22}$$

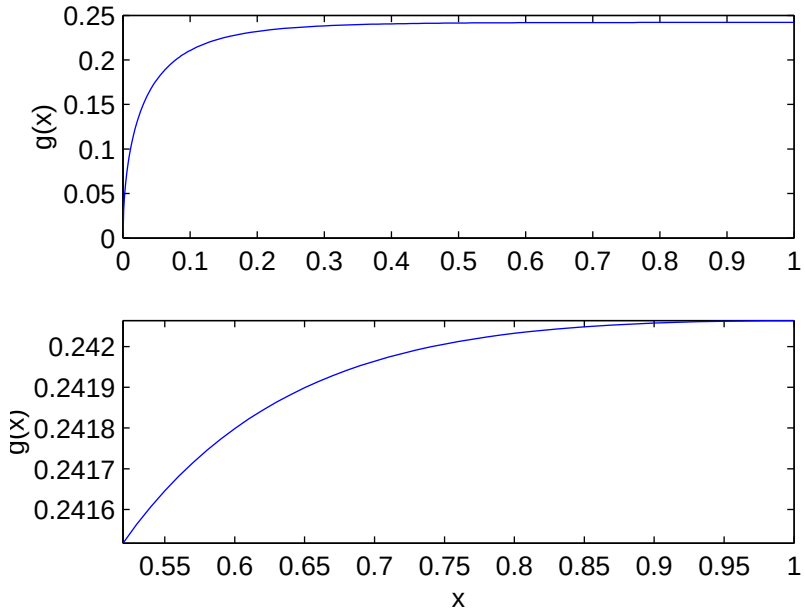

Figure C.3 The Hypergeometric Function $g(x)$

Or, equivalently, the expression Eq. (C.22) is not zero. To show this holds for $x_1 > x_2$, the same procedure is followed, resulting in the inequality Eq. (C.22) being reversed. There is no zero crossing for any segment (x_1, x_2) where $x_1 \neq x_2$. □

Lemma C.2.3. *The strengthened Jacobi condition holds, viz., that the interval* $[\theta_o, \theta_f]$, *where* $\theta_o > -\pi/2$ *and* $\theta_f < \pi/2$, *contains no points conjugate to the point* θ_o.

Proof. By Proposition C.2.1, Eq. (C.22) is not equal to zero, which implies the constant C_2 in Eq. (C.21) must be zero. Hence, from Eq. (C.20), $C_1 = 0$ and the solution to the differential equation resulting from the Jacobi equation is $y \equiv 0$. Hence, there are no conjugate points. □

Theorem C.2.1. *For the two radar exposure minimization problem, any segment of the Voronoi edge is locally minimizing.* □

In conclusion, in view of the above analysis, the problem with the Voronoi edge is the latter's ceasing to be a global minimum - this, according to the condition imposed by Theorem 6.3.1.

Bibliography

1. Andrews, Larry C. *Special Functions of Mathematics for Engineers* (Revised Edition). New York: McGraw-Hill, 1992.
2. Arkin, Ronald C., "Toward the Unification of Navigational Planning and Reactive Control." Working Notes of the AAAI Spring Symposium on Robot Navigation, Stanford University, March 1989.
3. Arkin, Ronald C. and Tucker Balch. "Cooperative Multiagent Robotic Systems." *Artificial Intelligence and Mobile Robots* edited by D. Kortenkamp and others, MIT Press, 1998.
4. Asseo, Sabi J. "In-Flight Replanning of Penetration Routes to Avoid Threat Zones of Circular Shapes." *Proceedings of the IEEE 1998 National Aerospace and Electronics Conference*. 383–391. IEEE Press, 1998.
5. Bortoff, Scott A., "Path-Planning for Unmanned Air Vehicles." In-house Report. AFRL/VAAD, Wright-Patterson AFB Ohio, 15 August 1999.
6. Brooks, Rodney A. "New Approaches to Robotics," *Science*, *253*:1227–1232 (September 1991).
7. Bryson, Jr., Arthur E. *Dynamic Optimization*. Menlo Park California: Addison–Wesley, 1999.
8. Bryson, Jr., Arthur E. and Yu-Chi Ho. *Applied Optimal Control*. Waltham Massachusetts: Ginn and Company, 1969.
9. Buzogany, Louis E. *Automated Control of Aircraft in Formation Flight*. MS thesis, AFIT/GE/ENG/92D-07, Graduate School of Engineering, Air Force Institute of Technology (AETC), Wright-Patterson AFB OH, December 92 (ADA259020).
10. Byrd, Paul F. and Morris D. Friedman. *Handbook of Elliptic Integrals for Engineers and Physicists*. Berlin Germany: Springer-Verlag, 1954.
11. Cash, J.R. and Margaret H. Wright. "A Defered Correction Method for Nonlinear Two-Point Boundary Value Problems: Implementation and numerical evaluation," *SIAM J. Sci. Stat. Comput.*, *12*:971–989 (1991).
12. Chandler, Philip R., et al. "UAV Cooperative Path Planning." *Proceedings of the 2000 AIAA Guidance, Navigation and Control Conference*. 2000.
13. Coleman, Thomas, et al. *Optimization Toolbox Users's Guide*. Natick Massachusetts: The MathWorks, Inc., January 1999.
14. Eves, Howard. "Analytic Geometry." *CRC Standard Mathematical Tables and Formulae*, (29th Edition) edited by William H. Beyer, Boca Raton Florida: CRC Press, 1991.
15. Freund, E. and H. Hoyer. "Pathfinding in Multi-Robot Systems: Solution and Applications." *Proceedings of the 1986 IEEE International Conference on Robotics and Automation*. April 1986.

16. Gelfand, I. M. and S. V. Fomin. *Calculus of Variations* (Revised English Edition). Englewood Cliffs New Jersey: Prentice–Hall, 1963.

17. Goldman, Jeffrey A. *A Survey of Three-Dimensional Path Planning in the Context of a Point-Like Aircraft Avoiding Danger Regions*. Technical Report WL-TR-93-1070, Wright-Patterson AFB Ohio: Wright Laboratory, May 1993 (ADA268395).

18. Gregory, John and Cantian Lin. *Constrained Optimization in the Calculus of Variations and Optimal Control Theory*. New York: Van Nostrand Reinhold, 1992.

19. Hebert, Jeffrey, et al. "Cooperative Control of UAVs." *Proceedings of the 2001 AIAA Guidance, Navigation and Control Conference*. 2001.

20. Helgason, R.V. and others. *Shortest Path Algorithms on Grid Graphs with Applications to Strike Planning*. Technical Report, Southern Methodist University, February 1997 (ADA321664).

21. Hunter, Maj. Mark, "Low Cost Autonomous Attack System (LOCAAS) Industry Day Briefing." Briefing. AFRL/MNAV, Eglin AFB Florida, 24 June 1998.

22. Isaacs, Rufus. *Differential Games*. New York: John Wiley and Sons, 1965.

23. Jacques, David R. and others. "A MATLAB Toolbox for Fixed-Order, Mixed-Norm Control Synthesis," *IEEE Control Systems Magazine*, *15*(5):36–44 (October 1996).

24. Koren, Yoram and Johann Borenstein. "Potential Field Methods and Their Inherent Limitations for Mobile Robotics." *Proceedings of the 1991 IEEE International Conference on Robotics and Automation*. April 1991.

25. Leahy, Lt. Col. Mike, "Unmanned Combat Air Vehicle Advanced Technology Demonstration Industry Day Briefing." Briefing. DARPA, Washington DC, 23 February 1998.

26. Leitmann, George. *The Calculus of Variations and Optimal Control: An Introduction*. New York: Plenum Press, 1981.

27. McFarland, Michael B., et al. "Motion Planning for Reduced Observability of Autonomous Air Vehicles." *Proceedings of the 1999 IEEE Conference on Control Applications*. New York: IEEE Press, 1999.

28. McLain, Timothy W., "Coordinated Control of Unmanned Air Vehicles." In-house Report. AFRL/VAAD, Wright-Patterson AFB Ohio, Summer 1999.

29. Milne-Thomson, L.M. "Elliptic Integrals." *Handbook of Mathematical Functions with Formulas, Graphs, and Mathematical Tables*, (Ninth Edition) edited by Milton Abramowitz and Irene A. Stegun, Washington DC: U.S. Government Printing Office, November 1970.

30. Novy, Michael C. *Air Vehicle Optimal Trajectories for Minimization of Radar Exposure*. MS thesis, AFIT/GAE/ENY/01M-07, School of Engineering and Management, Wright-Patterson AFB OH, March 2001.

31. Oberhettinger, Fritz. "Hypergeometric Functions." *Handbook of Mathematical Functions with Formulas, Graphs, and Mathematical Tables*, (Ninth Edition) edited by

Milton Abramowitz and Irene A. Stegun, Washington DC: U.S. Government Printing Office, November 1970.

32. Ogilvy, C. Stanley. *Excursions in Geometry*. New York: Dover Publications, Inc., 1990.

33. Okabe, Atsuyuki, et al. *Spatial Tessellations*. Chichester England: John Wiley and Sons, 1992.

34. Pendelton, Capt. Ryan R. *Use of Unusual Aircraft Orientations to Generate Low Observable Routes*. MS thesis, AFIT/GAE/ENY/00M-09, School of Engineering and Management, Wright-Patterson AFB OH, March 2000.

35. Polyanin, Andrei D. and Valentin F. Zaitsev. *Handbook of Exact Solutions for Ordinary Differential Equations*. Boca Raton Florida: CRC Press, 1995.

36. Press, William H. and others. *Numerical Recipes in FORTRAN 77* (Second Edition). Cambridge England: Cambridge University Press, 1992.

37. Ram, Aswin and others. *Case-based reactive navigation: A case-based method for on-line selection and adaptation of reactive control parameters in autonomous robotic systems*. Technical Report GIT-CC-92/57, Atlanta Georgia: College of Computing,Georgia Institute of Technology, 1992.

38. Ram, Aswin and others. "Using Genetic Algorithms to Learn Reactive Control Parameters for Autonomous Robotic Navigation," *Adaptive Behavior*, *2*(3):277–304 (1994).

39. Ram, Aswin and Juan Carlos Santamaría. "Multistrategy Learing in Reactive Control Systems for Autonomous Navigation," *Informatica*, *17*(4):347–369 (1993).

40. Roberts, Sanford M. and Jerome S. Shipman. *Two–Point Boundary Value Problems: Shooting Methods*. New York: American Elsevier, 1972.

41. RoboCup. *RoboCup: The World Cup Initiative*, Last Accessed: 16 August 2001. http://www.robocup.org.

42. Skolnik, Merril I., editor. *Radar Handbook* (Second Edition). New York: McGraw-Hill, 1990.

43. Visual Numerics, Inc. *IMSL Math Library*, *1*. Visual Numerics, Inc., 1997.

44. Weisstein, Eric W. *CRC Concise Encyclopedia of Mathematics*. Boca Raton Florida: CRC Press, November 1998.

45. Wolfram Research, Inc. *Mathematica* (Version 4 Edition). Champaign Illinois: Wolfram Research, Inc., 1999.

46. Zabarankin, M., et al., "Optimal Risk Path Algorithms." Presentation to the Workshop on Cooperative Control and Optimization, December 2000. To be published in a collection by Kluwer Academic Publishers.

Vita

Captain Jeffrey Hebert, a native of central Massachusetts, graduated from Grafton Memorial Senior High School in 1986. He then attended Worcester Polytechnic Institute to study electrical engineering, graduating in 1990 with a Bachelor of Science degree, with Distinction. Upon graduation, he was commissioned as a Second Lieutenant in the United States Air Force.

Captain Hebert's first assignment was to the Flight Control Division, Flight Dynamics Directorate, Wright Laboratory, Wright-Patterson Air Force Base, Ohio. As a simulation systems engineer, he was responsible for providing engineering solutions in support of several pilot-in-the-loop flight simulators. In 1994, Captain Hebert was selected to attend the Air Force Institute of Technology (AFIT), where he received the Master of Science in Electrical Engineering degree, specializing in guidance, control and navigation. Captain Hebert was subsequently assigned to the 746th Test Squadron, 46th Test Group (AFMC), Holloman Air Force Base, New Mexico, where he was involved in the testing of Global Positioning System user equipment for a wide variety of military weapon systems. In 1999, Captain Hebert returned to AFIT to pursue a PhD in Electrical Engineering. For his next assignment, Captain Hebert will report to Kirtland Air Force Base, New Mexico, where he will be involved in the operational test and evaluation of the Airborne Laser.

REPORT DOCUMENTATION PAGE

Form Approved
OMB No. 0704-0188

The public reporting burden for this collection of information is estimated to average 1 hour per response, including the time for reviewing instructions, searching existing data sources, gathering and maintaining the data needed, and completing and reviewing the collection of information. Send comments regarding this burden estimate or any other aspect of this collection of information, including suggestions for reducing the burden, to Department of Defense, Washington Headquarters Services, Directorate for Information Operations and Reports (0704-0188), 1215 Jefferson Davis Highway, Suite 1204, Arlington, VA 22202-4302. Respondents should be aware that notwithstanding any other provision of law, no person shall be subject to any penalty for failing to comply with a collection of information if it does not display a currently valid OMB control number.

PLEASE DO NOT RETURN YOUR FORM TO THE ABOVE ADDRESS.

1. REPORT DATE *(DD-MM-YYYY)*	2. REPORT TYPE	3. DATES COVERED *(From - To)*
30-11-2001	Doctoral Dissertation	Oct 1999 - Nov 2001

4. TITLE AND SUBTITLE
Air Vehicle Path Planning

5a. CONTRACT NUMBER

5b. GRANT NUMBER

5c. PROGRAM ELEMENT NUMBER

6. AUTHOR(S)
Hebert, Jeffrey M., Capt, USAF

5d. PROJECT NUMBER
ENR Proposal #01-062

5e. TASK NUMBER

5f. WORK UNIT NUMBER

7. PERFORMING ORGANIZATION NAME(S) AND ADDRESS(ES)
Air Force Institute of Technology
Graduate School of Engineering and Management (AFIT/EN)
2950 P Street, Building 640
WPAFB OH 45433-7765

8. PERFORMING ORGANIZATION REPORT NUMBER
AFIT/DS/ENG/01-04

9. SPONSORING/MONITORING AGENCY NAME(S) AND ADDRESS(ES)
Mr. Phillip R. Chandler, UAV Control Tech Lead
AFRL/VACA
Bldg 146 Rm 305
2210 8th Street
WPAFB OH 45433-7532

10. SPONSOR/MONITOR'S ACRONYM(S)

11. SPONSOR/MONITOR'S REPORT NUMBER(S)

12. DISTRIBUTION/AVAILABILITY STATEMENT
APPROVED FOR PUBLIC RELEASE; DISTRIBUTION UNLIMITED

13. SUPPLEMENTARY NOTES

14. ABSTRACT

An air vehicle exposed to illumination by a tracking radar is considered. The problem of determining an optimal planar trajectory connecting two prespecified points is addressed. An analytic solution yielding the trajectory minimizing the received radar energy reflected from the target is derived using the Calculus of Variations. The related problem of an air vehicle tracked by a passive sensor is also solved. Using the insights gained from the single air vehicle radar exposure minimization problem, a hierarchical cooperative control law is formulated to determine the optimal trajectories that minimize the cumulative exposure of multiple air vehicles during a rendezvous maneuver. The problem of one air vehicle minimizing exposure to multiple radars is also addressed using a variational approach, as well as a sub-optimal minmax argument. Local and global optimality issues are explored. A novel decision criterion is developed determining the geometric conditions dictating when it is preferable to go between or around two radars. Lastly, an optimal minimum time control law is obtained for the target classification and identification mission of an autonomous air vehicle. This work demonstrates that an awareness of the consequences of embracing sub-optimal and non-globally optimal solutions for optimization problems, such as air vehicle path planning, is essential.

15. SUBJECT TERMS
Planning, Optimization, Calculus of Variations, Unmanned, Uninhabited Air Vehicle, Aircraft

16. SECURITY CLASSIFICATION OF:			17. LIMITATION OF ABSTRACT	18. NUMBER OF PAGES	19a. NAME OF RESPONSIBLE PERSON
a. REPORT	b. ABSTRACT	c. THIS PAGE			Meir Pachter, AFIT/ENG
U	U	U	UU	195	19b. TELEPHONE NUMBER *(Include area code)* 937-255-3636 x4593